ISAS - INTERNATIONAL SCHOOL
FOR ADVANCED STUDIES

"A multidisciplinary study of neural coding underlying sensory-motor responses in the leech"

Thesis submitted for the degree of "Doctor Philosophiae"

CANDIDATE
Davide Franco Zoccolan

SUPERVISOR
Prof. Vincent Torre

SISSA - SCUOLA
INTERNAZIONALE
SUPERIORE
STUDI AVANZATI
TRIESTE
Via Beirut 2-4

TRIESTE

To my parents

TABLE OF CONTENTS

Acknowledgements

First of all, I wish to express my gratitude to Prof. Vincent Torre for his support and for carefully supervising my Ph.D. work.

I thank Prof. John Nicholls for inspiring our work on the leech nervous system and for his precious advice. I also thank Dr. Hugh Robinson for valuable scientific suggestions and helpful comments about reproducibility of motor behavior.

I thank all my colleagues and friends of the Torre's lab. I'm especially grateful to Giulietta Pinato and Ivan Arisi, who worked with me for the experiments on, respectively, local bending and whole-body shortening. I also thank the two new "leechers" of the lab: Sofija Andjelic and Elisabeth Garcia Perez. I thank Marco Cappello, Alessandro Bisso and Andrea Giachetti for the help in developing the software to compute and analyze the optical flow. I thank Manuela Schipizza Lough and Jane Wolfe for her careful work in editing the text.

I also thank the members of the Harchirudo leech database group: Fabio Venuti, Riccardo Brancaleon, Gerry Cargnelutti and Emanuela Cazzaniga.

I thank all my friends that helped me with computer: Sergio Graziosi, Walter Vanzella, Felice Pellegrino and Caterina Camus.

Finally, I thank Mr. Claudio Becciani for his invaluable technical support.

Note

The work described in this dissertation was carried out at the International School for Advanced Studies, Trieste, between November 1998 and September 2002. All work reported has not been submitted, as in whole or in part, to any other University or Institute.

Part of the data reported in the present thesis has been published in the articles listed below. In all cases the candidates personally performed the experimental work and the data analysis, and contributed to software and paper writing.

1. **Zoccolan D**, Pinato G & Torre V (2002). Highly variable spike trains underlie reproducible sensory-motor responses in the leech. *J. Neurosci.* (in press).

2. **Zoccolan D** & Torre V (2002). Using optical flow to characterize sensory-motor interactions in a segment of the medicinal leech. *J. Neurosci.* **22,** 2283-2298.

3. **Zoccolan D**, Giachetti A, & Torre V (2001). The use of optical flow to characterize muscle contraction. *J. Neurosci. Methods* **110**, 65-80.

4. Arisi I, **Zoccolan D**, & Torre V (2001). Distributed motor pattern underlying whole-body shortening in the medicinal leech. *J. Neurophysiol.* **86**, 2475-2488.

Davide Franco Zoccolan

Abbreviations used in the text

σ: standard deviation

AA: anterior anterior branch of the anterior root

AC: anterior connective

AE: annulus erector motor neuron

AFR: average firing rate

CNS: central nervous system

CPG: central pattern generator

C.V.: ventrolateral circular excitatory motoneuron

DE: dorsal excitatory motor neuron

DP: dorsal posterior branch of the posterior root

DP1: main trunk of the DP branch

FMRFamide: phe-met-arg-phe-amide

L: large longitudinal excitatory motoneuron

N_l: lateral nociceptive mechanosensory neuron

N_m: medial nociceptive mechanosensory neuron

P_d: dorsal pressure mechanosensory neuron

P_v: ventral pressure mechanosensory neuron

PP: posterior posterior branch of the posterior root

T_d: dorsal touch mechanosensory neuron

T_l: lateral touch mechanosensory neuron

T_v: ventral touch mechanosensory neuron

Abstract

The subject of my Ph.D. project is the study of the neural coding of sensory-motor responses in the leech *Hirudo Medicinalis*. I have used a combination of multielectrode recordings, videomicroscopy and computer vision methods to quantify the leech behavior and simultaneously measure its underlying neuronal activity. Based on this experimental approach, I was able to characterize the motor pattern underlying reflexive behavior in the leech, addressing fundamental issues of systems neuroscience such as population coding and distributed organization of motor responses. In this context, the specific aims of my Ph.D. project can be summarized in three main goals:

1) to develop a new method to quantify the two-dimensional pattern of deformation induced by muscle contraction on the leech body wall;
2) to investigate the distributed organization of leech reflexive behavior at the level of recruitment and activation of specific classes of motoneurons and muscle fibers;
3) to understand the neural basis of the reliability of leech motor responses, by quantifying their reproducibility at different levels of neural processing.

In this scheme, the accomplishment of a specific aim was the starting point to address the next one. Quantitative analysis of deformation occurring on leech body-wall was the necessary backdrop for characterizing leech sensory-motor responses at the behavioral level. This quantitative analysis of behavior, in turn, was fundamental for comparing reproducibility of leech motor responses with that of neural firing sustaining them. In the following paragraphs, I will summarize the major achievements of my Ph.D. project in relation to established main goals.

The first aim of my research was to develop a reliable and innovative method to quantify the pattern of deformation that muscle contraction induces on the leech body-wall. Muscle contraction is usually measured and characterized with force and displacement

transducers. The contraction of muscle fibers, however, evokes in the tissue a two and even three-dimensional displacement field, which is not properly quantified by these transducers because they provide just a single scalar quantity. I circumvented this problem by using videomicroscopy and standard tools of computer vision developed for the analysis of time varying image sequences. By computing the so called optical flow, i.e. the apparent motion of points in a time varying image sequence, it is possible to recover a two dimensional motion field, describing rather precisely the displacement caused by muscle contraction in a flattened piece of skin. The obtained two dimensional optical flow can be further analyzed by computing its origin (i.e. the singular point) and four elementary components that combine linearly: expansion, rotation, longitudinal shear and oblique shear. These elementary deformations provide a compact and accurate characterization of the contraction induced by different motoneurons. I demonstrated this technique by analyzing the displacement caused by muscle contraction on the leech body-wall. However, this method can be applied to monitor and characterize all contractions in almost flat tissues with enough visual texture.

The second aim of my Ph.D. project was to apply the method described above in order to characterize the pattern of activation of different classes of motoneurons and muscles during leech reflexive behavior. Activation of motoneurons innervating leech muscles causes the appearance of a two dimensional vector field of deformations on the skin surface that can be fully characterized by computing the optical flow. I found that all motoneurons can be classified and recognized according to the elementary deformations of the contractions they elicit: longitudinal motoneurons give rise almost exclusively to longitudinal negative shear, whereas circular motoneurons give rise to both positive longitudinal shear and significant negative expansion. Oblique motoneurons induce strong oblique shear, in addition to longitudinal shear and negative expansion. These results clearly showed that contractions induced by different classes of motoneurons and muscle

fibers form a set of basic behavioral units. I also investigated the way in which such behavioral units can combine to sustain motor responses and I found that optical flows induced by the contraction of longitudinal, circular and oblique fibers superimpose linearly. Complex patterns of skin deformation induced by mechanosensory stimulation can therefore be attributed rather reliably to the contraction of distinct longitudinal, circular and oblique muscle fibers. Based on this conclusion, I found that *local bending*, a motor response caused by local mechanical stimulation of the leech skin, is sustained by coactivation of two distinct classes of motoneurons: circular and longitudinal. I also compared the pattern of deformation produced by local bending with that produced by intracellular stimulation of mechanosensory pressure (P), touch (T) and nociceptive (N) cells: optical flows resulting from the activation of P cells were almost identical to those produced by mechanical stimulation. This confirmed that local bending is almost entirely mediated by excitation of P cells, with minor contributions from T and N cells. In conclusion, these results revealed the distributed nature of leech reflexive behavior at the level of muscle activation and motoneuron recruitment, showing that complex motor responses result from the linear sum of a small number of basic patterns of deformation.

The final step in investigating distributed motor behavior in the leech was to characterize the reproducibility of local bending and that of neural firing sustaining it. I analyzed variability at different levels of processing: mechanosensory neurons, motoneurons, muscle activation and behavior. I found that spike trains in mechanosensory neurons were very reproducible, unlike those in motoneurons. However, the motor response was much more reproducible than the firing of individual motoneurons sustaining it. I showed that this reliability of the behavior is obtained by two distinct biophysical mechanisms: temporal and ensemble averaging. The former is guaranteed by the low pass filtering properties of the leech muscles that contract very slowly and therefore are poorly sensitive to the jitter of motoneuron spikes. The latter is provided by the coactivation of a

population of motoneurons, firing in a statistically independent way. This statistical independence reduces the variability of the population firing. These results have a general significance, because they show that reproducible spike trains are not required to sustain reproducible behaviors and illustrate how the nervous system can cope with unreliable components to produce reliable action.

1 Introduction and background

A major aim of Systems Neuroscience is to understand how the nervous system processes sensory information and translates it into specific actions. This challenge requires the understanding of the neural code, i.e. identifying the relevant features of the neural activity that are reproducible from trial to trial during the execution of a repeated behavior (Bialek and Rieke, 1992; Mainen and Sejnowski, 1995; Gerstner et al., 1997; Shadlen and Newsome, 1998; Stevens and Zador, 1998; Lestienne, 2001). An adequate experimental analysis of this issue requires both quantitative observation of the behavior and the simultaneous measurement of a large fraction of its underlying neural activity. These measurements cannot be obtained in mammalian nervous systems, where it is possible to monitor the electrical activity of only a minimal fraction of neurons involved in any behavior. Such an endeavor can only be obtained in simpler nervous system of invertebrates, such as the *Aplysia* (Castellucci and Kandel, 1974; Tsau et al., 1994; Frost and Kandel, 1995), the lobster (Morris and Hooper, 1997; Morris and Hooper, 1998; Hoover et al., 2002), the cockroach (Camhi, 1988) and the leech (Nicholls and Baylor, 1968; Stuart, 1970; Stent et al., 1978; Kristan, 1982; Wittenberg and Kristan, 1992a; Arisi et al., 2001). These nervous systems are "solvable " in the sense that it is possible to quantify the behavior and at the same time to record the electrical activity of a significant fraction of neurons involved in the behavior. Since neurons, synapses, sensory receptors in mammalian and invertebrate preparations are rather similar, the understanding of information and parallel processing in these simple nervous systems provides a solid basis for unraveling how the brain of higher animals works.

In my Ph.D. project, I have used a combination of intracellular and extracellular multielectrode recordings, videomicroscopy and computer vision methods to investigate neural coding of sensory-motor responses in the leech *Hirudo Medicinalis*. Following the

direction of the information flow, I analyzed the reproducibility of *local bending*, a motor response caused by mechanical stimulation of the leech skin (Kristan, 1982; Lockery and Kristan, 1990a; Lewis and Kristan, 1998b), at different levels of processing: mechanosensory neurons, motoneurons, muscle activation and behavior (Chapter 5). I previously characterized local bending from the behavioral point of view, by quantitatively analyzing the pattern of skin deformation induced by mechanical stimulation of the skin and by activation of single and multiple motoneurons and mechanosensory neurons (Chapter 4). This quantitative analysis of behavior was based on the computation of the optical flow, a method derived from computer vision, whose utility in neurobiology I have demonstrated in the course of the present study (Chapter 3).

In this introductory chapter, I provide the rationale and the background of my thesis, by reviewing the main contributions to the topics I addressed during my Ph.D. project. Some basic information about anatomy and neurobiology of the medicinal leech is summarized in section 1.1. In section 1.2, a quick overview of typical motor behaviors and underlying neural circuits of the leech is provided together with a detailed description of the neural coding of the local bending. In section 1.3, the issue of variability of neural firing in the nervous system is reviewed. The last section of this chapter describes the aim of my Ph.D. thesis.

1.1 The central nervous system of the leech

In the last 35 years, several fundamental issues of neuroscience have been addressed in the leech central nervous system, in the last 35 years: action potential generation and conduction block (Yau, 1976a; Yau, 1976b; Gu, 1991; Mar and Drapeau, 1996; Melinek and Muller, 1996); neuronal basis of behavior, including the study of modulation, integration and coordination in sensory-motor responses (Lockery and Kristan, 1990a; Lockery and Kristan, 1990b; Wittenberg and Kristan, 1992a; Wittenberg and Kristan,

1992b; Kristan et al., 1995; Lewis and Kristan, 1998a; Lewis and Kristan, 1998b); oscillatory circuits (Pearce and Friesen, 1985b; Calabrese, 1995; Calabrese et al., 1995; Brodfuehrer et al., 1995b); sensory cells and signal transduction (Blackshaw, 1981; Blackshaw et al., 1982; Peterson, 1983; Peterson, 1984; Blackshaw, 1993); neural basis of learning (Boulis and Sahley, 1988; Sahley et al., 1994a; Sahley et al., 1994b); development, regeneration and repair of the nervous system (Jellies et al., 1995; Jellies and Johansen, 1995); neural network models of sensory-motor responses (Lockery and Sejnowski, 1992; Wittenberg and Kristan, 1992b; Lockery and Sejnowski, 1993; Lewis and Kristan, 1998a). The reason why these topics have been investigated in the leech CNS are both historical and related to the advantages offered by the system itself. In fact, this preparation has a simple structure, with the possibility to investigate the role of identified neurons in specific behaviors, easily follow the flow of information from the input (sensory neurons) to output (motoneurons) stages of the nervous system and to monitor the phases of its development and repair. More in detail, the leech CNS presents the following experimental advantages, compared to different animals preparations: high similarity between segmental nervous ganglia; a small number of cells in each ganglion of the nervous chain; easy parallel extracellular recordings from motoneurons and mechanosensory neurons; high accessibility of neurons to intracellular recording; long duration of experimental semi-intact preparations; a limited repertoire of stereotyped motor behaviors.

1.1.1 Anatomy of the leech and structure of its central nervous system

Leeches are segmented worms belonging to the class Hirudinea, which includes about 650 species and it is related to the class of the earthworms (Oligochaeta). The species *Hirudo medicinalis*, also called European medicinal leech, on which all the experiments explained in the present thesis have been performed and which is the most studied leech species in neurobiology, will be described here.

The leech is a segmented animal: its body is composed of a chain of highly stereotyped units, the segments, which are linked and coordinated to one another. The adult leech *Hirudo medicinalis* consists of 4 partially fused segments in the head region, 21 segments along the body and 7 modified segments in the posterior region, forming the tail (Muller et al., 1981); each segment consists of exactly 5 annuli, except for the head and tail regions (see **Fig. 1.1**).

The structure of the CNS reflects this segmentation. As shown in **Fig. 1.1A**, the leech CNS consists of a chain of segmental ganglia, linked to one another by bundles of axons (the connectives). The 21 segmental ganglia (G1-G21) are numbered sequentially from the anterior to the posterior region and are almost identical, except for G5 and G6, which innervate the sexual organs. The first 4 ganglia in the head region (H1-H4) are fused and modified to form the head brain, while the last 7 ganglia (T1-T7) are fused in the specialized tail brain.

Each of the segmental ganglia innervates a well defined segment of the body wall by two pairs of nerves (roots) arising symmetrically from the left and right sides (**Fig. 1.1B**). The four roots are defined as anterior and posterior, left and right. The two posterior roots bifurcate near the ganglion, each one originating two branches called posterior-posterior nerves (PP) and dorsal posterior nerve (DP). Through these nerves the ganglion innervates the whole segment. The anterior and PP nerves innervate the territory corresponding to the lateral and ventral part of the animal, while the DP nerves innervate the dorsal part of the animal. The leech performs its whole spectrum of behaviors, using four types of muscles (**Fig. 1.1B**). From the inner to the outer part of the body walls, three layers of muscle fibers are located: longitudinal, oblique, and circular. These muscles form the major portion of the body wall and are distributed evenly around the perimeter of the body. The longitudinal muscles, the thickest and deepest layer, shorten the leech in the longitudinal direction when contracting; the oblique muscles, an outer thin layer, twist the

body; the circular muscles lie just under the skin and are able to elongate the animal. Another class of muscles (dorso-ventral or flatteners) connects internally the dorsal and ventral sides of the animal and is responsible for the flattening of the body, for example during swimming. A further kind of muscles, the annulus erectors (not shown in **Fig. 1.1B**), are located immediately under the skin and are responsible for erecting annuli in ridges.

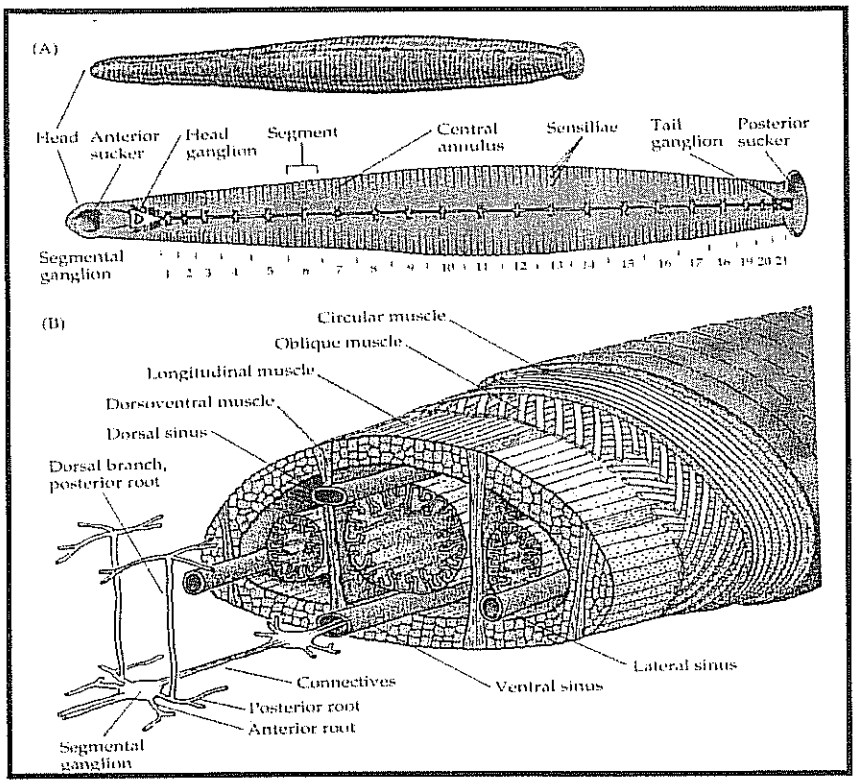

Figure 1.1 The leech central nervous system. (A): Schematic diagram of the leech showing the segmentation and the two specialized regions of anterior and posterior suckers. The CNS consists of a ventral nerve cord composed of a chain of 21 segmental ganglia and two more specialized head and tail ganglia, linked to one another by bundles of axons (connectives). Segments are indicated, composed of five annuli each. (B): Cross-section of the leech showing its anatomy. The body wall is made-up of three layers of muscles (circular, oblique and longitudinal), dorso-ventral muscle fibers run from the dorsal to the ventral side of the animal. Annulus erector muscles (not shown here), are located immediately under the skin. The nerve cord lies in the ventral part of the body and it is surrounded by the ventral blood sinus. Ganglia innervate the body wall through the anterior and posterior roots. The posterior root bifurcates near the ganglion and the dorsal branch crosses ventro-dorsally the body to innervate the dorsal region. The other roots innervate lateral and ventral regions. *(From: Muller et al., 1981)*

1.1.2 The segmental ganglion

The leech segmental ganglion contains the cell bodies of about 400 neurons (Macagno, 1981). Its aspect and structure are conserved from segment to segment and from animal to animal; indeed the same neurons are recurrent in each ganglion for their positions, dimensions and functions. All neurons in the leech ganglion are monopolar; the cell bodies are contained in six separated regions (packets), each enveloped by a glial cell, while their innervations take place in the central neuropil, a specialized region in which synapses are arranged, surrounded by two giant glial cells (Muller et al., 1981); two other glial cells form the nuclei of the connective nerves.

The neurons in the leech CNS can be divided into three categories on the basis of their function: interneurons, sensory neurons and motoneurons. The category of interneurons broadly contains all neurons whose entire arborization does not exit from the CNS, but often exits the ganglion through the connectives: they are involved in a variety of functions such as heartbeat, motor control, reproduction, learning (Brodfuehrer and Friesen, 1986; Lockery and Kristan, 1990a; Wittenberg and Kristan, 1992b; Sahley et al., 1994b; Baader and Kristan, 1995; Shaw and Kristan, 1995; Baader, 1997; Shaw and Kristan, 1999). Sensory cells are neurons that directly translate a physical input coming from the environment into membrane potentials, or more generally are specialized in transforming a physical quantity like pressure, heat, light into a change of their electrical properties (Nicholls and Baylor, 1968; Blackshaw, 1981; Blackshaw et al., 1982; Peterson, 1983; Peterson, 1984; Blackshaw, 1993). Motoneurons are responsible for the excitation or inhibition of muscles (Stuart, 1970; Nicholls and Purves, 1970; Ort et al., 1974; Stent et al., 1978; Mason and Kristan, 1982; Norris and Calabrese, 1987; Gu et al., 1991). Motoneurons and sensory neurons project outside the ganglion to the periphery through the roots; sensory neurons also project in the connectives. The neuron cell bodies in the ganglion are located in two layers, the dorsal and the ventral one. The cell bodies of all

mechanosensory neurons lie in the ventral side, while those of motoneurons mainly lie in the dorsal one, with few exceptions.

1.1.3 Properties of mechanosensory neurons

In the CNS there are sensory neurons responsible for three different mechanosensory modalities (**Fig. 1.2**) (Nicholls and Baylor, 1968; Yau, 1976a; Yau, 1976b; Blackshaw, 1981; Blackshaw et al., 1982; Blackshaw, 1993): T (touch) cells are three for each hemiganglion and respond to a light mechanical stimulus applied to the skin; P (pressure) cells are two for each hemiganglion and respond to stronger stimuli; N (noxious) cells are two for each hemiganglion and respond to a damaging stimulation of the skin, with a threshold more than three times higher than the P cells (Nicholls and Baylor, 1968; Blackshaw et al., 1982). Recent studies have demonstrated that N cells exhibit also functional properties similar to those of polymodal nociceptive neurons in mammals (Pastor et al., 1996), i.e. they are not simple mechanosensitive cells but respond to different

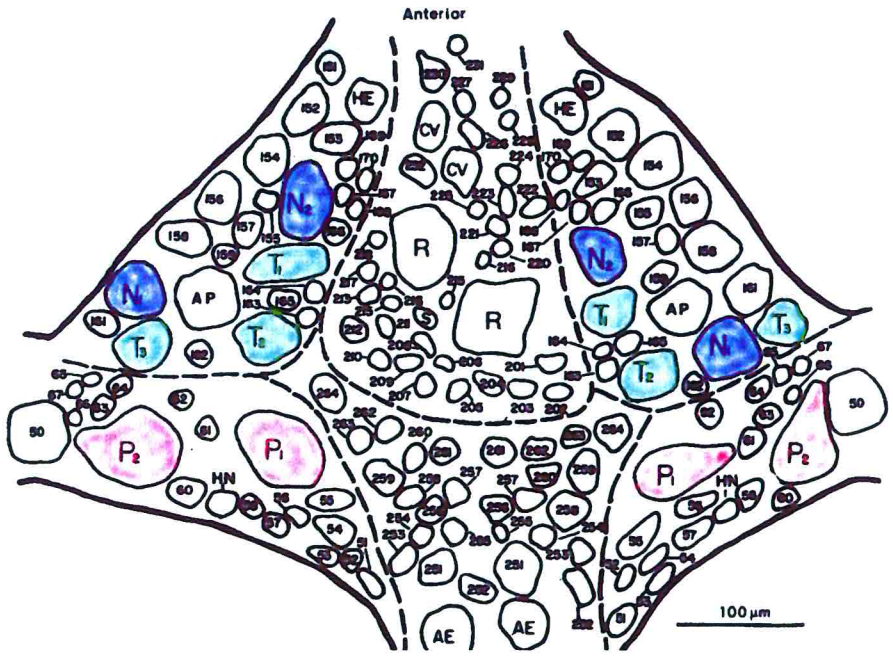

Figure 1.2 Map of leech ganglion from the ventral aspect, showing the recurrent positions of the different kinds of mechanosensory cells. In green are indicated the six Touch (T) cells, in red the four Pressure (P) cells and in blue the four Nociceptive (N) cells. *(From: Muller et al., 1981)*

sensory modalities of noxious stimulus like temperature rise and irritant chemical substances.

The mechanosensory cells in each ganglion innervate a well defined territory of the skin in the corresponding segment (Nicholls and Baylor, 1968; Blackshaw, 1981; Blackshaw et al., 1982), for example the three T cells respond respectively to the stimulation of the ventral (T_v), lateral (T_l) and dorsal (T_d) region of the segment. Similarly, P cells respond one to ventral (P_v) and the other to dorsal (P_d) pressure stimuli. For the two ipsilateral N cells (N_m , N_l) the receptive fields in the same ganglion are approximately coincident and span the entire hemisegment from dorsal to ventral midline.

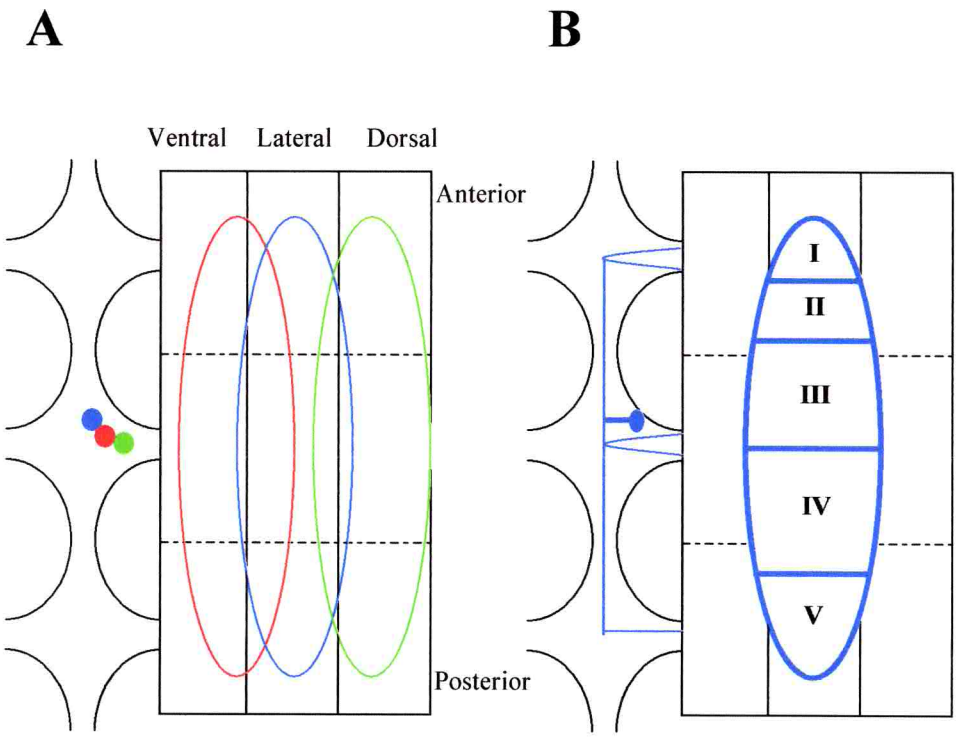

Figure 1.3 Organization of the receptive fields. (**A**): the boundaries of the receptive fields of three T cells in the same ganglion overlap. The cells are drawn in the same color as their receptive fields. T_v is represented in red, T_l in blue, T_d in green. (**B**): adjacent subfields (I II III IV V) of a T_l cell, innervated by separate branches, do not overlap.

Mechanosensory neurons are characterized by a main process arising from the cell body that gives rise to several branches projecting through the ipsilateral roots and the connectives to innervate the roots of adjacent ganglia. The receptive fields span 12-13 annuli over the central and the two adjacent segments; they appear to be composed of several non overlapping sub-fields (**Fig. 1.3**) innervated by separate branches of the same cell (Nicholls and Baylor, 1968; Yau, 1976a; Yau, 1976b). By comparing the extension of receptive fields of cells responsible for the same sensory modality in the central segment or in the two adjacent ones, a considerable overlapping between receptive fields has been observed, as shown in Fig. 1.3A (Nicholls and Baylor, 1968).

1.1.4 Properties of motoneurons

In each hemiganglion there are 21 excitatory and 7 inhibitory identified motoneurons (Nicholls and Baylor, 1968; Stuart, 1970; Ort et al., 1974; Stent et al., 1978; Mason and Kristan, 1982; Norris and Calabrese, 1987; Baader, 1997). When the ganglion is observed in transmitted light, 25 are visible on the dorsal side and 3 are visible on the ventral side (**Fig. 1.4**). All motoneurons are in pairs, one lies in the left hemiganglion and the other in the right hemiganglion, with a corresponding location.

With the exception of the Annulus Erector (AE), which erects the skin at the center of annuli and the heart excitor (HE), which supplies the lateral heart tubes, they are all responsible for the leech locomotion and movement. They can be divided into four groups, according to the muscle fibers they innervate: longitudinal, circular, oblique, dorsoventral. With the only exception of cell 4, a ventral longitudinal excitor, and cell 117, a dorsoventral excitor, all motoneurons exit the ganglion via the contralateral roots to innervate the corresponding body wall (Ort et al., 1974). Their fields of innervation extend longitudinally into adjacent body segments (Blackshaw, 1981) and frequently overlap with those of neurons supplying the same muscles group. The motoneurons probably innervate

muscle fibers by many terminals along their length, as it happens in crustacean (Stuart, 1970).

Excitatory motoneurons induce a smooth contraction of muscle fibers when increasing the firing frequency above a certain threshold level and over a functional range. Each motoneuron in the ganglion shows a distinctive kinetics of the contraction. Rising the firing frequency over the characteristic active range of the neuron, increases the contraction rate and its peak amplitude (Mason and Kristan, 1982). Since leech muscles (Mason and Kristan, 1982; Norris and Calabrese, 1987; Arisi et al., 2001), as those of other invertebrates and lower vertebrates (Morris and Hooper, 1997; Morris and Hooper, 1998), contract very slowly and integrate the incoming spike trains over a very long time window (several hundred milliseconds), muscle contraction normally reaches its stationary phase, which is purely spike frequency dependent, only after many seconds of sustained motoneuron firing (Mason and Kristan, 1982; Morris and Hooper, 1997). Based on this observation, Morris and Hooper (1997) suggested that contraction of leech muscles during performance of natural behaviors - which require modulation of motoneuron firing on a time scale of tens-hundreds ms - primarily depends on the number of spikes fired by the activated motoneurons rather than on their firing frequency.

Inhibitory motoneurons counteract the effect of excitors. Since inhibitor activity does not reduce basal tension, it is necessary for the excitors to be active in order for the inhibitors to exert a peripheral effect. The ability of inhibitors to oppose strongly the effects of excitors suggest they contact most of the fibers contacted by the excitors (Mason and Kristan, 1982). In addition to their direct action on body wall, they also inhibit centrally the excitatory motoneurons, which innervate the same muscle (Granzow et al., 1985; Granzow and Kristan, 1986). Unlike the contraction, the relaxation of muscles is much slower, but the leech provides a modulation system.

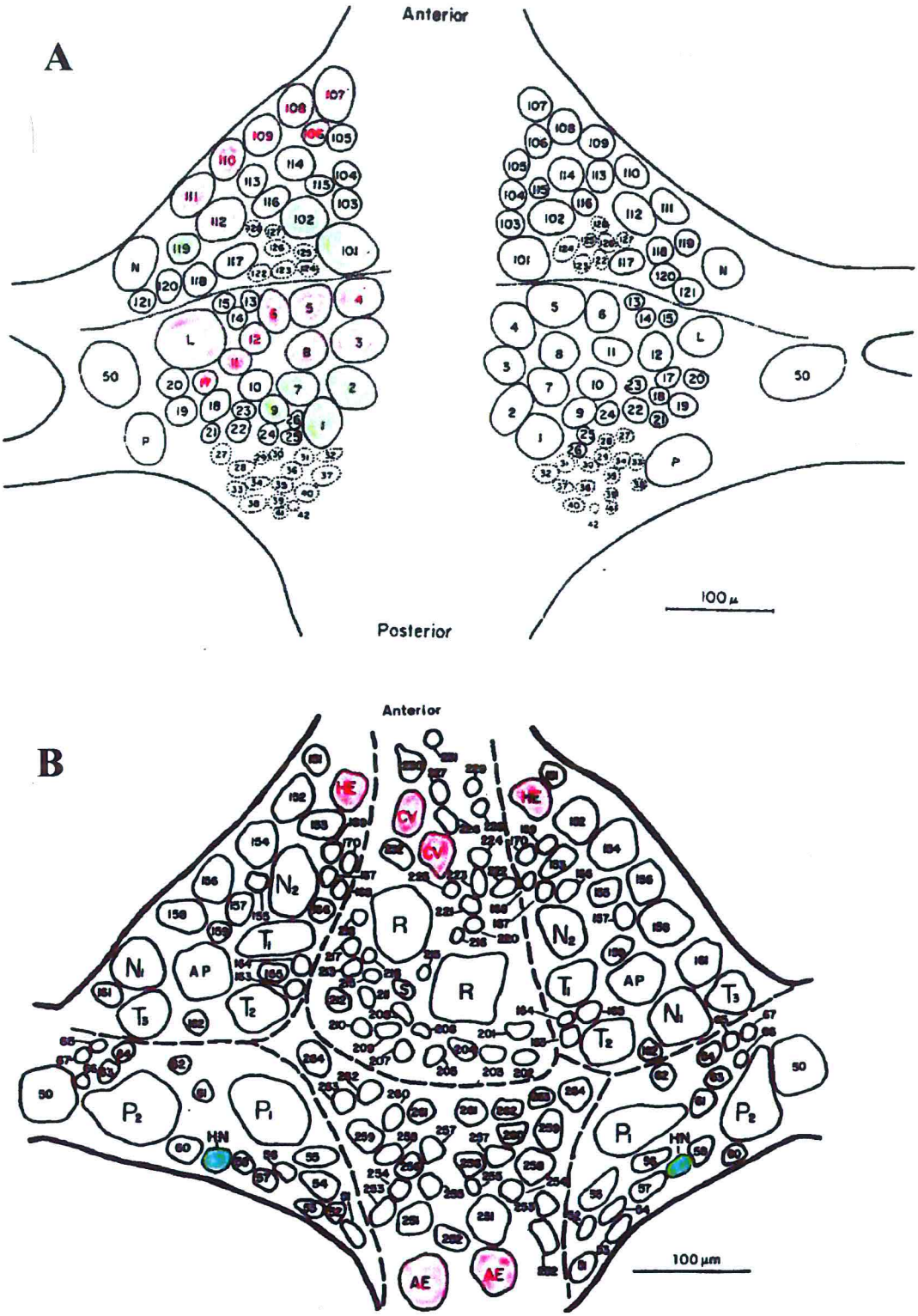

Figure 1.4 Recurrent positions of the inhibitory (green) and excitatory (red) motoneurons in the leech ganglion. (**A**): map of the ganglion from the dorsal aspect; only left side motoneurons are colored. (**B**): map of the ganglion from the ventral aspect; all visible ventral motoneurons are colored. *(From: Muller et al., 1981)*

Stimulation of Retzius cells evokes slow reduction of tone in the longitudinal muscle and increases the rate of the slow phase of relaxation following a contraction; these effects have a long latency and duration and are mimicked by direct application of serotonin (Mason and Kristan, 1982).

The soma and the proximal axonal region of leech motoneurons are unexcitable; the action potentials arise at a site distant from the soma, near the primary bifurcation of the axon (Gu et al., 1991). For this reason, very small action potentials (few mV in amplitude), which passively propagate from the spike generation site to the soma, are visible in the intracellular recordings performed from the motoneuron cell bodies (Stuart, 1970). There is consistent evidence that the leech longitudinal nerve muscle junction is cholinergic (Gardner and Walker, 1982) and more generally that excitatory motoneurons synthesize, accumulate and release acetylcholine (Norris and Calabrese, 1987). The leech inhibitory motoneurons are thought to be GABAergic (Blackshaw and Nicholls, 1995), since the longitudinal motoneurons take up and synthesise GABA from the precursor glutamate and further, central and peripheral inhibitory synaptic effects are mimicked by GABA.

1.2 Leech motor behaviors and underlying circuits

1.2.1 Overview

The leech exhibits a variety of motor behaviors. Some of them, such as local bending, local shortening and whole-body shortening, are escape reflexes, whose aim is to withdraw the animal from potential danger. More complex motor behaviors, such as crawling and swimming, are locomotory movements, used by the leech to explore its environment, to direct itself towards a source of food or to escape from danger. Both escape and locomotory behaviors are elicited (and regulated) by interaction with the environment, mediated by central mechanosensory neurons and/or mechanoreceptors, chemoreceptors and photoreceptors of the peripheral nervous system (Kristan and Stent, 1976; Brodfuehrer

and Friesen, 1986; Lockery and Kristan, 1990a; Wittenberg and Kristan, 1992a; Carlton and McVean, 1993; Baader and Kristan, 1995; Shaw and Kristan, 1995; Brodfuehrer et al., 1995a; Baader, 1997; Lewis and Kristan, 1998a; Lewis and Kristan, 1998b).

The way in which the leech responds to external stimuli depends upon their intensity and location. The same sensorial stimulus, mechanical stimulation of the skin detected by central mechanosensory neurons, is able to evoke a set of different behaviors. A moderate mechanical stimulus produces local bending of the stimulated segment (Kristan, 1982; Lockery and Kristan, 1990a). A stronger stimulus elicits stronger bending movement at the site of stimulation and shortening in nearby segments (Wittenberg and Kristan, 1992a), if delivered in the midbody region. A strong mechanical stimulation elicits whole-body shortening if delivered to the rostral region (Shaw and Kristan, 1995), whole-body shortening or swimming if delivered in the posterior region (Shaw and Kristan, 1997).

As previously mentioned, one of the main advantages offered by the leech is the possibility to perform experiments on semi-intact preparations, in which quantitative analysis of leech behavior and measurement of its underlying neural activity can be simultaneously obtained. Using appropriate semi-intact preparations, the neural basis of all the behaviors previously described has been extensively investigated. In the following, I will briefly review the main achievements in understanding the neural circuits responsible for the various behaviors of the leech. The neural network mediating local bending will be described in more detail, since neural coding of local bending is the subject of my Ph.D. thesis.

Swimming

Historically, the neural circuit generating the swimming has been one of the first to be investigated in the leech (Stent et al., 1978). The swimming rhythm consists of a periodical continuous antero-posterior undulation of the whole body, produced by an antiphasic

contraction of dorsal and ventral longitudinal muscles. The whole swimming circuit can be considered as a chain of coupled oscillators (Pearce and Friesen, 1985a; Pearce and Friesen, 1985b), one per ganglion. The local swimming network in each ganglion is a Central Pattern Generator (CPG), composed of a set of interneurons and motoneurons, mostly connected by inhibitory synapses (Brodfuehrer et al., 1995a). The mechanism that generates the swimming oscillations is based on reciprocal inhibition between several pairs of oscillating interneurons (Friesen et al., 1976; Stent et al., 1978). The interganglionic connections are essentially replicas of the intraganglionic ones, most of them being also inhibitory. A leading role is played by the head brain, which contains trigger interneurons (Brodfuehrer and Friesen, 1986) that are at the highest level in the hierarchy of the swimming circuit and project caudally along the nerve cord in order to elicit or inhibit the swimming rhythm. The mechanical feedback, provided by activation of stretch receptors (peripheral mechanosensory neurons), has recently been also shown to play a primary role in intersegmental coordination during swimming (Yu et al., 1999; Cang and Friesen, 2000; Cang et al., 2001; Cang and Friesen, 2002).

Crawling

Neural basis of crawling, the locomotory behavior of the leech in the terrestrial environment, has started to be investigated only recently (Baader and Kristan, 1995). A crawling locomotion cycle consists of an elongation phase and a contraction phase, sustained respectively by contraction of circular and longitudinal muscles. Front and rear suckers are alternatively released and attached during the cycle (Cacciatore et al., 2000). The crawling circuit, which is rather complex, is a Central Pattern Generator (CPG), as the animal is able to produce several successive crawling cycles, and a neural correlate of crawling occurs in the isolated nerve cord (Baader, 1997; Eisenhart et al., 2000; Cacciatore et al., 2000). The crawling CPG differs from the swimming one in that precise intersegmental coordination is not essential and much more flexibility is needed to make

variable exploratory movements of the environment before deciding where to attach and continuing the cycle (Cacciatore et al., 2000). Therefore, a crucial role is played by sensory feedback to modulate the CPG activity. The CPG is certainly located partly in the head and tail brains and partly in the mid-body ganglia (Cacciatore et al., 2000). In mid-body ganglia several active interneurons during crawling has been identified, in particular some multifunctional cells, already known to be part of the swim-generating circuit (Kristan et al., 1988).

Whole-body shortening

Whole-body shortening is a withdrawal response from a strong mechanical or electrical stimulus delivered to the anterior part of the animal. This escape reflex is produced by the contraction of longitudinal muscles in the whole leech body. It is mediated by the activation of multiple P and T sensory neurons (Shaw and Kristan, 1995) and is sustained by the coactivation of probably all excitatory motoneurons of longitudinal muscles in the leech CNS. Fast interneuronal pathways together with the S cell network are responsible for coordinating the shortening of the body segments (Shaw and Kristan, 1995; Shaw and Kristan, 1997; Shaw and Kristan, 1999).

1.2.2 Local Bending

When the skin of the leech is touched, the animal bends its body to withdraw from the stimulus. This simple response, referred to as local bending, is initiated by a moderate, localized mechanical stimulation of the skin and is classically described as contraction of longitudinal muscles on the stimulated side of the segment and relaxation on the opposite side, leading the segment away from the stimulus in the opposite direction (Kristan, 1982; Lockery and Kristan, 1990a). Depending on its location, the mechanical stimulus can elicit dorsal, ventral or lateral bending (**Fig. 1.5**). In the following, I will briefly review the role

of mechanosensory neurons, motoneurons and interneurons in mediating the bending reflex.

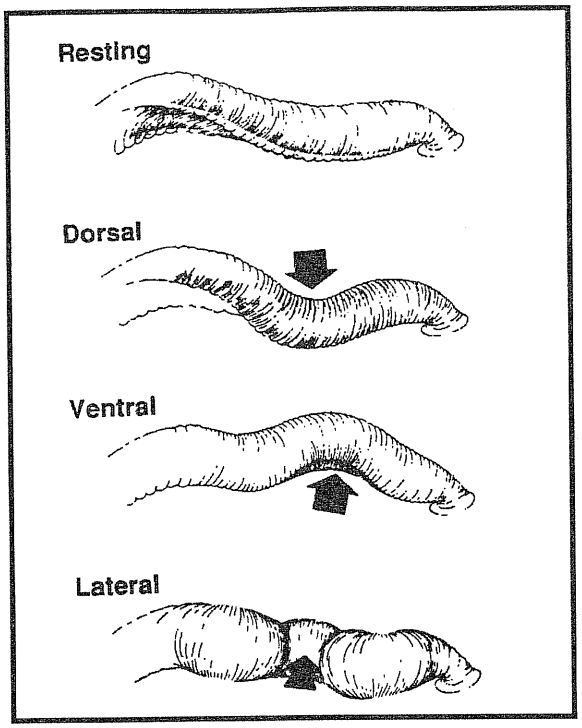

Figure 1.5 Local bending reflex in the leech. The posterior half of the animal is shown in the resting state and following mechanical stimulation of the dorsal, ventral and lateral body wall (arrows). *(From Lockery & Kristan, 1990)*

Mechanosensory neurons

The role of mechanosensory neurons in encoding mechanical stimuli and initiating local bending has been extensively investigated (Kristan, 1982; Lockery and Kristan, 1990a; Lewis and Kristan, 1998a; Lewis and Kristan, 1998b; Pinato and Torre, 2000). These studies have shown four major properties: i) moderate mechanical stimuli are precisely encoded by a population of three touch (T) and two pressure (P) cells in each side of the ganglion (Lewis and Kristan, 1998a; Lewis and Kristan, 1998b; Pinato and Torre, 2000); ii) the firing of these neurons is highly reproducible (Pinato and Torre, 2000); iii) local bending is almost completely mediated by P cell activation (Kristan, 1982; Lockery and Kristan, 1990a); a population vector formed by the spike counts of the active P cells

precisely accounts for the bending direction (Kristan et al., 1995; Lewis and Kristan, 1998a; Lewis and Kristan, 1998b).

Motoneurons

The pattern of activation of motoneurons during local bending has been precisely characterized by simultaneous intracellular recordings from pairs of P cells and individual motoneurons representative of the eight classes of longitudinal motoneurons involved in the reflex: dorsal excitors (DE), ventral excitors (VE), dorsal inhibitors (DI) and ventral inhibitors (VI), ipsilateral and controlateral (according to the innervation field of the body walls) to the stimulated P cells (Lockery and Kristan, 1990a). As shown in **Fig. 1.6**, paired dorsal, ventral and lateral P cell stimulation produced a pattern of motoneuron activation consistent with the behaviors shown in **Fig. 1.5**: the longitudinal muscles would be excited on the stimulated side and inhibited on the opposite side. Stimulation of individual P cells lead to similar conclusions (Lockery and Kristan, 1990a).

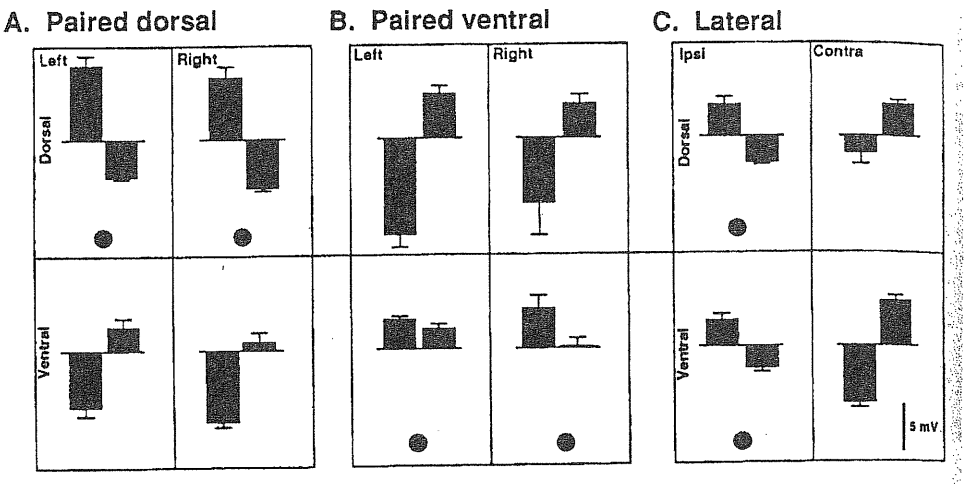

Figure 1.6 Response of representative DE's and VE's innervating four different quadrant of the leech body wall to 3 patterns of paired P cell stimulation. A, Average peak synaptic potential in millivolts following simultaneous stimulation of the two PDs. B, Stimulation of two PVs. C, Stimulation of PD and the ipsilateral PV. *(From Lockery & Kristan, 1990a)*

Interneurons

Seventeen interneurons involved in the dorsal local bending have been found: eight bilateral pairs and one unpaired interneurons (Lockery and Kristan, 1990b). The most intriguing property of their connectivity pattern was that all these interneurons received substantial synaptic input not only from the ipsilateral dorsal P cell, but also from the ipsilateral ventral P cell and most of them received substantial input from all four P cells. This is consistent with the idea of a distributed architecture of the neural circuit underlying local bending. Interneurons are not dedicated to detect input from a specific P cell or a specific pair of P cells. They can receive inputs from 1-4 P cells and detection of particular stimuli, with consequent activation of appropriate motoneurons, would be achieved by the set of interneurons as a whole (Lockery and Kristan, 1990b; Kristan et al., 1995).

Further studies revealed that a subset of local bending interneurons is also part of the circuit producing local shortening (Wittenberg and Kristan, 1992b; Kristan et al., 1995). This reflex, paired to local bending, is evoked by a moderate mechanical stimulation of the skin and produces a rapid shortening of the adjacent segments to the stimulated one, where local bending takes place (Wittenberg and Kristan, 1992a; Wittenberg and Kristan, 1992b).

1.3 Variability and reliability of the nervous system

A major goal of System Neuroscience is to understand the neural code, i.e. to identify the relevant features of neural activity that nervous system uses to encode and process sensory inputs and to translate them into actions or a specific behavior. As widely recognized (Bialek and Rieke, 1992; Mainen and Sejnowski, 1995; Gerstner et al., 1997; Shadlen and Newsome, 1998; Stevens and Zador, 1998), the issue of reproducibility is essential for understanding the core of the nervous code. In other words, it is essential to identify which

features of the neural activity, underlying a given perception or computation or behavior, are reproducible across repeated trials of the same neural process. These features could be the temporal pattern of spikes fired by a given neuron, the timing of specific action potentials, the instantaneous firing rate of a neuron or the average firing rate of a population of neurons (Shadlen and Newsome, 1994; Shadlen and Newsome, 1995).

An intrinsic property of the nervous system seems to be that neuronal firing patterns are affected by high variability. Several experiments performed on cortical neurons in vivo (Softky and Koch, 1993; Holt et al., 1996; Reich et al., 1997; Gur et al., 1997; Shadlen and Newsome, 1998; Stevens and Zador, 1998; McAdams and Maunsell, 1999; Kara et al., 2000) and on invertebrate nervous systems (Bialek and Rieke, 1992; Wu et al., 1994; Warzecha and Egelhaaf, 1999; Warzecha et al., 2000) revealed large variability in discharge patterns of action potentials fired by recorded neurons. The more widespread interpretation of such variability is that it results from stochastic forces (Shadlen and Newsome, 1994; Mainen and Sejnowski, 1995; Shadlen and Newsome, 1995; Shadlen and Newsome, 1998). In this view the irregular firing of a neuron is due to noise and does not reflect some specific temporal pattern of synaptic inputs from the neuron's afferents. The neuron carries information in its firing rate, computed on a time window varying from tens to hundred ms, depending on the computational task in which it is involved. An instantaneous estimate of the average firing rate can only emerge from the pooled responses of many individual coactivated neurons (Shadlen and Newsome, 1994; Shadlen and Newsome, 1995). An alternative interpretation is that irregularity in neural firing can result from precise coincidences of presynaptic events. In this view, the temporal pattern of spikes can convey information about the temporal pattern of activation of presynaptic afferents (Softky and Koch, 1993; Softky, 1995). On the other hand, the capability of sensory systems to respond reproducibly to time-varying external stimuli and to encode their dynamics in precisely timed spike trains has been observed in both

mammals and lower animals (Bialek et al., 1991; Bialek and Rieke, 1992; de Ruyter van Steveninck RR et al., 1997; Heil and Irvine, 1997; Heil, 1997; Middlebrooks et al., 1998; Kara et al., 2000; Reinagel and Reid, 2000; Furukawa and Middlebrooks, 2002; Reinagel and Reid, 2002).

The critical problem of interpreting irregular firing in the nervous system, i.e. understanding if neurons convey a noisy rate code or a precise temporal code, is strictly related to understanding the origin of such irregularity. Possible sources of unreliability in spike generation have been investigated experimentally and theoretically by many authors. Allen and Stevens (1994), in their analysis of unreliability in the transmission at individual synaptic contacts on CA1 hippocampal pyramidal neurons, took into account many possible sources of variability: threshold fluctuations, conduction failures, temperature dependence and stochastic release of neurotransmitter. Their study lead to the conclusion that probabilistic release mechanisms at low capacity synapses are mainly responsible for the unreliability of synaptic transmission. Other studies provided a direct measure of the probabilities of transmitter release in individual hippocampal synapses (Hessler et al., 1993; Murthy et al., 1997), while the evidence of unreliability at central excitatory synapses has been confirmed by several other investigators (Wahl et al., 1995; Markram and Tsodyks, 1996; Wahl et al., 1997; Hardingham and Larkman, 1998).

Another biophysical mechanism that can account for irregular firing of a neuron is the integration it performs on a large number of excitatory and inhibitory presynaptic inputs. The random walk model of synaptic integration and spike generation, originally proposed by Gerstein and Mandelbrot (1964) and then developed by Shadlen and Newsome (94, 95, 98), yields, when model neurons are fed with appropriate balance of excitation and inhibition, to irregular firing patterns consistent with those found in cortex.

Other studies aimed at investigating the intrinsic noise level of neurons in spike generation. In their renowned work, Mainen & Sejnowsky (95) assessed that intrinsic noise

in cortical neurons is low. They injected rat cortical neurons with a time-varying current mimicking the large and rapid random fluctuations of somatic current due to many independent synaptic inputs and found that the mechanism of transformation of such somatic currents in spike trains is very reliable. This could allow cortical neurons to precisely transform synaptic input into spike sequences, supporting a possible role for spike timing in neural coding. On the other hand, this finding suggests that synaptic transmission, being subject to both release failure and quantal fluctuation, and the integration properties of neurons are mainly responsible for observed variable neuronal firing.

1.4 Aim of the work

1.4.1 Open questions on neural coding of leech reflexive behavior

The finding that the same subset of interneurons (see Section 1.2.2) contributes to mediate local bending in the stimulated segment (Lockery and Kristan, 1990b) and local shortening in a number of segments around the stimulus site (Wittenberg and Kristan, 1992b), strongly supports the idea of a distributed nature of reflexive behaviors in the leech (Kristan et al., 1995). There are two main advantages for nervous systems to use distributed networks in producing motor behaviors (Kristan et al., 1995). The first is efficiency: a population of interneurons coding for different behavioral tasks can produce many more output patterns than the same number of interneurons, each dedicated to a specific behavior. The second advantage is that distributed neural networks allow for graceful degradation of the motor output in the case of death of individual interneurons.

At the level of interneurons, distributed processing of leech motor behaviors has been extensively investigated (see Section 1.2.2). The data reported until now by different authors, all support a partially distributed organization of the leech motor circuits, with some dedicated interneurons and some multifunctional interneurons taking part in different

behaviors. Not only have interneurons involved in both local bending and local shortening been found (Lockery and Kristan, 1990b; Wittenberg and Kristan, 1992b; Kristan et al., 1995), but also, one of these neurons, cell 115, is known to be part of the CPG of the swimming circuit. Moreover, the swimming, crawling and whole-body shortening circuits are partially superimposed, since some interneurons are active during different motor behaviours: cells 204 and 208 during swimming and crawling; S cell during shortening and crawling (Brodfuehrer and Friesen, 1986; Wittenberg and Kristan, 1992b; Brodfuehrer et al., 1995a; Baader, 1997).

At the level of mechanosensory neurons, population coding of local bending, based on the population vector formed by the spike counts of coactivated P cells, has been shown to precisely account for stimulus location and bending direction (Lewis and Kristan, 1998a; Lewis and Kristan, 1998b).

At the level of motoneurons, the distributed organization of the leech motor behaviors is also evident. It has been found that the same excitors and inhibitors of longitudinal muscles attend to all leech behaviors. The pattern of activation of these motoneurons depends on the sustained behavior. They can be rhythmically activated, as in the case of locomotory behaviors (swimming and crawling), or can be transiently activated, as during escape reflexes (bending and shortening). Motoneurons in all body segments can almost simultaneously take part in the process (whole-body shortening) or motoneurons of only a few segments can be involved (local bending and shortening).

Despite this evidence of distributed processing across motoneurons, the pattern of motoneuron activation at the population level and the distributed nature of motor responses have been, so far, poorly investigated. At the muscle level too, the pattern of body-wall deformations induced by muscle activation during the execution of reflexive behaviors has been poorly studied. Recent advances on spinal motor systems suggest that complex motor behaviors in vertebrates can result from a flexible combination of a small number of

behavioral units, each unit corresponding to the control of a group of functionally related muscles (d'Avella and Bizzi, 1998; Tresch et al., 1999; Bizzi et al., 2000; Mussa-Ivaldi and Bizzi, 2000). This means that motoneurons and muscles are not a simple relay of supraspinal motor commands to the periphery but actively attend to the computation underling motor behaviors. A similar quantitative assessment of the interaction between basic behavioral units in the leech is necessary to clarify the relevance of motoneurons and muscles in the processing of motor responses.

The issue of distributed processing underlying motor behavior is strictly related to the issues of variability in neural firing and coding strategies mediating sensory-motor responses. As described in Section 1.3, a number of studies investigated the basis of neural coding in presence of highly variable neuronal discharges and explored possible sources of such variability across nervous systems. The key question is to understand how unreliable firing patterns can be consistent with the capability of nervous systems to process information and perform behavioral tasks in a reproducible and reliable way across different trials of the same sensorial stimulation. At present, I am not aware of studies focusing on the comparison between reproducibility of a specific motor behavior and of the neural activity sustaining it. The nervous system of the leech is a particularly suitable model for such a comparison because it allows both quantitative observation of behavior and the simultaneous measurement of a large fraction of its underlying neuronal activity.

1.4.2 Specific aims of the project

The aim of my Ph.D. project was to study the distributed motor pattern underlying reflexive behavior in the medicinal leech. Specifically, I investigated the computational role of motoneurons and muscles activated during the bending reflex (see Section 1.2.2), addressing the following main questions:

1) Which are the basic patterns of body-wall deformation produced by activation of different classes of the leech muscles?

2) How can these patterns combine to sustain motor reflexes such as local bending?

3) How many motoneurons are coactivated during local bending?

4) How concerted is their firing activity? Are they responses correlated?

5) How reliable is the motoneurons firing (see Section 1.3) compared to the motor behavior?

6) Is local bending mediated by a population code at the level of motoneurons?

Chapter 4 focuses on the first two issues, Chapter 5 on the last four. Chapter 3 explains the method used to quantify the pattern of deformation occurring at the surface of the leech skin during muscle activation: this is the backdrop for the quantitative analysis of behavior on which the results presented in Chapters 4 and 5 are based.

2 Materials and methods

All the experiments described in this thesis were performed in the leech CNS using different kinds of preparations and experimental protocols. In this chapter all the experimental procedures are explained with attention to technical questions and data analysis. The method used to quantify skin deformation and muscle contraction is only mentioned here, since it is part of my Ph.D. project and it will be the main subject of the next chapter.

2.1 Animals and preparations

Specimens of *Hirudo medicinalis* were obtained from a commercial supplier (Ricarimpex, Eysines, France) and kept at 5° C in tap water dechlorinated by aeration for at least 24 hours. The leeches were dissected under a stereomicroscope. Two kinds of preparation were arranged for the experiments: isolated ganglion and semi-intact body-wall preparation.

2.1.1 Isolated ganglion

For analyzing motoneuron firing during local bending, a single midbody ganglion (chosen between the 7th and the 16th) was isolated from the leech CNS and its roots were carefully cleaned and cut in order to draw them into suction pipettes used for extracellular recordings (**Fig. 2.1**). The ganglion was then pinned through the connectives on a Sylgard-coated dish, with the ventral or dorsal side up. Since mechanosensory neurons are visible from the ventral side of the ganglion (see **Fig. 1.2**), ventral side up configuration was used for impaling and stimulating pressure P cells in order to evoke local bending and simultaneously record extracellular spike trains of activated motoneurons. On the other hand, since most motoneurons are contained in the dorsal side of the ganglion (see **Fig. 1.3**), dorsal side up configuration was used for impaling and stimulating motoneurons in

order to obtain a clear signature of the extracellular voltage signals produced by their action potentials.

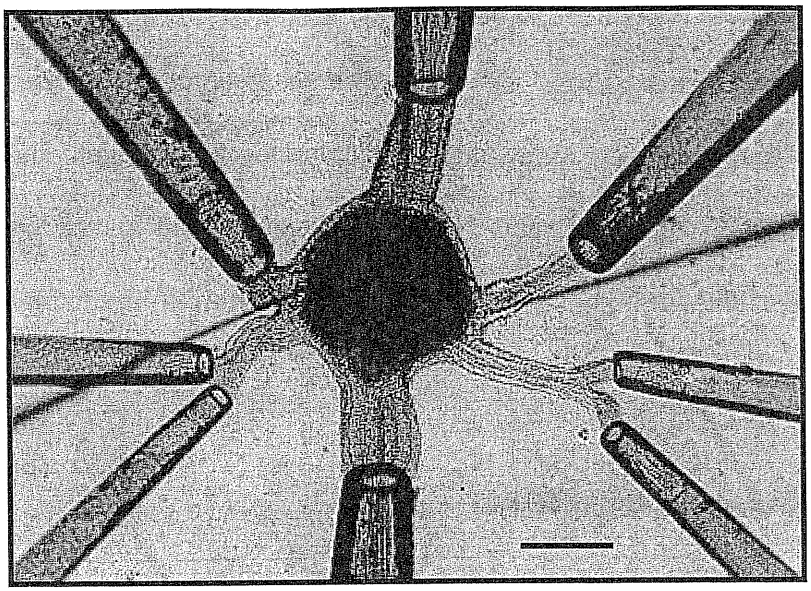

Figure 2.1 Example of isolated ganglion preparation. In the picture, two sharp electrodes for intracellular recordings from neuronal cell bodies and eight suction pipettes for extracellular recordings from nerve roots are clearly visible. Scale bar 250 μm. *(From: Pinato et al., 2000)*

2.1.2 Body-wall preparation

For the analysis of behavior and the assessment of its reproducibility, a body-wall preparation was used. **Fig. 2.2** shows a typical body-wall preparation used to monitor muscle contractions evoked by intracellular stimulation of motoneurons or mechanosensory neurons or by mechanical stimulation of the skin. A hemisection of the leech skin, three segments in length (15 annuli), was isolated from the rest of the body, of which one boundary was formed by the dorsal midline of the animal (top of **Fig. 2.2**). The other boundary (bottom of **Fig. 2.2**) was between the lateral line (longitudinal light gray strip in **Fig. 2.2**) and the ventral midline of the animal. The skin was flattened and fixed with small pins to the bottom of the recording chamber, but allowing the skin to deform during muscle contraction (two of these pins, inserted in the dorsal edge of the body wall, are visible in the top of **Fig. 2.2**). In **Fig. 2.2** the annular margins appear as vertical

crevices (14 annuli are clearly visible); the dorsal skin is dark (top of the figure) while the ventral skin is light gray (bottom of the figure). The dark and light longitudinal strips mark the skin at the lateral margin. The anterior part of the animal is on the left side of the picture. All pictures and drawings of the leech skin in the present thesis have this orientation.

The middle segment, whose central annulus is indicated by the white arrow in **Fig. 2.2**, was kept innervated to its ganglion. The ganglion is not shown in **Fig. 2.2**, but its roots, which innervate the body wall, are clearly visible at the bottom of the figure. A suction pipette recording en passant from the posterior posterior (PP) nerve is also visible. The connective and the roots emerging from the opposite side of the ganglion were pinned so as to allow easy intracellular recordings from the cell bodies of mechanosensory neurons (ventral side up) and motoneurons (dorsal side up) in the ganglion.

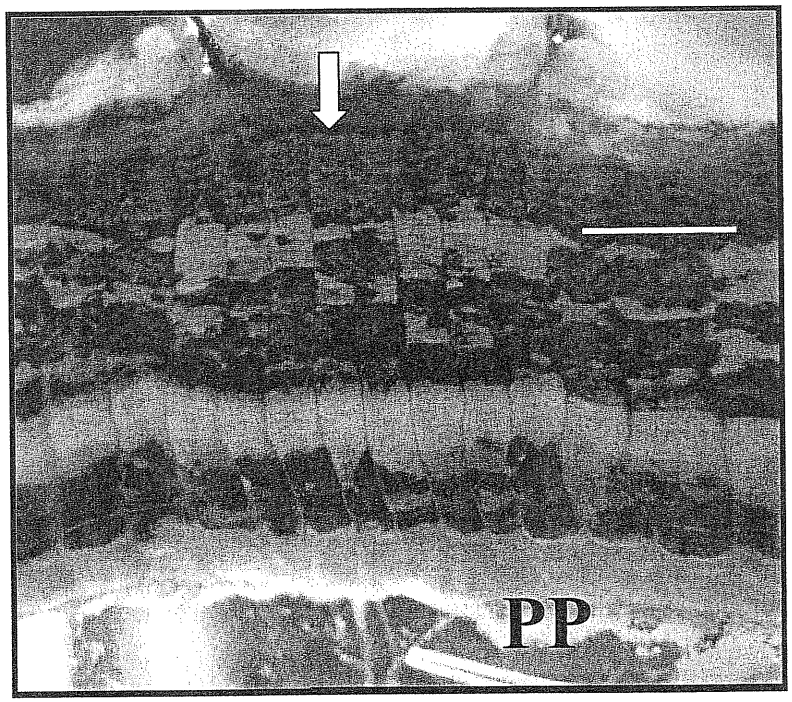

Figure 2.2 Example of body-wall preparation. A hemisection of the leech skin, three segments in length (14 annuli are visible). The longitudinal boundaries are: near to the dorsal midline (top of the panel); between the ventral line (the gray longitudinal strip) and the ventral midline (bottom of the panel). The middle segment (whose central annulus is indicated by the arrow) is innervated by its ganglion (not shown). At the bottom of the panel a pipette suctioned onto the PP nerve emerging from the ganglion is shown.

The portion of body wall innervated by motoneurons extends longitudinally beyond the boundary of the middle segment (central annulus plus two annuli on either side of it). The extent of the territories innervated by the longitudinal motoneurons is slightly more than one segment while the circular motoneurons and the annulus erector innervates muscle fibers over an extent of nine to ten annuli (the central annulus of a segment and four annuli on either side of it) (Stuart, 1970).

2.1.3 More intact preparations

The surgery to obtain the body-wall preparation described above requires careful cleaning of the roots and cutting the skin before the ventral midline. For these reasons, in some control experiments, more intact preparations were used to verify that motor responses observed in the body-wall preparation were not affected by some dissection induced abnormality in muscle and skin innervation. The other preparations used in the present study are briefly described below.

Intact body-wall preparation

In comparison with the body-wall preparation described in Section 2.1.2, the differences were: i) the inferior boundary coincided precisely with the ventral midline of the animal body and ii) the ganglion innervating the central segment was not exposed. This preparation offered two main advantages: i) the skin could be mechanically stimulated near the ventral midline and ii) the roots innervating skin and muscles were perfectly intact because they had not been cleaned and exposed.

Intact leech

In this preparation, the head and the tail of the animal were pinned on a sylgard dish and the body was stretched. Two or three central segments were flattened and secured to the sylgard dish with 4 pins. This portion of body wall and various free segments along the

body were mechanically stimulated to verify the consistency of the motor responses in the intact animal and reduced preparations.

2.1.4 Solutions

All the preparations were kept in a Sylgard-coated dish at room temperature (20-24°C). During dissection and during experiments, the preparations were bathed in a Ringer solution with the following composition in mM: 115 NaCl, 1.8 $CaCl_2$, 4 KCl, 12 glucose, 10 Tris maleate buffered to pH 7.4 with NaOH) (Muller et al., 1981).

2.2 Electrophysiology

2.2.1 Extracellular recordings

Suction pipettes were used to perform extracellular recordings from the nerve roots emerging form the segmental ganglion (see **Fig. 2.1**). The pipettes were obtained by pulling (P-97 puller, Sutter Instruments) thick walled glass capillaries (GC100-10, Clark Electromedical Instruments). After pulling, the capillaries were cut on the tip and shaped with a microforge, in order to match the section diameter of the root we had decided to record from. The pipettes were positioned near roots using micromanipulators (Narishige, Japan).

In the experiments performed on the isolated ganglion, five suction pipettes were used to perform parallel extracellular recordings from the anterior anterior (AA), anterior medial (MA), and posterior posterior (PP) roots and from the two bifurcations (DP:B1 and DP:B2) of the dorsal posterior root (Ort et al., 1974; Stent et al., 1978; Pinato et al., 2000). Spikes recorded from these roots were classified according to dimension and shape using semi-automatic spike sorting techniques (see Section 2.5.1) (Ort et al., 1974; Pinato and Torre, 2000; Pinato et al., 2000) and were identified by impaling each motoneuron with a sharp intracellular microelectrode (see next Section). In this way, it was possible to

characterize the firing activity of a large fraction of all leech motoneurons: the excitatory motoneurons of longitudinal muscles (cells 3, 4, 5, 6, 8, 107, 108 and L), the excitor of flattener muscles (cell 109), the annulus erector (AE), and two inhibitory motoneurons of longitudinal muscles (cells 102 and 119) (Ort et al., 1974; Stent et al., 1978). Since the voltage signals of excitatory motoneurons of circular muscles are unreliably identifiable in the extracellular recordings from the nerve roots, it was possible to monitor the activity of only one circular excitor: cell CiV.

In some experiments performed on the body-wall preparation, the firing rate of motoneurons activated by intracellular stimulation was monitored with en passant suction electrode on the roots innervating the body wall, to obtain, in such a way, extracellular recordings of the action potentials traveling along these fibers. A suction pipette close to the posterior posterior root is visible in the bottom of **Fig. 2.2**.

2.2.2 Intracellular recordings

In both isolated ganglion and body-wall preparation, intracellular recordings from the soma of selected neurons were obtained by impaling those neurons with sharp electrodes. The electrodes were pulled (P-97 puller, Sutter Instruments) using thin walled glass capillaries (TW100F-4, WPI). The input resistance was in the range 20-40 MΩ. Potassium acetate 4.0 M solution was used to fill the electrodes (Muller et al., 1981). The electrode holders, including head stage, were mounted on micromanipulators (Narishige, Japan).

Intracellular stimulation of selected motoneurons was performed in the body-wall preparation, in order to characterize the pattern of skin deformation induced by individual motoneurons. In these experiments, depolarizing current pulses were passed through the electrodes into the cell bodies to evoke a spike discharge at physiological rate (from 10 up to 40 Hz), lasting from some hundred milliseconds to few seconds. Similar spike trains were evoked in motoneurons impaled in the isolated ganglion, in order to obtain a template

of their extracellular action potentials and perform spike identification on extracellular recordings (see previous Section).

Intracellular stimulation of P cells was performed in both isolated ganglion and body-wall preparation, in order to initiate local bending. In these experiments, depolarizing current pulses were passed through the electrodes into the cell bodies to evoke a short spike train (2-8 spikes in 200-400 ms). Similar intracellular stimulation was performed in other mechanosensory neurons (T and N cells). Moreover, intracellular recordings from mechanosensory neurons were performed to monitor their responses to mechanical stimulation of the skin, in the body-wall preparation.

Relevance of motoneuron coupling

As mentioned above, quantifying the pattern of deformation characteristic of individual motoneurons required stimulation of these motoneurons in the body-wall preparation. Since it is well know (Ort et al., 1974) that motoneurons are electrically coupled, simultaneous extracellular recordings from the roots in the isolated ganglion were used to verify that electrical coupling between pairs of motoneurons (Ort et al., 1974) is not strong enough to induce a sustained firing in other motoneurons while stimulating a specific one. 77 intracellular stimulations of individual motoneurons were performed in five different preparations (about 15 motoneurons impaled in each experiment). Low frequency (10-15 Hz) bursts in stimulated motoneurons were always unable to affect the spontaneous firing pattern of other simultaneously recorded motoneurons. Higher frequency (20-40 Hz) and long lasting (up to 1 s) bursts in stimulated motoneurons generally evoked only few spikes in other recorded motoneurons, in some cases transiently increasing their spontaneous firing rate 2 or 4 Hz, although in 2 cases of the 77, a high frequency burst (>40 Hz) in the stimulated motoneuron increased the firing rate of a motoneuron coupled to it up to ~15 Hz. These data indicate that, in experiments in which skin deformations were evoked by

stimulating an individual motoneuron (see Chapters 3, 4 and 5), the contribution to the response by other motoneurons is minimal.

2.2.3 Data collection and storage

Extracellular voltage signals were recorded using a homemade 8-channel amplifier, whose head-stage has a bandwidth of 200-2500 Hz (2-pole filter) and a fixed gain of 10^3. The peaks of the action potentials recorded by the suction electrodes from the roots, ranged between 15 and 500 μV. The standard deviation of the noise was about 10 μV. The intracellular recordings were performed using the amplifier Axoclamp-2b (Axon Instruments).

Both intracellular and extracellular recordings were digitized at 10 kHz and stored on a personal computer using the acquisition board Digidata 1200B and the software Clampex 8 (Axon Instruments) (see **Fig. 2.3**).

2.2.4 Mechanical stimulation

In some experiments a brief (200-400 ms) mechanical stimulus was delivered to the skin to evoke local bending. The stimulus consisted of a poke with a nylon filament driven by a solenoid (347-652 RS components), as described by Lewis and Kristan (1998a). Different stimulus intensities were achieved by changing the diameter and the length of the filaments (Levin et al., 1978). A force transducer (HONEYWELL FSG-15N1A) measured the force exerted by each filament that was used (Pinato and Torre, 2000). Filaments delivering stimulus intensities of about 20 and 50 mN were used.

2.2.5 Measurement of muscle tension

In a series of experiments the accuracy of the proposed method for quantifying muscle contraction was tested by comparing its results with those obtained by a usual force transducer. These measurements were performed by connecting the force transducer FT03 (Grass Instruments, Astro-Med, Inc) to the leech body-wall by means of a stiff nylon wire

ending in a hook inserted in the skin edge (see Chapter 3). The voltage signal provided by the sensor was amplified, digitized at 10 KHz and stored on a personal computer using Clampex 8 (Axon Instruments).

2.3 Optics

A stereomicroscope (SMZ-2B, Nikon) was used during the dissection. The preparation was then transferred on an anti-vibration table, where a second stereomicroscope (SZ-11, Olympus) was mounted to impale neurons under visual control in dark field transmitted light. This microscope was also used for imaging the body-wall preparation (see next Section).

2.4 Video recordings

A standard CCD camera (640 × 480 pixels) was mounted on a dissecting microscope (see previous Section) and used to image the body-wall preparation. Images of the contracting leech skin were acquired at 5 or 8.3 Hz and stored on a personal computer using a frame grabber DT3155 (Data Translation) and the acquisition software Axon Imaging Workbench 2.2 (Axon Instruments). Axon Imaging Workbench and Clampex 8 can run simultaneously on the same computer, allowing the synchronized acquisition of images and of electrical signals. The drawing of **Fig. 2.3** shows the scheme of the acquisition system to simultaneously record the neural activity and the motor behavior of the leech in the body-wall preparation.

All pictures of the leech skin in the present thesis have a resolution of 640 × 480 pixels.

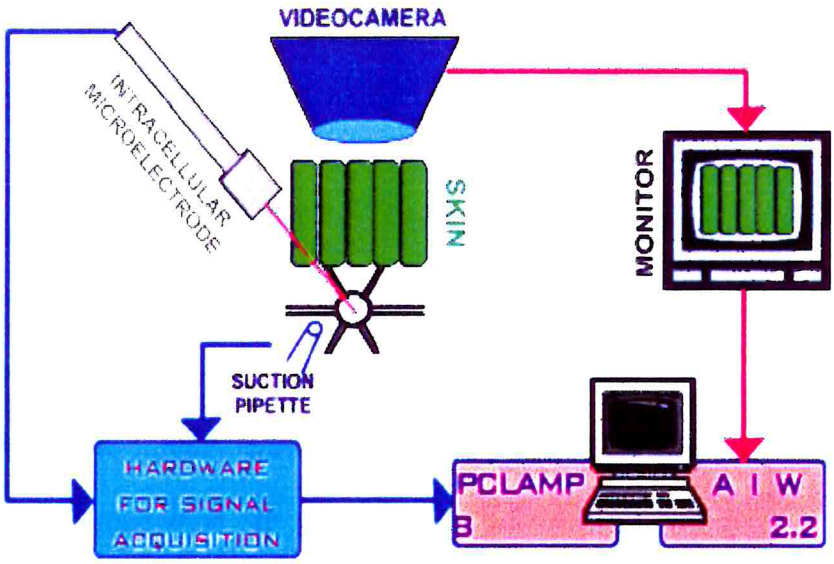

Figure 2.3 Scheme of the acqisition system. Electrophysiological intracellular and extracellular signals are conveyed to the acquisition board Digidata 1200B mounted on a personal computer after a filtering and amplification stage (hardware for signal acquisition). At the same time, a CCD camera acquires images of the contracting body-wall preparation. The images are conveyed to the frame grabber DT3155 (Data Translation) mounted on the same computer. The software for imaging (Axon Imaging Workbench 2.2) and signal acquisition (Clampex 8) can run simultaneously on the same computer and can be synchronized to one another.

2.5 Data analysis

2.5.1 Spike clustering and statistics

Preliminary data display and analysis were performed with Clampex 8 and Axoscope 8 software (Axon Instruments). However, since the experiments performed on the isolated ganglion involved parallel recordings from populations of coactivated neurons, it was necessary to develop a suitable method for further analysis of these multi-electrode

recordings. The possibility of discriminating in parallel signals produced by different neurons is based on the assumption that action potentials produced by the same neuron have almost identical extracellular signals. Hence, a crucial problem was the classification of the shapes of action potentials. In most experiments, this task was accomplished in a semi-automatic way. The development of software to face this problem was part of my Ph.D. work, carried out in collaboration with several other people in my laboratory. A multi-purpose program, composed of several different modules for semi-automatic spike extraction, spike sorting, statistical analysis and display of results, was realized in Matlab language (Math Works Inc.). I personally wrote the module for detecting spikes fired by the same neuron in different channels (different roots). Routinely computed first order statistics of sorted neurons included: average firing rate of identified neurons, coefficient of variation, histograms of the time occurrences of the 1^{st}, 2^{nd}, ...,n^{th} spikes in each trial. Second order statistics included time cross-correlations and joint firing probabilities and entropies.

2.5.2 Variability of neural firing

The variability of action potentials identified as originating from the same neuron N was characterized by computing the coefficient of variation CV of the firing rate of the neuron. It is defined as CV = σ/AFR, where σ is the standard deviation of the firing rate and AFR is the average firing rate of the neuron, over the number of trials of a given stimulation, in a given time window Δt. When the electrical activity of several neurons $i = 1, \ldots, n$ was analyzed, the CV of the random vector $X = (x_1, x_2, \ldots, x_n)$, with x_i being the firing rate of neuron N_i, was considered. In this case the covariance matrix Γ replaced the unidimensional variance σ^2 and the CV was defined as $CV_X(t) = \sqrt{\sum_{i,j} |\Gamma_{i,j}(t)|} \Big/ \sum_i AFR_i(t)$, where AFR_i is the average firing rate of neuron N_i. When the random variables x_i are statistically independent, the covariance matrix Γ is

diagonal and the CV reduces to $\mathrm{CV}_X(t) = \sqrt{\sum_i \sigma_i^2(t)} \Big/ \sum_i \mathrm{AFR}_i(t)$. In this case (Pinato et al., 2000) the CV of random vector X is equal to the CV of the random variable $X = x_1 + x_2 + \ldots + x_n$. The CV of the ensemble of motoneurons in **Fig. 5.8** was computed as the CV of the random variable $X = x_1 + x_2 + \ldots + x_n$.

2.5.3 Statistical independence of neural firing

Statistical independence in motoneuron firing was measured by computing, for each pair of coactivated motoneurons i and j, the following quantities: 1) the probability p_i that motoneuron i fires at least one spike in a given time interval Δt; 2) the joint probability p_{ij} that both motoneurons i and j fire at least one spike in the same Δt; 3) the entropy for the activity of motoneuron i, defined as $H_i = -\sum_m P_i^m \log_2 P_i^m$, where P_i^m is the probability that motoneuron i fires m spikes in Δt; 4) the joint entropy $H_{ij} = -\sum_{mn} P_{ij}^{mn} \log_2 P_{ij}^{mn}$, where P_{ij}^{mn} gives the probability that motoneuron i fires m spikes and motoneuron j fires n spikes in Δt. When the joint probability of firing p_{ij} is equal to the product $p_i\ p_j$ and the joint entropy H_{ij} is equal to the sum $H_i + H_j$, the firing of the two neurons is statistically independent (Pinato et al., 2000). Notice that computation of joint entropies is the proper way to evaluate pair-wise statistical independence, because entropy takes into account all possible firing states (neuron i firing 0, 1, 2, ..., m spikes) of the neurons, while joint probability only gives the probability that the neurons fired. However, since calculation of joint entropies for many pairs of motoneurons with many possible firing states requires an extremely long computation time, I used joint probabilities to obtain a first estimate of statistical independence. More precisely, p_{ij} can be used to evaluate statistical independence if the probability for the neurons to fire more than one spike in Δt is very low. For this reason, I computed probabilities for a time window of 20 ms, chosen for a low probability of firing more than one spike. Such a choice not only allows using joint probabilities to estimate statistical independence but also guarantees reasonable

computation times for evaluation of joint entropies. This is because the number of different firing states of leech motoneurons, when activated by a moderate mechanosensory stimulus, is usually not bigger than 4 or 5 in a 20 ms time window.

2.5.4 Analysis of motor behavior

Image sequences of the contracting skin of the leech were collected as described in Section 2.4 and then analyzed in order to obtain a quantitative characterization of the undergoing deformation. This quantitative analysis was based on the computation of the optical flow, a method derived from computer vision, whose utility in neurobiology I have demonstrated in the course of the present study. And, since the application of this method to the analysis of muscle contraction and skin deformation is one of the achievements of my Ph.D. work, it will be explained in detail in Chapter 3.

3 The use of optical flow to characterize muscle contraction

The first aim of my Ph.D. project was to develop a reliable method to quantify the pattern of deformation that muscle contraction induces on the leech skin. This chapter describes the approach adopted to solve such problem. The resulting method, based on the computation of the optical flow, is enough general to be applicable to the analysis of contractions in every kind of flat tissue with enough visual texture.

3.1 Introduction

Muscle contraction is commonly measured by force and displacement transducers (Joyce et al., 1969; Burke et al., 1970; Stuart, 1970; Mason and Kristan, 1982; Kristan, 1982; Norris and Calabrese, 1987; Ghez, 1991). These transducers are small, cheap and convenient to use. They provide a direct measure of the force along a given direction, i.e. a scalar quantity. However, muscle contraction induces in the tissue a displacement field, i.e. a vector field, which cannot be precisely characterized by using these sensors, which provide only scalar quantities. I circumvented this problem by using recent advances obtained in computer vision for the analysis of time varying sequence of images.

Research into computer vision has developed many tools for the analysis of image sequences (Horn and Schunck, 1981; Lucas and Kanade, 1981, Aggarwal and Nandhakumar, 1988; Anadan 1989), such as those taken by a CCD camera monitoring traffic at street intersections (Giachetti et al., 1995) or by a CCD mounted on a moving vehicle (Giachetti et al., 1998). Some of these algorithms identify important features of the viewed scene and track them from one frame to the next one (Aggarwal and Nandhakumar, 1988; Nagel, 1983). Other algorithms aim at computing the vector field of the image motion on the CCD sensor, usually called optical flow, by differential methods, requiring

the computation of various - temporal and spatial - derivatives of the original image sequences (Horn and Schunck, 1981; Lucas and Kanade, 1981). Once optical flow is obtained, i.e. a two-dimensional vector field describing the image motion, it is possible to recover from it important information of motion (Verri et al., 1989) and deformations (Giachetti and Torre, 1996) of viewed objects. These algorithms, which have been extensively studied and tested in a large variety of image sequences, provide reliable data and accurate measurements in specific cases. Indeed, performances and reliability of all these algorithms depend crucially on the presence of enough textures on the images: the absence of textures and landmarks makes very difficult any analysis of motion and deformation based on image sequences.

Conditions for the success of the algorithms developed by research into computer vision are met in some relevant neurobiological cases. They are met, for instance, when deformations of a piece of skin or of an almost flat tissue with enough texture or landmarks are imaged with a CCD camera. In this chapter I describe the use of video miscroscopy and of tools of computer vision to measure and characterize the displacement field induced on leech body-wall preparation (see Section 2.1.2) by muscle contraction. The approach is based on the presence of natural landmarks on leech skin: indeed the whole body of the animal is covered by a rich texture, ideal for the computation of the optical flow.

The chapter is divided into three main sections. In Section 3.2 the tracking algorithm is discussed and explained step by step. In Section 3.3 it is shown how to compute a reliable and dense optical flow from a sequence of images of the leech skin during muscle contraction induced by tactile or electrical stimulation. In Section 3.4 the linear deformation theory is used to characterize and describe skin deformations induced by different stimuli.

The proposed method, here demonstrated for the characterization of muscle contractions in the leech skin, is expected to provide good results for the analysis of all

contractions evoked in almost flat tissues with enough landmarks. In this case the proposed method provides a complete characterization of the induced deformations, which cannot be obtained with usual force transducers.

3.2 Tracking a feature in an image sequence

3.2.1 The tracking algorithm

One of the most useful computer vision techniques for recovering the three-dimensional motion of objects viewed by a CCD camera, is the computation of optical flow. This is a planar vector field, which is the perspective projection, on the image plane, of the original three-dimensional field of displacements occurring on the surface of the viewed object (Horn and Schunck, 1981; Verri and Poggio, 1989). Different approaches have been proposed to compute the optical flow (Horn and Schunck, 1981; Nagel, 1983; Verri et al., 1990; Anadan, 1989; Aschwanden and Guggenbuhl, 1992). The most suitable for my application is the window matching or correlation algorithm, which tracks points from one image to the next one in the image sequence (Aggarwal and Nandhakumar, 1988; Anadan, 1989; Aschwanden and Guggenbuhl, 1992; Giachetti, 2000). The correlation algorithm is described step by step, with the graphic aid provided by **Fig. 3.1**, in the following way. In essence, the algorithm tracks a window of gray levels (defined by the red square) in image n, centered on the point (x',y'), by looking at the most similar window of gray levels in image n+1, centered in the point (x'',y''), within the blue square, representing the possible search space.

More in detail: let $I(x,y,n)$ be an image sequence, with I representing its gray level at location (x,y) in image n. Two consecutive images of a sequence of a contracting leech skin are shown in **Fig. 3.1**, where panel ***A*** and ***B*** reproduce the images at time n and n +1 respectively. Let (x',y') be a point in image n and $W(x',y',n,h,k)$ a window centered in (x',y'), with width h and height k. The point (x',y') and the window W are indicated respectively by

a white X and by a red box in **Fig. 3.1*A***. If the image brightness I undergoes a smooth deformation starting with image n, the point (x',y') will move to the new location (x'',y'') in image $n+1$ (white X in **Fig. 3.1*B***) according to the following algorithm:

1. Consider the set of points $N_{x',y'}$, in the image $I(x,y,n+1)$, such that:

$$x'-h_0 < x < x'+h_0 \quad \text{and} \quad y'-k_0 < y < y'+k_0 .$$

This set of points $N_{x',y'}$ is simply a rectangle (centered on the original position (x',y') of the feature to be tracked) which delimits the region in which the feature is expected to move in the next frame. This rectangle is drawn in blue in both panels of **Fig. 3.1**.

2. Consider all windows $W(x,y,n+1,h,k)$ with (x,y) belonging to $N_{x',y'}$. In other words, consider the windows centered on all the points belonging to the blue rectangle of **Fig. 3.1*B***. These windows must have the same size of the window centered on the original point (x',y') at frame n (the red box in panel ***A***). The blue rectangle represents the possible search space for the final displacement of the original patch of gray levels.

3. Evaluate the similarity between each of these windows and the window $W(x',y',n,h,k)$ in the image $I(x,y,n)$ (the red window of panel ***A***), computing the value of the correlation function

$$f_{CORR}(W(x,y,n+1,h,k),W(x',y',n,h,k)), \qquad (1)$$

for each point (x,y) belonging to $N_{x',y'}$.

4. The point (x',y') will move to the new location (x'',y'') in the image $I(x,y,n+1)$ (white cross in panel ***B***), such that (x'',y'') maximizes the value of (1) over the set of points $N_{x',y'}$. In other words, the algorithm finds the window $W^*(x'',y'',n+1,h,k)$ in the image $n+1$ (the red box in panel ***B***, with center inside the blue rectangle), which is most similar to the window centered on the original point (x',y') in the image n (the red box in panel ***A***). The center (x'',y'') of this window W^* is the new position of the tracked point.

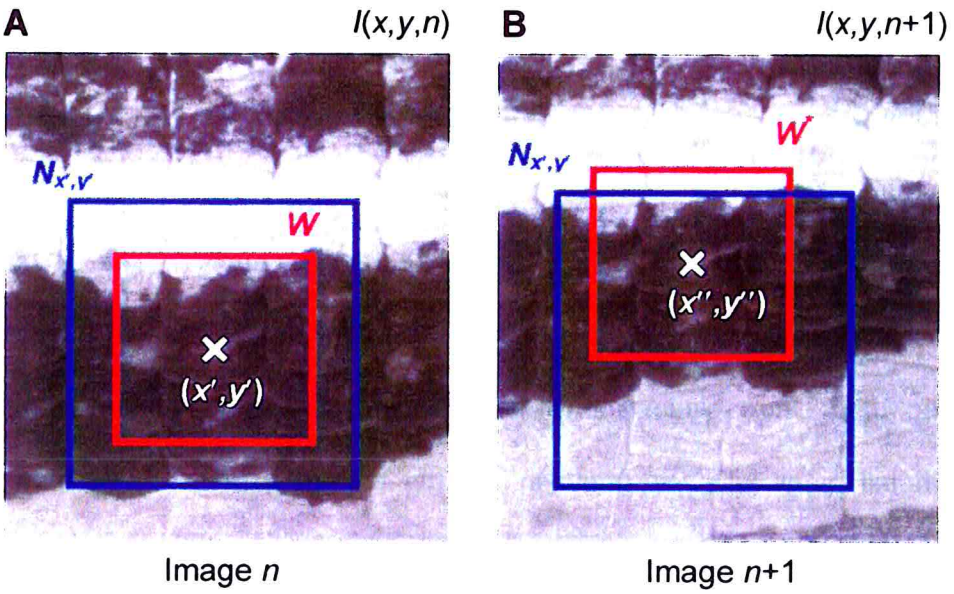

Figure 3.1 The tracking algorithm. A detail of the leech skin is shown at two different times during a contraction that induces a strong deformation on the skin surface. *A*, Skin at frame *n*. The white X indicates the feature to be tracked. The red window is that used to compute the correlation, as described in Section 3.2.1. The blue window is the search space in which the point is expected to move. *B*, Skin at frame *n* +1. The white X indicates the new position of the tracked feature. The red window is the one maximizing the correlation with the red window of panel *A*. The blue window is the same as that in panel *A*.

This algorithm depends on four parameters, namely h, k and h_0, k_0. h and k are the dimensions of the window centered around the moving point and h_0 and k_0 are the dimensions of the rectangle in which the moving point is supposed to move. The size of this window can be estimated by the expected velocity of the deformation. A simplified version of the algorithm assumes that $h = k = h_0 = k_0$ equal to a value between 10 and 20 pixels.

3.2.2 Selection of the similarity/distance function

Different choices are available for the correlation function (1) (see Aschwanden and Guggenbuhl, 1992). One possibility is to use the classical cross-correlation (CC) function, defined for square windows with side amplitude $m \equiv h = k$, as:

$$CC(W(x,y,n+1,m),W(x',y',n,m)) = \sum_{i,j=-m/2}^{m/2} I(x+i,y+j,n+1)I(x'+i,y'+j,n) \qquad (2)$$

This standard CC function is overly sensitive to noise and it is usually replaced by the normalized one (NCC) or by the zero-mean normalized version (ZNCC) (see Giachetti, 2000 for a definition).

As an alternative, a distance function may be used to evaluate the difference between the pattern of gray level of the two windows. In this case the new location (x'',y'') of the tracked point is obtained by minimizing the distance function. A widely used distance functions is the SAD function (sum of the absolute values of the differences of the gray level in corresponding pixels of the two images), defined, for square windows with side amplitude m, as:

$$SAD(W(x,y,n+1,m),W(x',y',n,m)) = \sum_{i,j=-m/2}^{m/2} \left| I(x+i,y+j,n+1) - I(x'+i,y'+j,n) \right| \qquad (3)$$

Another widely used distance function is the SSD function (sum of the squared differences of the gray level in corresponding pixels of the two images) (see Giachetti, 2000 for a definition). The SAD and the SSD functions can be modified to consider the effect of global gray-level variations, setting the average gray level difference equal to zero (ZSAD, ZSSD) or locally scaling the intensity (LSAD, LSSD) (Aschwanden and Guggenbuhl, 1992; Giachetti, 2000).

An analysis of the robustness of these distance/similarity functions against several types of noise and image distortion can be found in Aschwanden and Guggenbuhl (1992). A comparison among their performances (Giachetti 2000) indicates that all the standard measures based on the comparison of the gray levels (SAD, SSD, NCC, ZSAD, ZSSD, LSAD, LSSD) provide an accurate tracking, with the exception of the simple CC, which is extremely sensitive to noise. Their performances are similar and they are substantially equivalent. In the present work I chosen to use a tracking algorithm based on the SAD function, which provided an accurate and fast tracking of all the analyzed sequences.

Sometimes local changes in the light intensity can occur due to highlights on the bathing solution or to the presence of shadows projected by the nylon filament used to stimulate the skin mechanically (see **Fig. 3.2*D*** and ***E***). These regions are usually small and the distortion in the optical flow produced by their presence does not invalidate its use. Some distortion in the optical flow can also occur at the cut edges of the preparation, where the skin deformation can be very strong and irregular (the skin at the edges can slightly rise and twist). Part of the skin can move out the field of view of the camera, thereby making measurements near edges less reliable.

3.2.3 Selection of the reference image

Section 3.2.1 describes how the window-matching algorithm can track a feature from image n to image n +1 of an image sequence. If the sequence starts at image 0 and

terminates with image N, a selected feature in image 0 can be tracked along the whole sequence of images in two different ways, namely:

1. In every image of the sequence always look for the original features contained in the image $I(x,y,0)$, and seek the highest correlation with the gray levels over $W(x',y',0,h,k)$.

2. If the point (x',y') has moved to point (x'',y'') from image n to image $n+1$, at image $n+2$ seek for the highest correlation with the gray levels over $W(x'',y'',n+1,h,k)$.

The first algorithm is based on tracking the original features contained in the initial image, while the second algorithm follows a changing feature.

The second algorithm is appropriate, for example, to track cars and vehicles in outdoor scenes, where the features to be followed do not return to the original position and their shape changes considerably with time (Giachetti et al., 1995). The first algorithm can be suitable to follow slow rhythmic events, such as muscle contraction and relaxation, where the tracked features do not undergo substantial changes in their shape and always come back to the original resting state. As discussed in Section3.3.1, the results of the first algorithm proved to be more appropriate to monitor deformations on the surface of the leech skin. For this reason most of the data presented in the following sections were analyzed using the first algorithm.

3.3 Monitoring muscle contraction by videomicroscopy

3.3.1 Tracking features on the leech skin

Fig. 3.2*A* illustrates an image of a leech body-wall preparation (see Section 2.1.2) taken with a dissecting microscope at a low magnification before passing a depolarizing current

step, lasting 3 seconds, in motoneuron 8, which is an excitor of the ventral longitudinal muscles. Panel *A* illustrates the skin at rest, before the stimulus application, while panel *B* illustrates the portion of skin enclosed in the white rectangle of panel *A*, at the time of the maximal contraction and at a higher magnification. The spike discharge (~20 Hz) evoked in the neuron is visible both in the intracellular (see lowest trace of panel *C*) and in the extracellular recording from the PP nerve root, as shown in the middle trace of panel *C*. The white X's in panels **A** and *B* indicate the position of four selected features, while the white lines in panel *B* are the consecutive displacements of the features during the movement. The upper part of panel *C* reproduces the time course of the displacement for the four selected features. The latency between the beginning of the contraction and the first spike of the discharge was between 230 ms and 430 ms, the uncertainty of 200 ms was equal to the image sampling period (image sampling rate was 5 Hz). The contraction reached its maximum at the end of the spike train. The skin remained contracted for about 1.5 s and then relaxed to the initial state. Similar results were obtained when the skin was touched for 100 ms with a nylon filament (visible in the bottom of panels *D* and *E*) exerting a force of 50 mN. Panels *D* and *E* show the skin at rest and at the maximal contraction respectively. The white X's indicate the position of the selected features, while the white tracks are the consecutive displacements of the features during the movement.

Fig. 3.3 illustrates the trajectory of six points on the leech skin during contraction and relaxation of the oblique muscles, induced by stimulating motoneuron 110 intracellularly (Stuart, 1970). Panel *A* and *B* of **Fig. 3.3** show respectively the piece of skin at rest and at the time of the maximal contraction, with superimposed trajectories (red lines) of the tracked points (white X's). Panels *C* and *D* show the skin at the end of the relaxation phase when it returned to its rest position. The trajectories of the selected points from rest to maximal contraction and from maximal contraction to maximal relaxation are drawn respectively in red and yellow.

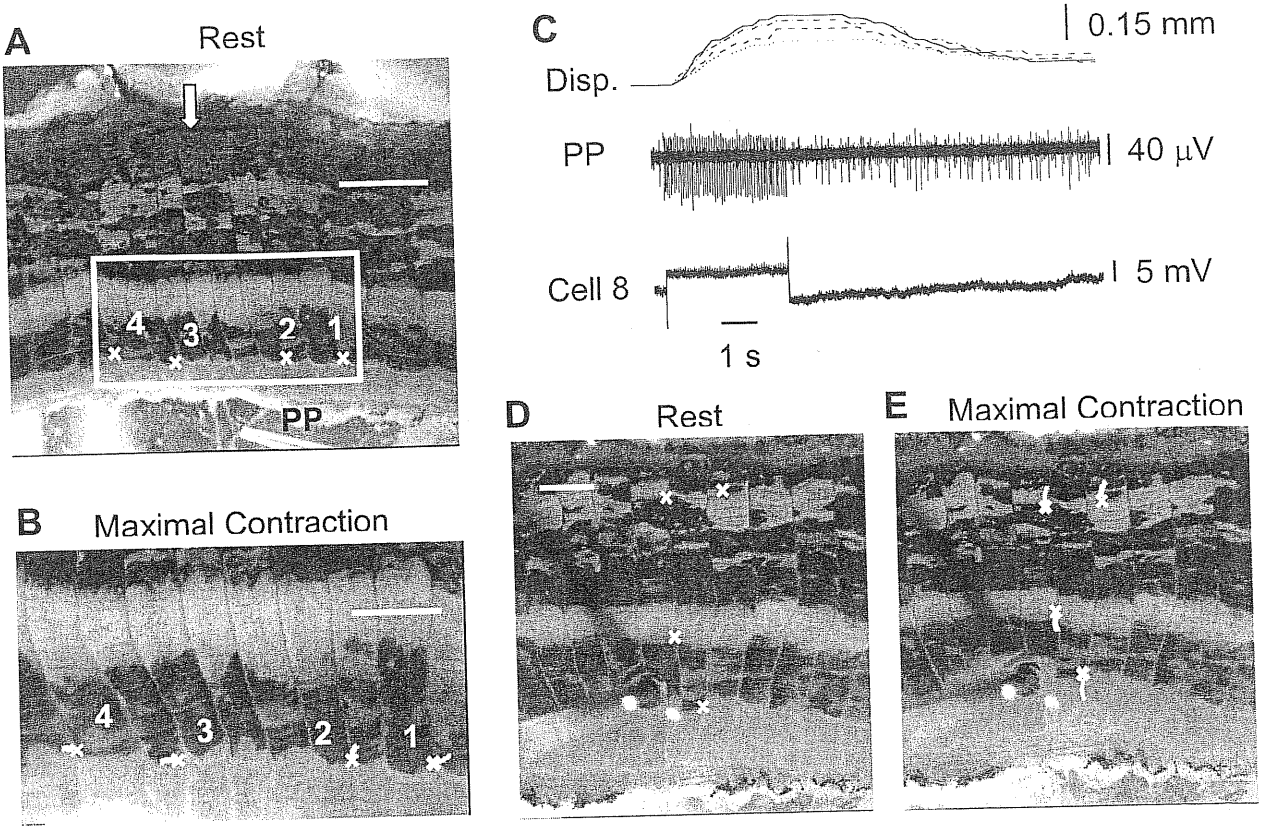

Figure 3.2 Deformations on the leech skin. *A*, A leech body-wall preparation, three segments in length. The middle segment (whose central annulus is indicated by the arrow) is innervated by its ganglion, where the intracellular recording shown in *C* was obtained. The skin is at rest. At the bottom of the panel a pipette suctioned onto the PP root is shown. White X's indicate the selected features to be tracked. These features were selected in zones with high contrast, namely on the border of the dark longitudinal strip. This allowed the use of very small windows to compute the correlation-based tracking. Scale bar 3 mm. *B*, The portion of skin in the white box of *A*, shown at a higher magnification at the time of maximal contraction after passing a depolarizing current step in motoneuron 8. White X's correspond to the new positions of the tracked points. White lines indicate the trajectories of these four points during muscle contraction. The square window used to compute the correlation was 10 pixels wide. This corresponds roughly to the size of the X's. Scale bar 2 mm. *C*, Bottom trace: Intracellular recording from motoneuron 8 during its stimulation with a depolarizing current step. Middle trace: extracellular recording with a suction pipette from the posterior posterior (PP) root, during the stimulation of motoneuron 8. The largest signals on the trace are the extracellular action potentials of motoneuron 8 observed in the bottom trace (fire rate ~ 20 Hz). Top trace: time course of the displacement of the features tracked in *B*. *D* and *E*, Same markers as in *A* and *B*, but during the mechanical stimulation with a nylon filament, which can be seen in the two panels. Scale bar 2 mm.

In panel ***C*** features were tracked using the first algorithm described at the end of Section 3.2.3, in panel ***D*** using the second. When the first algorithm was used, features were properly tracked also when muscles relaxed after contraction (see yellow lines in panel ***C***). The second algorithm was not able to track exactly the same features: in panel ***D*** there are no yellow trajectories reaching the white X's, i.e. the original position at the end of the relaxation. Panel ***E*** illustrates the time course of the displacement for the three points labeled in the previous panel as 1, 2 and 3. The solid lines refer to the points tracked in panel ***C*** with the first algorithm, and the dotted lines, with corresponding colors, refer to the same points tracked in panel ***D*** with the second algorithm. During contraction all points were well tracked by both algorithms. When the contraction became slower the second algorithm failed to follow the features, which were completely lost during the relaxation phase. The reason is that slow deformations at the skin surface lead to sub-pixel displacements in consecutive frames and the second algorithm, computing the correlation between successive images, is no longer able to perceive the movement. To avoid this problem, the tracking algorithm can be improved to allow sub-pixel resolution (Giachetti, 2000). This algorithm is necessary when high spatial resolution is required (see **Fig. 3.6*B***), but its computational cost becomes significant when applied over a dense grid of points, which are required to compute the optical flow (see next Section). For this reason, all the optical flows presented in the following figures were obtained using the first algorithm, which provides a correct tracking with a reasonable computation time. As an alternative, it is possible to modify the second algorithm forcing it to compute the correlation with the last frame in which the detected displacement is not zero (for example two or three frames before the current one). This revised version of the second algorithm has the same performance of the first algorithm in terms of tracking accuracy and computation time.

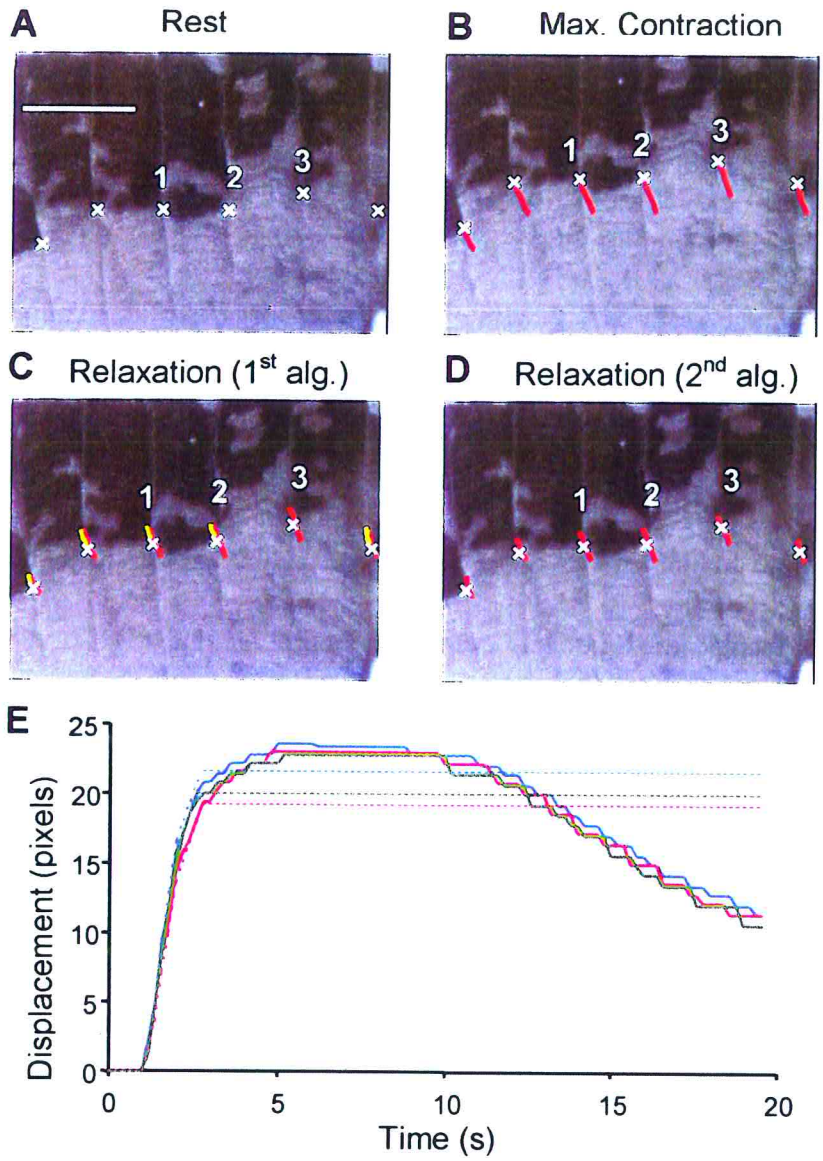

Figure 3.3 Comparison between the two tracking algorithms described at the end of Section 3.2.3. *A*, Detail of a patch of leech skin at rest, before passing a depolarizing current step in motoneuron 110 (OE). Six features are indicated by white X's. They were selected in zones with high contrast to minimize the size of the windows used to compute the correlation. Scale bar 2 mm. *B*, Skin at the end of the contraction phase, after stimulation of cell 110. The red lines are the consecutive displacements of the selected features (white X's) from rest to maximal contraction, as detected by the first tracking algorithm. The windows used to compute the correlation were 10 pixels wide. This corresponds roughly to the size of the X's. *C* and *D*, Skin at the end of the relaxation phase. White X's and red lines are the same as in previous panels. In *C* the yellow lines indicate the consecutive displacements of the selected features from maximal contraction to maximal relaxation, as detected by the first tracking algorithm. In *D* the second algorithm is not able to follow the features during relaxation. In *B*, *D* and *C* the scale is the same that in *A*. *E*, Time course of the displacement for the three points labeled in the previous panel as 1, 2 and 3. The solid lines refer to the tracking with the first algorithm and the dotted lines refer to the tracking with the second one.

3.3.2 Computing the optical flow

It is possible to track all features on a regular grid and obtain a dense representation of the occurring displacements, referred in computer vision as *optical flow*. Given a sequence of images $I(x,y,i)$, with $i=1,\ldots,N$, and given a grid of points $\vec{x}=(x,y)$ on the image plane, the optical flow $\vec{O}_{Ti}(\vec{x})=(u_{Ti}(\vec{x}),v_{Ti}(\vec{x}))$ is the total displacement of the features centered on $\vec{x}$ from image 1 to image i. $u_{Ti}(\vec{x})$ and $v_{Ti}(\vec{x})$ are respectively the x and y component of the displacement in every point $\vec{x}$.

Fig. 3.4 illustrates a case when the cell L, a motoneuron innervating longitudinal muscles, was stimulated with a depolarizing step of current, inducing a spike discharge of about 40 Hz (see bottom trace in **Fig. 3.3*C***). The time course of the displacement, for a given point on the skin (indicated by a red X in **Fig. 3.4*A***), is shown in **Fig. 3.4*C***, where the duration of the contraction and of the relaxation phase are indicated. Features on a 30×20 pixel grid were tracked from the resting state to the maximal contraction (see panel ***A***) and from the maximal contraction to the end of the relaxation phase (see panel ***B***). In panels ***A*** and ***B*** the head of the arrows indicates the direction of the movement while the length of the arrows indicates the amplitude of the displacement. During contraction the main component of the deformation was a strong contraction in the longitudinal direction along the leech body. Since the body wall of the leech is an elastic medium, this longitudinal shortening induced also a transverse elongation. During relaxation there was the opposite deformation: an elongation in the longitudinal direction and an associated shortening in the transverse direction. The skin was motionless in a region above the intersection of the longitudinal gray strip with the central annulus of the innervated segment (6^{th} annulus from the left). The amplitude of the displacement increased while moving away from this region in both longitudinal and transverse directions.

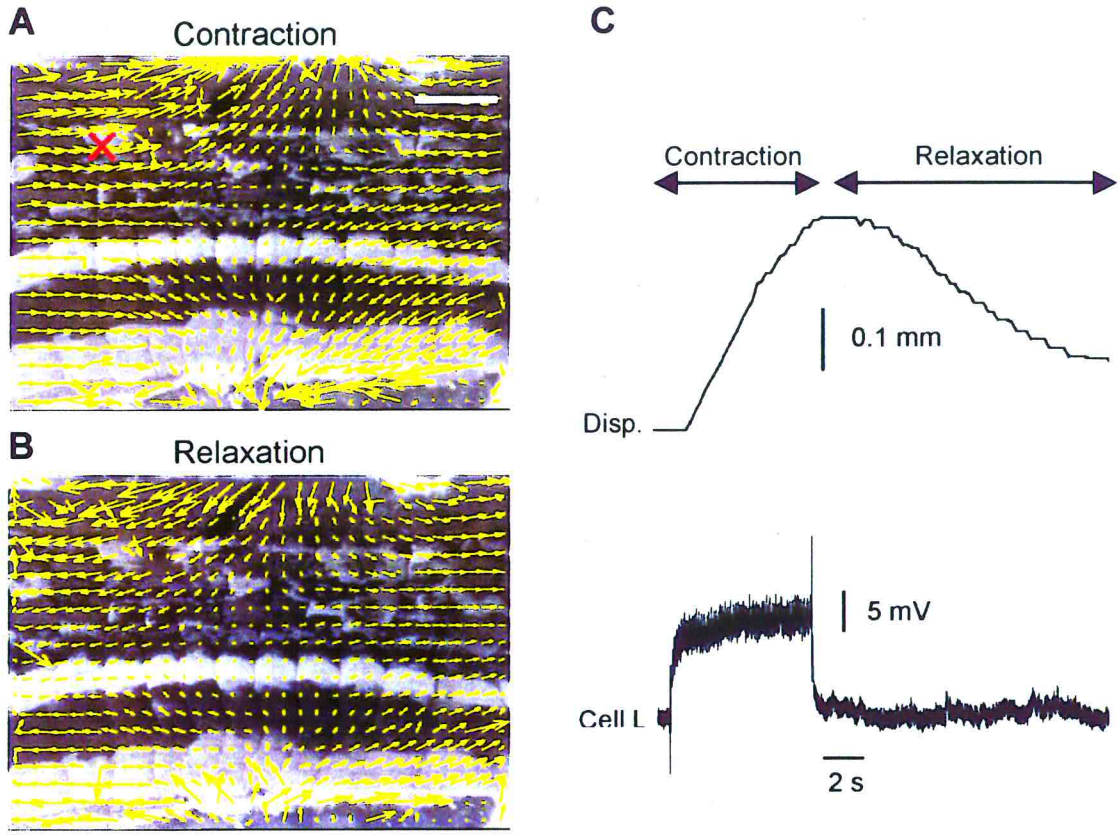

Figure 3.4 Optical flows during skin deformation caused by the stimulation of the L motoneuron. *A* and *B*, Dense optical flows (grid 30 × 20) at maximal contraction and relaxation. Vectors have yellow head and body, indicating respectively the direction and the amplitude of the movement. Scale bar 2 mm. The arrows were amplified twice (2 ×) in order to make the direction of the movement more clear. *C*, Bottom trace: intracellular recording from the L motoneuron during its stimulation with a depolarizing current step (firing rate ~ 40 Hz). Upper trace: the displacement of a representative point of the skin (indicated by the red X in *A*) during contraction and relaxation. The square window used to compute the correlation was 20 pixels wide. This corresponds roughly to 2/3 the size of the red X of panel A.

The major movement occurred at the edges of the preparation, well beyond the boundary of the territory innervated by the cell L (see Section 2.1.2). This is because the longitudinal muscles strongly pull the skin even in denervated regions of the body wall. This pattern of displacements is typical of a planar deformation whose intensity grows with the distance

from its stationary point. In Section 3.4 it is shown that this growth is linear in a wide area around the stationary point (see **Fig. 3.8*A***).

Fig. 3.5 illustrates the optical flows obtained during maximal contraction produced by the stimulation of 4 different motoneurons: the longitudinal L motoneuron (A), the dorsal excitatory (DE) motoneuron 3 (B), the oblique excitor (OE) motoneuron 110 (C) and the circular ventral (CV) motoneuron (D). These motoneurons were stimulated with a depolarizing step of current causing a spike discharge between 30 and 40 Hz lasting from 1 to 6 seconds. This produced a strong and sustained contraction. Each optical flow was computed following the displacements of a grid of 30×20 pixels from the resting state to the maximal contraction. The flows are drawn on a gray background reproducing the texture of the skin, where the body annuli can be seen. For each panel, the central annulus of the innervated segment is indicated in the legend.

These flows are in excellent agreement with the deformation expected from the traditional role of all motoneurons (Stuart, 1970). Motoneurons 3 and L innervate the longitudinal muscles, which are the muscle fibers running parallel to the length of the leech and responsible for its shortening (Stuart, 1970; Nicholls and Purves, 1970; Mason and Kristan, 1982; Kristan, 1982). The L motoneuron innervates the whole half-segment and indeed the corresponding contraction involves all the skin, with the center approximately in the middle of the half-segment. Motoneuron 3 is a dorsal excitor, innervating only the dorsal fibers of the longitudinal muscles, and its contraction involves mainly the dorsal side of the half-segment. The cell 110 (Stuart, 1970) is an excitor of the oblique muscle fibers and induces a contraction in an oblique direction in respect to the length of the leech. The CV motoneuron innervates the circular fibers situated in the lateral ventral side of the half segment (Stuart, 1970) and induces a contraction in the transverse direction with a displacements field opposite to that induced by the longitudinal motoneurons.

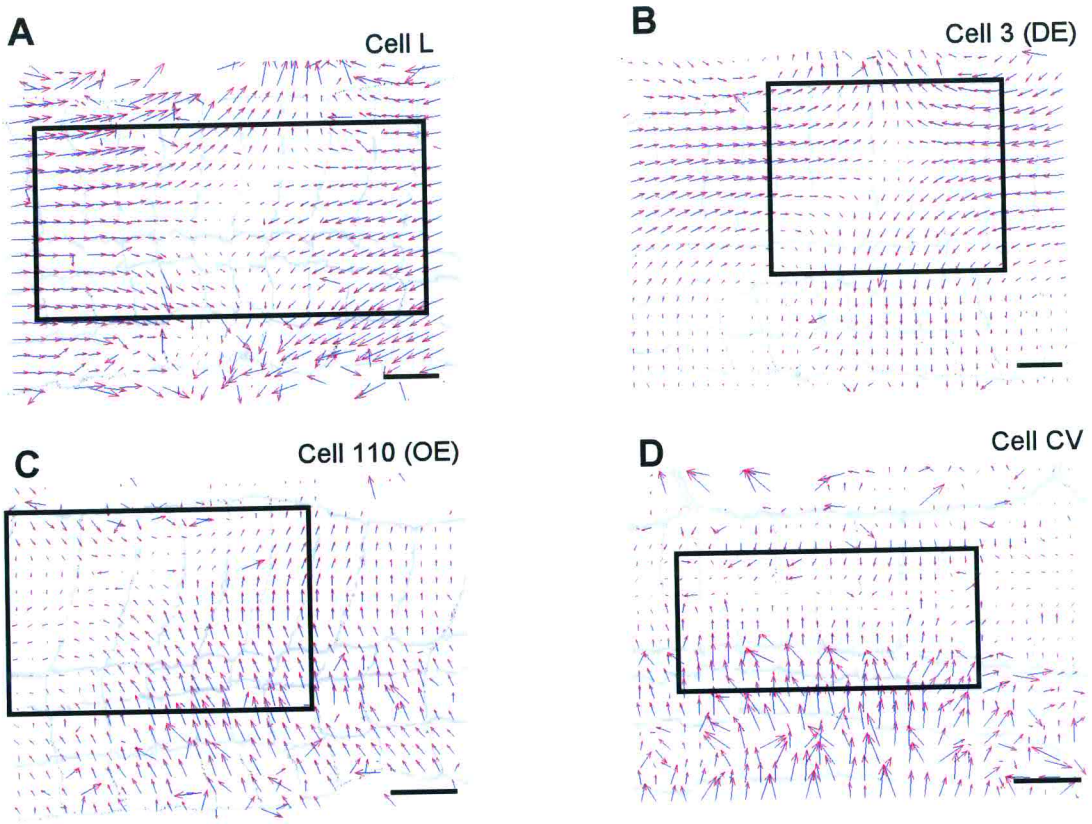

Figure 3.5 Examples of optical flows associated with different leech motoneurons. *A-D*, Optical flows computed on a 30 × 20 grid for the skin deformations caused by the intracellular stimulation of motoneuron L, 3(DE), 110(OE) and CV, respectively. The data are obtained from four different preparations. The firing rates of the spike discharges ranged from 30 to 40 Hz, lasting from 1 to 6 s. The arrows were amplified twice (2 ×) in order to make the direction of the movement more clear. A drawing of the segmental annuli is shown in gray in each panel. The central annulus of the innervated segment is, starting from the left, the 7th for panels *A* and *B*, the 4th for panel *C* and the 6th for panel *D*. In each panel, the window indicates the area in which the linear approximation shown in Fig. 3.8 was computed. Scale bars 2 mm. The square window used to compute the correlation was 15 pixels wide.

3.3.3 Comparison with direct measurement

I verified the usefulness and the accuracy of the tracking algorithm by direct measurement of the force exerted by leech muscles during the execution of a movement. In a series of experiments, I intracellularly stimulated a number of motoneurons. The evoked movements on the surface of the skin were recorded by the camera, while simultaneously the force

produced by the muscles was measured by a force transducer connected to the skin (see Section 2.2.5).

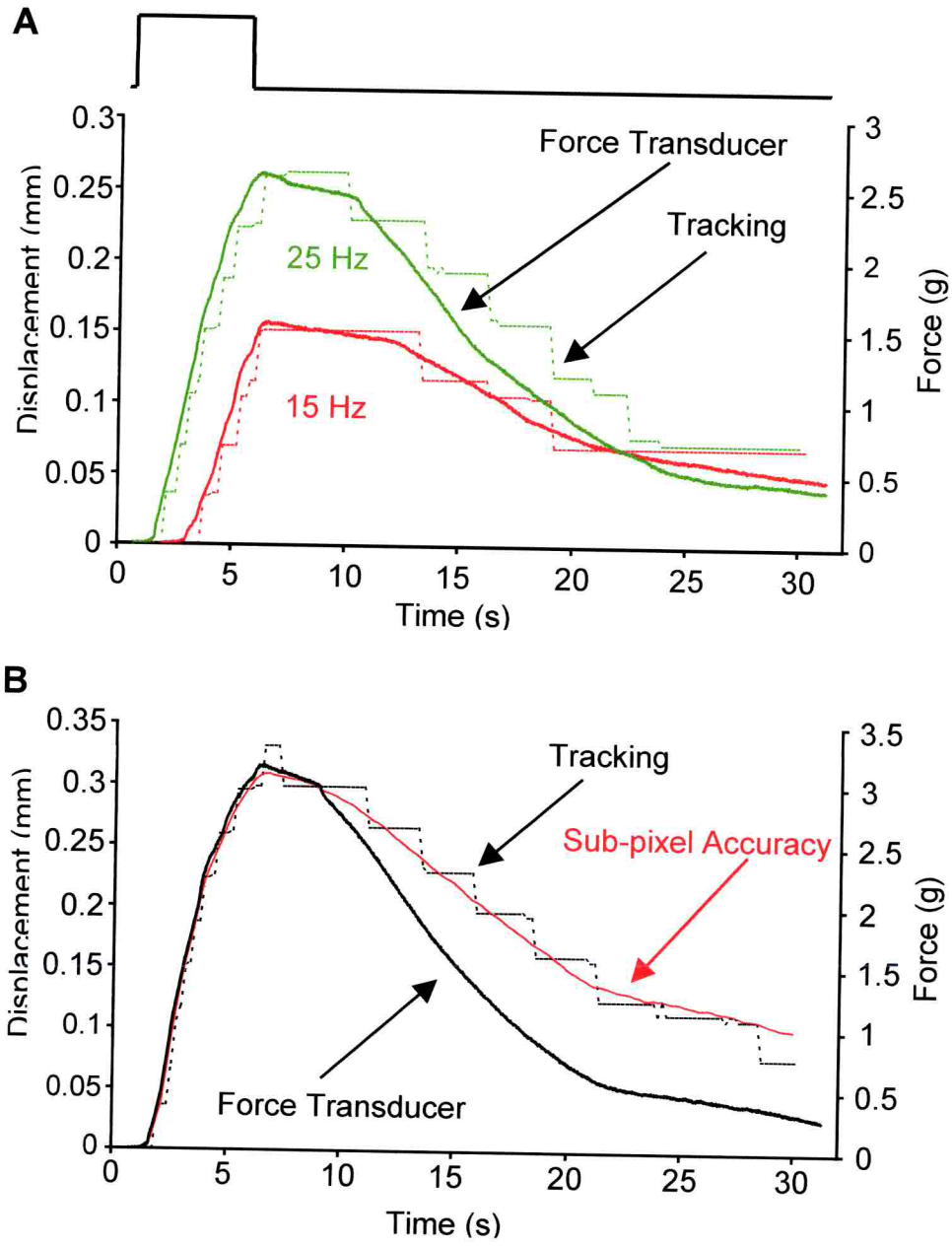

Figure 3.6 Comparison between the proposed approach and direct measurement of tension with a mechanical transducer. *A*, Time course of the deformations induced on a piece of skin by stimulating the motoneuron L to fire at 15 Hz (red lines) and at 25 Hz (green lines) for 5 seconds. The time course of the depolarizing current injected into the motoneuron is shown in the upper trace. Dotted lines represent the absolute displacement of a tracked feature on the skin in the two stimuli. The feature was chosen near to the insertion point of the hook in the skin (see Section 2.2.5). Solid lines of corresponding colors are the measurements of the force exerted by longitudinal muscles in the same two stimuli. *B*, Motoneuron L was stimulated to fire at ~30 Hz. Here the red solid line represents the sub-pixel tracking.

Fig. 3.6*A* shows the results of one of these experiments, in which I induced motoneuron L to fire at two different frequencies (~15 and 25 Hz) for 5 seconds. Dotted lines represent the absolute displacements from the resting position of a selected feature, as detected by the tracking algorithm in the two stimuli. I chose the feature near the insertion point of the hook in the skin (see Section 2.2.5). The solid lines of corresponding colors are the measurements of the force exerted by the longitudinal muscles in the same two stimulations, as recorded by a force transducer connected to the skin. The upper trace represents the time course of the depolarizing current injected into the motoneuron. For each stimuli, the time course of the detected displacement and muscle tension were almost identical during the initial rapid contraction and during the plateau phase. On the contrary, in the relaxation phase the force exerted by the muscle decayed towards zero much more rapidly than the displacement, indicating that the same skin displacement was sustained by different values of muscle tension during the rising and falling phase of the contraction (see also panel ***B***). This behavior is likely due to the passive biomechanical properties of the leech skin. Indeed, hysteresis in the leech body wall has been recognized and extensively studied in denervated whole animals (Wilson et al., 1996; Wilson et al., 1995).

Fig. 3.6*A* illustrates the usefulness of the proposed tracking method in investigating biomechanical properties, such as hysteresis, present in many muscle fibers and tissues (Wilson et al., 1995; Rembold, 1992; Galbraith et al., 1993). When comparison between displacement and some other measurable quantity (like muscle tension) requires high spatial resolution, displacements of just a few microns can be detected simply using appropriate objectives and a tracking algorithm allowing sub-pixel detection. The method used to track features with sub-pixel accuracy is the "mixed" algorithm, described in Giachetti (2000). It computes the integer part of the displacement with the correlation

method described in Section 3.2.1 and then computes the sub-pixel correction using differential techniques (Horn and Schunck, 1981; Bertero et al., 1988 ;Verri et al., 1990;). **Fig. 3.6*B*** reports the result of a sub-pixel tracking, where solid and dotted black lines correspond respectively to muscle tension and normal tracking, as in **Fig. 3.6*A*;** the red line is the sub-pixel tracking. In this experiment, I induced motoneuron L to fire at high frequency (~30 Hz). The higher spatial resolution of the sub-pixel tracking leads to a smooth red curve, which is more suitable for a quantitative comparison with the smooth black curve that represents the muscle tension measured by the force transducer.

3.4 Processing of the optical flow

Once the optical flow is obtained, how can the deformations on the leech skin be characterized? Is it possible to obtain an accurate and possibly simple characterization of muscle contraction? By using well-known results of the theory of deformable bodies, (Sommerfeld, 1974) I will provide a simple answer to these questions in the following sections.

3.4.1 Linear deformation theory

The optical flow computed from a sequence of time-varying images, as defined in Section 3.3.2, is a planar vector field, which often can be very well approximated by a simple linear vector field (Giachetti and Torre, 1996).

Let $\vec{x} = (x, y)$ be a point on the image plane. The motion field on the plane can be studied around the point $\vec{p} = (p_x, p_y)$. In the case of a general non-rigid motion, both points will experience changes in position, which will be denoted with $\vec{V} = (V_x, V_y)$ and $\vec{V}^0 = (V_x^0, V_y^0)$ for $\vec{x}$ and $\vec{p}$ respectively. By using a Taylor expansion up to the first order around the point $\vec{p}$, we have:

$$\vec{V}(\vec{x}) = \vec{V}^0 + \mathbf{L}(\vec{x} - \vec{p}), \tag{4}$$

where $\mathbf{L}$ is

$$\mathbf{L} = \begin{pmatrix} \left.\frac{\partial V_x}{\partial x}\right|_{\vec{x}=\vec{p}} & \left.\frac{\partial V_y}{\partial x}\right|_{\vec{x}=\vec{p}} \\ \left.\frac{\partial V_x}{\partial y}\right|_{\vec{x}=\vec{p}} & \left.\frac{\partial V_y}{\partial y}\right|_{\vec{x}=\vec{p}} \end{pmatrix} \tag{5}$$

Equation (4) defines a linear planar vector field of deformations in a sufficiently small element of the image plane, around the point $\vec{p}$. In (4) the term $\vec{V}(\vec{p}) = \vec{V}^0$ is the rigid translation, while the second term, represented by the linear operator $\mathbf{L}$, represents the rotation and the non-rigid component of the motion. Studying the contraction of the leech skin, the only interesting term in equation (4) is the second one, which accounts for the deformations occurring at the skin surface. Therefore the 2D motion field can be approximated by the linear deformation $\vec{V}_D$, with a stationary point $\vec{p}$, given by:

$$\vec{V}_D(\vec{x}) = \mathbf{L}(\vec{x} - \vec{p}), \tag{6}$$

where $\mathbf{L}$ is the Jacobian matrix defined in the (5). It is well know (Sommerfeld, 1974) that the matrix $\mathbf{L}$ describing the deformation can be decomposed as:

$$\mathbf{L} = \begin{pmatrix} L_{11} & L_{12} \\ L_{21} & L_{22} \end{pmatrix} = E\begin{pmatrix} 1 & 0 \\ 0 & 1 \end{pmatrix} + \omega\begin{pmatrix} 0 & 1 \\ -1 & 0 \end{pmatrix} + S_1\begin{pmatrix} 1 & 0 \\ 0 & -1 \end{pmatrix} + S_2\begin{pmatrix} 0 & 1 \\ 1 & 0 \end{pmatrix}, \tag{7}$$

where

$$E = \frac{L_{11} + L_{22}}{2} \quad \omega = \frac{L_{12} - L_{21}}{2}$$
$$S_1 = \frac{L_{11} - L_{22}}{2} \quad S_2 = \frac{L_{12} + L_{21}}{2} \tag{8}$$

are the elementary deformation components: expansion, rotation and shears respectively. Equations (5) to (7) mean that the linear planar deformation $\vec{V}_D$ is completely described knowing the coordinates of the stationary point $\vec{p}$ and the values of the parameters (8), which are the eingenvalues of the Jacobian matrix **L**, computed in $\vec{p}$. In the following, the stationary point $\vec{p}$ will be referred to as the *singular point*. This is because the motion field can be seen as the *phase portrait* of a dynamical system, whose singular points coincide with the points where the optical flow vanishes. This analogy enables the dynamical systems theory to be used for extracting the essential features of the motion field around the singular point. This is achieved by decomposing it in its elementary components as rotation, expansion, and shear deformations (Verri et al., 1989; Verri and Aicardi, 1990; Giachetti and Torre, 1996).

3.4.2 Geometrical meaning of the elementary deformations

Equation (6) defines a linear planar vector field over the image plane. Equation (7), in turn, states that each linear planar vector field can be decomposed as the linear sum of four elementary deformations, defined by the four matrixes in wich matrix **L** is decomposed. These four matrixes, in the order in which they appear in the right hand side of equation (7), define respectively: pure expansion (E), pure rotation (ω), pure horizontal shear (S_1), and pure oblique shear (S_2). The coefficients E, ω, S_1 and S_2 are the weights of the linear sum defined by equation (7).

The four elementary deformations are drawn in **Fig. 3.7**. The X's, in the center of each vector field, indicate the position of the singular points. The left side of **Fig. 3.7** shows the elementary deformations when the coefficients E, ω, S_1 and S_2 are set positive.

The elementary deformations are: expansion (panel *A*); counterclockwise rotation (panel *C*); positive horizontal shear, with elongation in the horizontal direction and contraction in the vertical direction (panel *E*); and oblique shear (panel *G*). When the coefficients E, ω, S_1 and S_2 are set negative the elementary deformations simply change their direction (right side of **Fig. 3.7**). They become: compression (panel *B*); clockwise rotation (panel *D*); negative horizontal shear, with contraction in the horizontal direction and elongation in the vertical direction (panel *F*); and oblique shear (panel *H*) with direction opposite to the shear of panel *G*.

Each linear vector field $\vec{V}_D$ is simply the superposition of the elementary fields shown in the left of **Fig. 3.7**. The coefficients E, ω, S_1 and S_2 determine which is the relative weight of each elementary deformation in building $\vec{V}_D$. This means that the parameters E, ω, S_1 and S_2, together with the coordinates p_x and p_y of the singular point $\vec{p}$, completely determine every linear planar vector field $\vec{V}_D$. For this reason, in the following, this set of six parameters is referred to as the *motion parameters*.

The singular point coordinates p_x and p_y are measured in pixels. The elementary deformation components E, ω, S_1 and S_2 are pure numbers and their magnitude varies from deformation to deformation. Usually a component can be considered negligible when its absolute value is one or more order of magnitude lower than the absolute value of the biggest component (see Section 3.4.4).

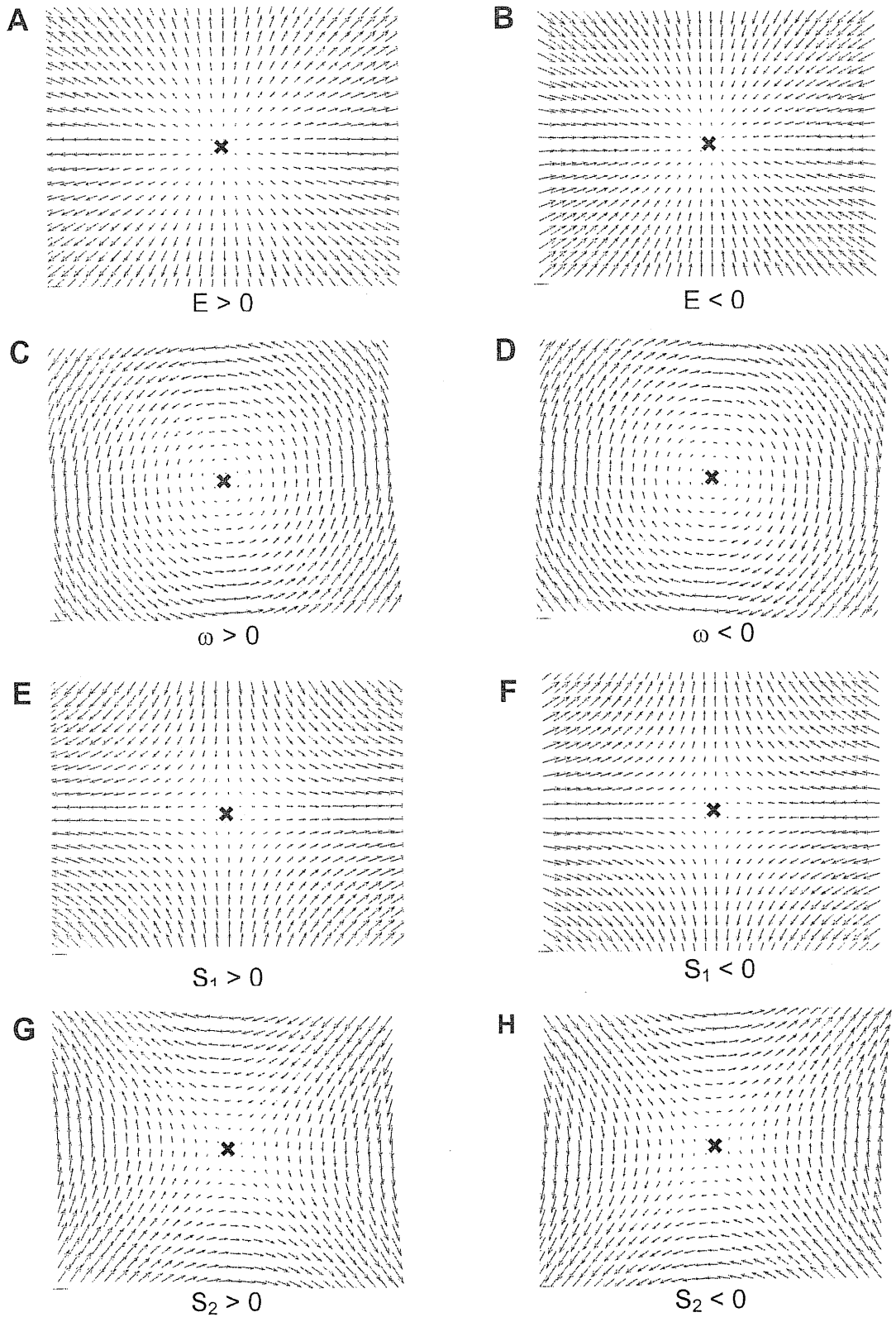

Figure 3.7 The elementary deformations. The sign of each elementary deformation component is reported at the bottom of each panel. *A*, Expansion. *B*, Negative expansion (compression). *C*, Counterclockwise rotation. *D*, Clockwise rotation. *E*, Horizontal positive shear. *F*, Horizontal negative shear. *G*, Oblique positive shear. *H*, Oblique negative shear.

3.4.3 Sequences of optical flows and their analysis

The computation of the optical flow and its linear approximation can be a powerful tool to study the dynamics of deformation. As described in the following, an instantaneous optical flow can be evaluated frame by frame in order to follow the time evolution of a contraction.

Given a sequence of images $I(x,y,i)$, $i = 1, \ldots, N$ of a deforming piece of skin, two kinds of optical flows can be considered: $\vec{O}_{Ti}$ and $\vec{O}_i$. The first optical flow $\vec{O}_{Ti}$, defined in Section 3.3.2, describes in image i the total displacement of the original features from image 0 to image i. The second optical flow $\vec{O}_i$ describes at every image i the instantaneous displacement of the features, i.e. the displacement from image $i-1$ to image i. The difference between the two optical flows is obvious when muscle contraction has reached a steady state: in this case $\vec{O}_i$ is null, while $\vec{O}_{Ti}$ is maximal.

The linear approximation described in Section 3.4.1 can be applied to the instantaneous optical flows $\vec{O}_i$ to obtain a sequence of instantaneuous linear fields $\vec{V}_{Di}$. This allows the computation of the motion parameters as functions of time and it allows their dynamical changes during deformation to be monitored. The units in which the time-varying deformation components (E_i, ω_i, S_{1i} and S_{2i}) are expressed are s^{-1} (or $frame^{-1}$) because they provide the strength of the elementary deformations in each time interval between two consecutive frames.

3.4.4 Linear vector flows on the leech skin

The total optical flows $\vec{O}_{Ti}$ shown in **Fig. 3.5** can be approximated with linear vector fields (see Section 3.4.1). Panels from ***A*** to ***D*** in **Fig. 3.8** illustrate the best linear vector fields (black arrows) approximating the corresponding optical flows reported in **Fig. 3.5**, which are associated to the skin maximal deformation caused by the stimulation of the L, 3 (DE),

110 (OE) and CV motoneurons. For each deformation, the linear approximation was computed in the region defined by the window drawn in each panel of **Fig. 3.5**. To allow a better comparison between raw optical flows and their linear approximations, the raw fields were also drawn (red arrows) inside the window selected to compute the linearization, in each panel of **Fig. 3.8**. The approximation with a linear vector field is quite satisfactory in the area of the skin defined by the windows. This area corresponds to the middle segment that is innervated by the impaled motoneurons. The linear approximation is less reliable near the pins used to fix the preparation, and also at the image borders.

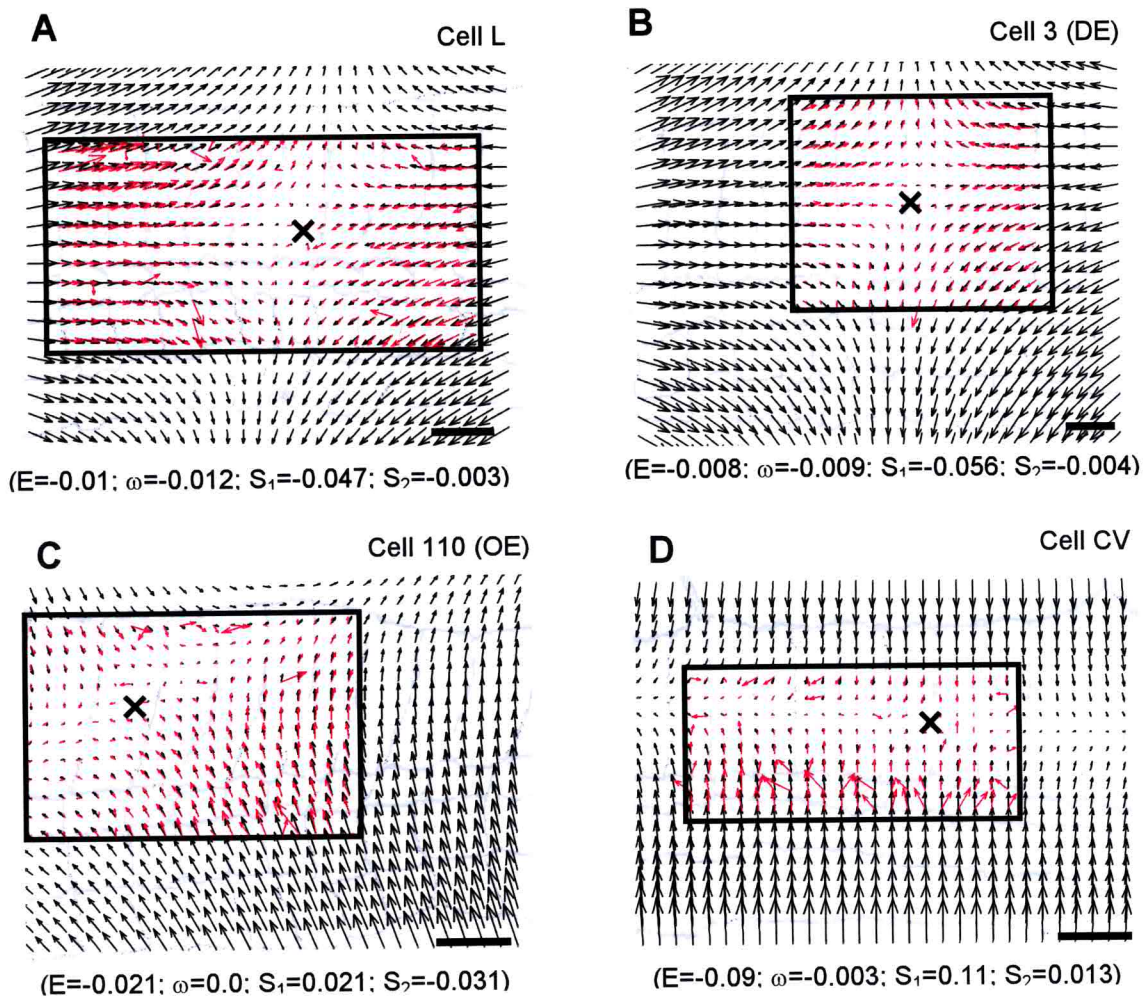

Figure 3.8 Linear approximation of optical flows and their analysis. *A-D*, The best linear approximations of optical flows shown in corresponding panels of Fig. 3.5. In each panel the linear approximation (black arrows) was computed in the area defined by the black window. Inside each window the corresponding raw field is also shown (red arrows). In each panel the X indicates the position of the singular point. The values of the elementary deformation components are reported at the bottom of each vector field. Scale bars 2 mm.

I reported the values of the elementary deformations E, ω, S_1 and S_2 at the bottom of each field in **Fig. 3.8**, and I indicated the position of the singular point by a cross. As expected from visual inspection, the main component for the longitudinal contractions (panels *A* and *B*) is a negative horizontal shear ($S_1 = -0.047$ and $S_1 = -0.056$ respectively for the cell L and the cell 3), while the other components are negligible (their ratio with S_1 varies between 0.05 and 0.2). The contraction produced by the CV motoneuron (panel *D*) is substantially different. It is the combination of two main elementary deformations: a positive horizontal shear ($S_1 = 0.11$) and a negative expansion ($E = -0.09$). The deformation induced by the motoneuron 110 (panel *C*) is still different, resulting from the combination of three main components: a negative oblique shear ($S_2 = -0.031$), a positive horizontal shear ($S_1 = 0.021$), and a negative expansion ($E = -0.021$).

Validity of linear approximation and choice of the linearization region

The reason for approximating optical flows, such as those shown in **Fig. 3.5**, with linear vector fields (**Fig. 3.8**), is to obtain a compact and quantitative description (i.e. based on few computable parameters) of the analyzed tissue deformation (see Section 3.4.2). The mathematical considerations recalled in Section 3.4.1 show that every planar and regular vector field can be locally approximated by a linear field by using a Taylor expansion up to the first order around its singular point. This means that: i) the linear approximation is always good in a sufficiently small region around the singular point; ii) the raw optical flow and its linear approximation are more and more different while moving away from the singular point. The critical question is to understand how large is the region in which the linear field provides an accurate approximation of the raw field. The size, shape and position of this region vary from case to case and must be appositely evaluated for each examined deformation.

I verified that, in the leech body-wall preparation, skin deformations caused by muscle contraction are usually very suitable for linear approximation, for two main reasons. First, in almost all experiments I performed, the optical flow had just one singular point. Not only when individual motoneurons were activated, as shown in **Figs. 3.5** and **3.8**, but also when skin or mechanosensory neurons were stimulated (see next Chapter). Second, in the skin area more strongly activated by the contraction, the amplitude of the raw optical flow usually increased smoothly and regularly while moving away from the singular point. These observations suggest that the pattern of deformation induced by muscle contraction on the leech body-wall can be well approximated by a linear field in a wide region around the center of the deformation.

Based on these considerations, a suitable region for computing the linear approximation of a raw optical flow can be a rectangular box satisfying the following properties: i) it must be centered on the presumed position of the singular point; ii) it must be positioned in the skin area strongly activated by the contraction (see Sections 4.2.1 and 4.3.2 for further comments on this issue); iii) it must include the most regular part of the raw filed. I used this procedure to compute the linear fields of **Fig. 3.8** and all other linear approximations shown in the present thesis. These rules impose rather precise limits to the shape and size of the linearization region. For example, when the contraction involves all the skin, as in the case of cells L and 110 (see **Figs. 3.5** and **4.1**), the linearization region can be very large. In this case, its size is decided by excluding from the linear approximation the zones of the skin in which the raw field is more irregular - near the edges of the preparation, because of the presence of the pins, or where highlights and shadows make the computation of the optical flow unreliable. Other deformations, for example those induced by motoneurons that selectively innervate a specific region of the body-wall, require linearization regions necessarily much smaller (see **Figs. 3.5** and **4.1** and discussion in Sections 4.2.1 and 4.3.2).

Every linearization region selected on the basis of these qualitative rules was accepted or rejected according to the accuracy of the resulting linear approximation. I estimated the goodness of the linear approximation by computing the following approximation error:

$$Err = \frac{\sum_i \left| \vec{V}_D(\vec{x}_i) - \vec{O}(\vec{x}_i) \right|^2}{\sum_i \left| \vec{V}_D(\vec{x}_i) \right|^2}, \qquad (9)$$

where $\vec{O}$ is the raw optical flow, $\vec{V}_D$ is its linear approximation, given by Equation (6), and i runs over all the points $\vec{x}_i$ framed by the rectangular box in which the linear approximation is computed. All the linearization regions used in the present study were selected in such a way to obtain an approximation error $Err \leq 0.15$. It was not necessary to develop an automatic procedure to find out the optimal region that minimizes the approximation error given by Equation (9). This is because, in general, the linear approximations resulted to be weakly sensitive to variations in size and shape of the selected region, provided this region satisfied the qualitative rules previously described. In most of the cases, varying the size of the linearization region in such a way as to increase the approximation error by 50%, I could affect the amplitude of the main elementary deformations by no more than 5%.

In conclusion, the linear approximations are very robust against variations of the region of the optical flow in which they are computed. This guarantees that, in general, the linear analysis of the contractions on the leech body-wall is meaningful, accurate and consistent from experiment to experiment and from preparation to preparation.

Monitoring the time course of muscle contraction

The qualitative shape of the optical flows $\vec{O}_{Ti}$ shown in **Fig. 3.5** and their linear approximation reported in **Fig. 3.8** did not change during development of contraction or during muscle relaxation: each vector just reversed its direction. This property is best shown by analyzing how the location of the singular point and the values of the four elementary deformations changed for the linear approximations of the instantaneous optical flows $\vec{O}_i$. **Fig. 3.9** shows the time evolution of the deformation parameters for the contraction induced by the cell L, previously described in **Fig. 3.5*A*** and **Fig. 3.8*A***. The instantaneous values of the parameters are obtained by computing and linearizing a sequence of 19 optical flows every 5 frames of the original image sequence (200 images). Namely, each flow $\vec{O}_i$ was computed by evaluating the displacement of the features from frame $i-5$ to frame i (the optical flows were under-sampled because the movement on the skin was too weak to be appreciated computing the flow frame by frame). The contraction phase lasted from second 1 to second 8; the relaxation phase started at second 11. From second 8 to second 11 the skin reached a stationary phase with unappreciable movements, where the optical flow vanished. As shown in panel ***A***, neither during contraction nor during relaxation did the location of the singular point change significantly in comparison to the width of a skin annulus (~80 pixels). The maximal change in the x position (x_p) was smaller than 50 pixels; the maximal change in the y position (y_p) was smaller than 80 pixels during contraction and slightly larger than 100 pixels during relaxation. This means that the singular point remained inside the central annulus of the segment for the whole duration of the movement, with some little oscillation only in the y direction. The singular point position changed only when the vector field vanished (time window from 7 to 12 seconds, data not shown). Similarly the relative amplitude of the four elementary deformations did not appreciably change (see panel ***B***) and S_1 was constantly the main

component of the motion, simply reversing its sign in the transition from the contraction to the relaxation phase.

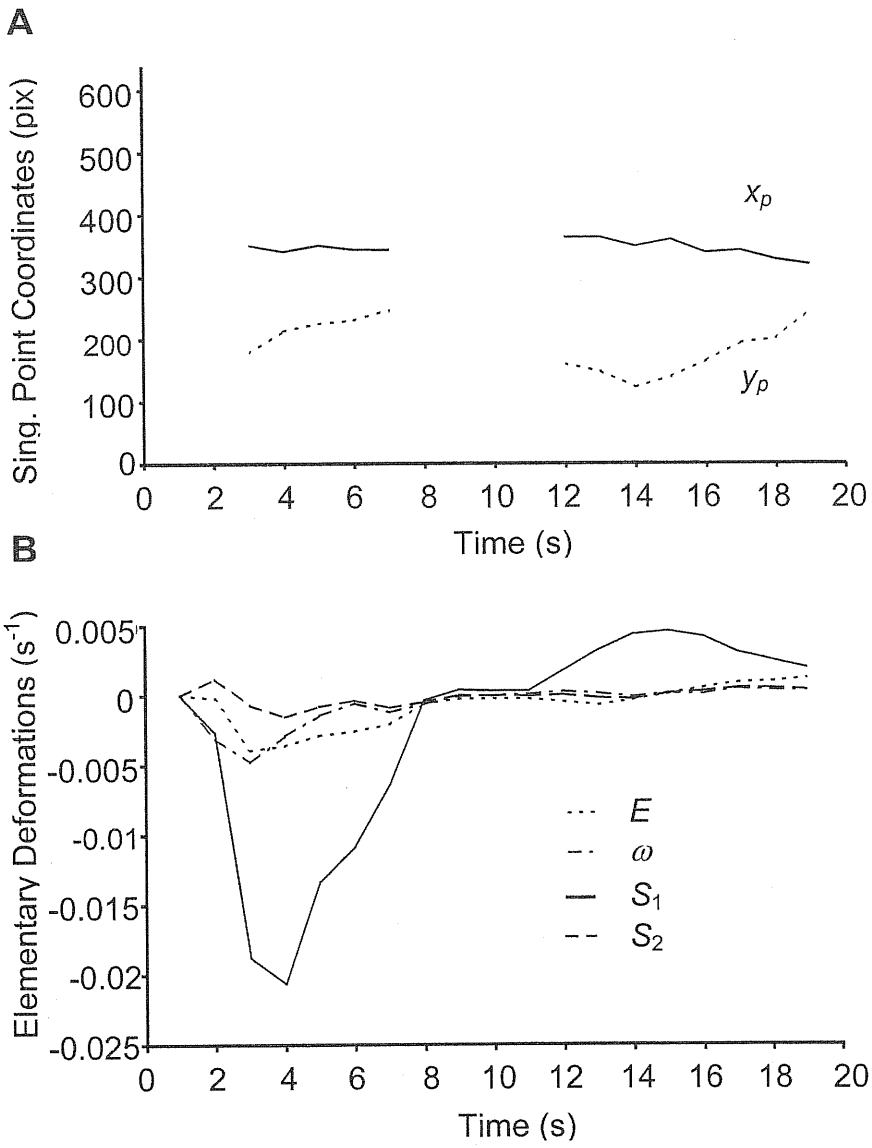

Figure 3.9 Time course of the motion parameters. *A*, Time evolution of the singular point location for the contraction induced by the cell L, previously described in Fig. 3.5*A* and Fig. 3.8*A*. Optical flows were computed every five frames of the original image sequence and then linearized to obtain the motion parameters. *B*, Time evolution of the four elementary deformation components for the same contraction.

The characterization of the skin deformation induced by the stimulation of specific motoneurons was consistent in different segments of the same preparation and in segments

dissected from different animals. In all the experiments the longitudinal motoneurons are characterized by a high negative S1 component. The motoneurons inducing transverse contractions, as the excitors of the circular muscles, are characterized by a high positive S1 and a high negative E coefficient. The oblique motoneurons, as cell 110, are characterized by a high S2 component in addition to a high positive S1 and a high negative E coefficient. These examples of contractions induced by motoneurons illustrate how it is possible to associate to each motoneuron in the leech ganglion a specific linear flow field and a set of parameters to identify it in a unique way, i.e. the coordinates of the singular point and the elementary deformation components. This procedure allows the construction of a basis of elementary deformations in which to decompose more complex contractions evoked, for example, by touching the skin of the animal (See Chapter 4).

3.5 Discussion

The results presented in this chapter show that usual tools of image processing developed in computer vision can be used to analyze image sequences of a contracting piece of skin and to quantify muscle contraction in a new and useful way. The proposed method can be applied to characterize contractions and deformations of any biological tissue with enough landmarks or visual texture. The analysis of elementary deformations (see Section 3.4) will be successful with almost flat tissues where relevant deformations are in essence two-dimensional.

As shown in Section 3.2, the movement of selected features on the leech skin can be followed - from one image to the next - by computing the correlation between patterns of gray levels in windows centered on the feature in consecutive images. This algorithm provides a dense optical flow, which is the displacements' map of points on an arbitrary grid. This optical flow is a simple and efficient way to obtain a 2D vector representation of the contraction induced on the skin by the activation of the underlying muscle fibers.

The proposed approach is superior in some important aspects to the classical way of quantifying tissue deformations by means of a displacement transducer in that it provides also the direction of these displacements. In addition, the proposed method does not need the insertion of a hook in the tissue, which to some extent can disturb the contraction itself. The proposed optical method provides measurements which are in excellent agreement with those obtained by transducers in physical contact with the tissue (see **Fig. 3.6**) and can help to investigate biomechanical properties of biological tissues. The absolute sensitivity depends on the optics used and with the appropriate objectives the displacements of just a few microns can be reliably detected. Small displacements, leading to sub-pixel displacements in successive images, are not easily detected. In this case three options are available: first, use a higher magnification; second, sub-sample the image sequence; and third use an algorithm allowing sub-pixel accuracy. The temporal resolution of the proposed method depends on the speed of the image acquisition system in use: in order to have the temporal sensitivity of usual transducers - higher than 1 kHz - it is necessary to use ultra-fast and expensive cameras and acquisition systems. Therefore when it is necessary to have a high temporal resolution, usual transducers offer a simple and cheap solution. Besides, force transducers are necessary when a direct measurement of the force exerted by a contracting tissue is required.

The proposed technique for the analysis of image sequences of contracting muscles provides highly precise and reliable data and results because many of the problems commonly encountered using the optical flow are not present. Namely: i) no changes of light intensity affect the preparation because the illumination is under the control of the experimenter and can be kept constant; ii) the imaged object is flat and its surface can be considered as flat or almost flat, thus greatly simplifying the analysis; iii) no relative motions are present in the scene and the resulting optical flow does not have any discontinuity and can be well approximated by a linear 2D vector field.

The experimental results and the analysis reported in Section 3.4 show how mathematical tools of the theory of linear deformations can be used to process these optical flows. The approximation of the optical flow with a linear vector field allows the matrix of the linear transformation to be computed and to recover the elementary components of the deformation: expansion (E), rotation (ω) and shear (S_1 and S_2) coefficients and the coordinates of the singular point. These motion parameters completely characterize every local contraction induced on a planar surface, such as a piece of skin flattened in a measuring set-up. The proposed approach is rather powerful because it provides a compact and reliable measure of the global deformation occurring at the surface of the leech skin. The time evolution of these parameters, obtained from sequences of instantaneous optical flows of the same experiment, allows the dynamics of the contraction to be monitored and to separate the contribution of different motoneurons in different phases of the movement (See Chapter 4).

The amount of stretching exerted on the leech muscles depended on the pinning of the skin and was quite variable from preparation to preparation. Nevertheless, the classification of the contractions, which was made on the base of the motion parameters (Section 3.4.4), was robust and slightly sensitive to the way in which the skin was pinned. As expected, the variability of the stretching of the body wall affected the amplitude of the detected displacement on the skin. But the shape of the optical flows and the relative amplitude of the main deformation components were constant from preparation to preparation. The singular point position was more sensitive to the pinning, but a typical trend for each motoneuron was found. This strongly suggests (see **Fig. 3.8**) a practical and powerful way to classify the skin deformations induced by all the excitor motoneurons in the leech ganglion: each motoneuron contraction belongs to a specific class characterized by a unique set of motion parameters (See Chapter 4).

The proposed method, demonstrated here by characterizing muscle contractions in the body wall of the leech, is expected to be widely applicable to the measurement of displacement in flat tissues rich in landmarks. Such a characterization cannot be obtained with force transducers. The present method can also be applied to analyze less texture rich preparations by adding artificial markers, such as beads, on their surface.

4 Using optical flow to characterize sensory-motor interactions in a segment of the medicinal leech

Once verified that computation of the optical flow from image sequences of the contracting leech skin is a powerful and reliable tool to quantify leech motor behavior (see previous Chapter), I extensively applied this method to characterize local sensory-motor interactions involving a body segment of the leech.

The part of my Ph.D. project described in this Chapter aimed at investigating the distributed processing of leech motor responses at the level of muscle activation. Namely, the goal of the experiments described below was to demonstrate that complex motor behaviors induced by mechanosensory stimulation of the leech skin result from a flexible combination of a small number of basic behavioral units. These behavioral units correspond to the functional patterns of deformation that activation of different sets of motoneurons and muscles induces on the leech body-wall.

4.1 Introduction

As recalled in Section 1.1.3, in the leech, mechanical inputs are transduced by 7 pairs of mechanosensory neurons; 3 specific for light pressure (touch or T cells), 2 for strong pressure (pressure or P cells), and 2 for noxious mechanical stimuli (N cells). The leech motor system consists of 21 pairs of excitatory motoneurons in each ganglion that innervate longitudinal, oblique and circular fibers (see Section 1.1.4 and **Fig. 1.1**). Muscle contractions induced by activation of these motoneurons have been extensively investigated using force and length transducers, electromiography and electrophysiology tools (Stuart, 1970; Mason and Kristan, 1982; Kristan, 1982; Norris and Calabrese, 1987; Lewis and Kristan, 1998). However, exhaustive analysis of the relationship between local

mechanosensory stimulation and pattern of muscle contraction induced by consequent motoneuron activation has not been performed, so far.

This Chapter describes how muscle contractions underlying sensory-motor responses in the body-segment of a leech were characterized by using videomicroscopy and computing the optical flow (see Chapter 3). The first step in my analysis was to characterize the deformations induced by longitudinal, circular, and oblique motoneurons. Experiments performed on many different body-wall preparations (see Section 2.1.2) showed that these deformations are sufficiently different so that motoneuron classes can be easily distinguished. The next step was to understand how these basic deformations, associated to individual motoneurons, could combine when more than one motoneuron were simultaneously active. Experiments in which I simultaneously stimulated pairs of motoneurons showed that deformations induced by different motoneurons sum linearly, i.e., add in the simplest way. This means that any given skin deformation can be decomposed into components caused by contraction of longitudinal, circular, and oblique muscles: by viewing a piece of skin when a mechanosensory neuron is stimulated, it is possible to identify which classes of motoneurons are activated. Therefore, the final step in my analysis was to investigate the pattern of deformation produced by activation of different mechanosensory neurons and by mechanical stimulation of the skin. These experiments showed that the local bending, during which the leech bends away from the stimulated site (see Section 1.2.2), is sustained by coactivation of circular and longitudinal motoneurons and is almost entirely mediated by P cell activation (Kristan, 1982).

4.2 Results

4.2.1 Characterization of the contractions induced by leech motoneurons

I used the body-wall preparation described in Section 2.1.2 to characterize the leech skin contractions induced by excitatory motoneurons. I stimulated individual leech

motoneurons to obtain a strong, sustained contraction of the corresponding muscles. The resulting skin movements were viewed with a CCD camera mounted on a dissecting microscope (see Section 2.4). Image sequences of the contracting skin were acquired at 5 Hz and analyzed as described in Chapter 3 to obtain optical flows: the two dimensional vector fields that described the displacement of a 30x20 point grid on the leech skin. Each optical flow was computed from the resting state to the time of maximal contraction.

Fig. 4.1 shows the optical flows obtained during maximal contraction produced by the stimulation of 9 motoneurons: longitudinal L (A); dorsal longitudinal excitatory (DE) 3 (B); dorsal longitudinal excitatory (DE) 5 (C); dorsal longitudinal excitatory (DE) 107 (D); ventral longitudinal excitatory (VE) 8 (E); ventral longitudinal excitatory (VE) 108 (F); oblique excitatory (OE) 110 (G); circular ventral (CV) (H); and flattener excitatory (FE) 109 (I). In each panel the arrow heads indicate movement direction and the arrow length indicates displacement. The optical flows are drawn on a gray background showing pieces of body wall whose contractions were analyzed.

These flows are in excellent agreement with the deformations expected from prior descriptions of these motoneurons (Stuart, 1970). Motoneurons L, 3, 5, 107, 8, and 108 innervate longitudinal muscles, muscles that run parallel to the length of the leech and are responsible for its shortening (Stuart, 1970; Nicholls and Purves, 1970; Mason and Kristan, 1982; Kristan, 1982). The L motoneuron innervates the whole half-segment and the corresponding contraction involves all of the skin, with the center approximately in the middle of the half-segment. Motoneurons 3, 5 and 107 are dorsal excitors, innervating only the dorsal fibers of the longitudinal muscles, and their contraction involves mainly the dorsal side of the half-segment. Motoneurons 8 and 108 are ventral excitors and deform the ventral part of the skin. Cell 110 (Stuart, 1970) excites oblique muscle fibers and induces a contraction in an oblique direction in respect to the length of the leech.

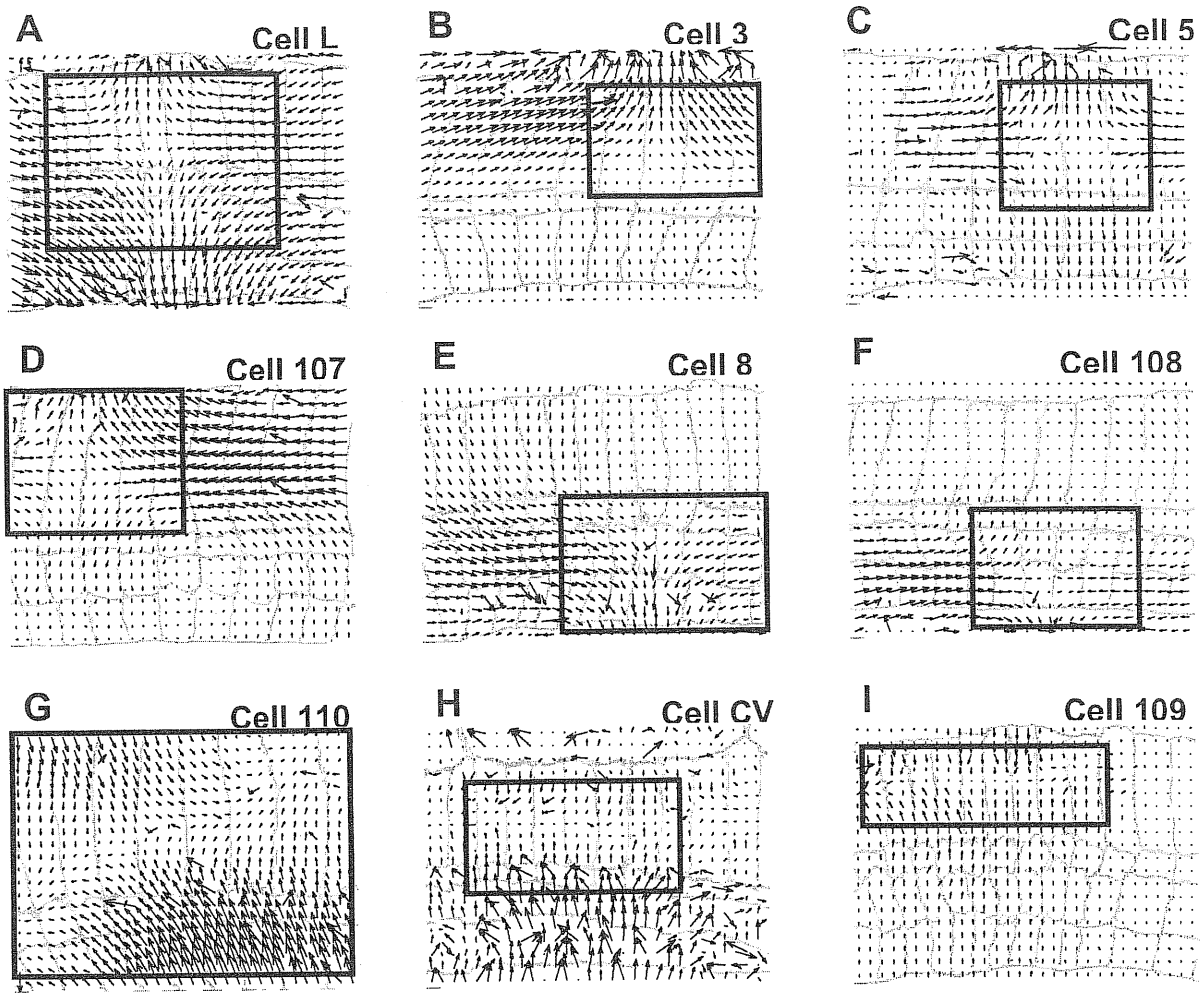

Figure 4.1 Optical flows associated to 9 different leech motoneurons. Panels *A* to *I* show the optical flow computed on a 30x20 grid for the skin deformations caused by intracellular stimulation of motoneurons L, 3, 5, 107, 8, 108, 110, CV and 109, respectively. The data were obtained from 7 different preparations. Each motoneuron was stimulated with a depolarizing step of current causing a spike discharge between 30 and 40 Hz lasting from 1 to 6 seconds. Optical flows were obtained as described in Chapter 3. A drawing of the segment annuli is shown in gray in each panel, annulus width is between 0.5 and 0.8 mm. Scale bars in the bottom of each panel are 2 mm wide. The top boundary of the preparation is the dorsal midline of the body; the bottom boundary is between the lateral line and the ventral midline. Anterior is to the left. The central annulus of the innervated segment is, starting from left: the 6th for panels *A*, *G*, *H* and *I*; the 5th for panels *B*, *D*, and *F*; the 4th for panel *C*; and the 8th for panel *E*. The region of optical flow framed by the solid box was used to compute the linear approximations shown in Fig. 4.2. In order to make the direction of the movement more clear, the fields shown in *E*, *F*, *G* and *I* are drawn with a magnification respectively 1.5, 2, 1.5 and 2 times larger.

The CV motoneuron innervates circular fibers situated in the lateral ventral side of the half segment (Stuart, 1970) and induces a contraction in the transverse direction with a displacement field perpendicular to that induced by the longitudinal motoneurons. Motoneuron 109, referred to as the flattener (Stuart, 1970), innervates dorsoventral fibers, responsible for the flattening of the leech body. Its activation induces a transverse contraction similar to that produced by the CV motoneuron.

The optical flows shown in **Fig. 4.1** can be approximated with linear vector fields. Panels A to I in **Fig. 4.2** illustrate the best linear vector fields approximating the corresponding optical flows reported in **Fig. 4.1**. For each deformation, the linear approximation was computed in a region surrounding the stationary point. This linearization region is indicated by the window drawn in each panel of **Fig. 4.1** and **Fig. 4.2** (the position of the stationary point is indicated by the X). Comparison of corresponding panels in **Figs. 4.1** and **4.2** shows that the linear approximation is satisfactory in the area of skin where the original optical flow (**Fig. 4.1**) is large and poor outside it. This is not surprising because almost all leech motoneurons innervate selectively just a narrow region of muscles in a half segment. For this reason, in almost all the panels of **Fig. 4.1** the contraction is restricted to a small area of the skin. By definition, the amplitude of a planar vector field increases linearly while moving away from the singular point (see **Fig. 4.2**). This explains why linear approximations have large amplitude in areas where corresponding real optical flows are almost zero. For example, in cell 3 (a dorsal excitor) the linear approximation is good not only inside the linearization region but also in a wider dorsal area of the skin where the deformation amplitude is significantly greater than zero (compare **Figs. 4.1*B*** and **4.2*B***). On the contrary, in the ventral region the deformation is almost zero and a comparison with the linear approximation is not appropriate. In summary, the contraction induced by each motoneuron is approximately

linear in the skin area that is being functionally innervated. In this area, the optical flow and its linear approximation are highly repeatable from preparation to preparation, allowing a precise classification of the different classes of motoneurons (see **Fig. 4.4**). Outside this area the optical flow is almost null and its shape is variable from preparation to preparation. This is because the observed deformation is passively driven by the active part of the skin and it is significantly influenced by the location of pins holding the preparation.

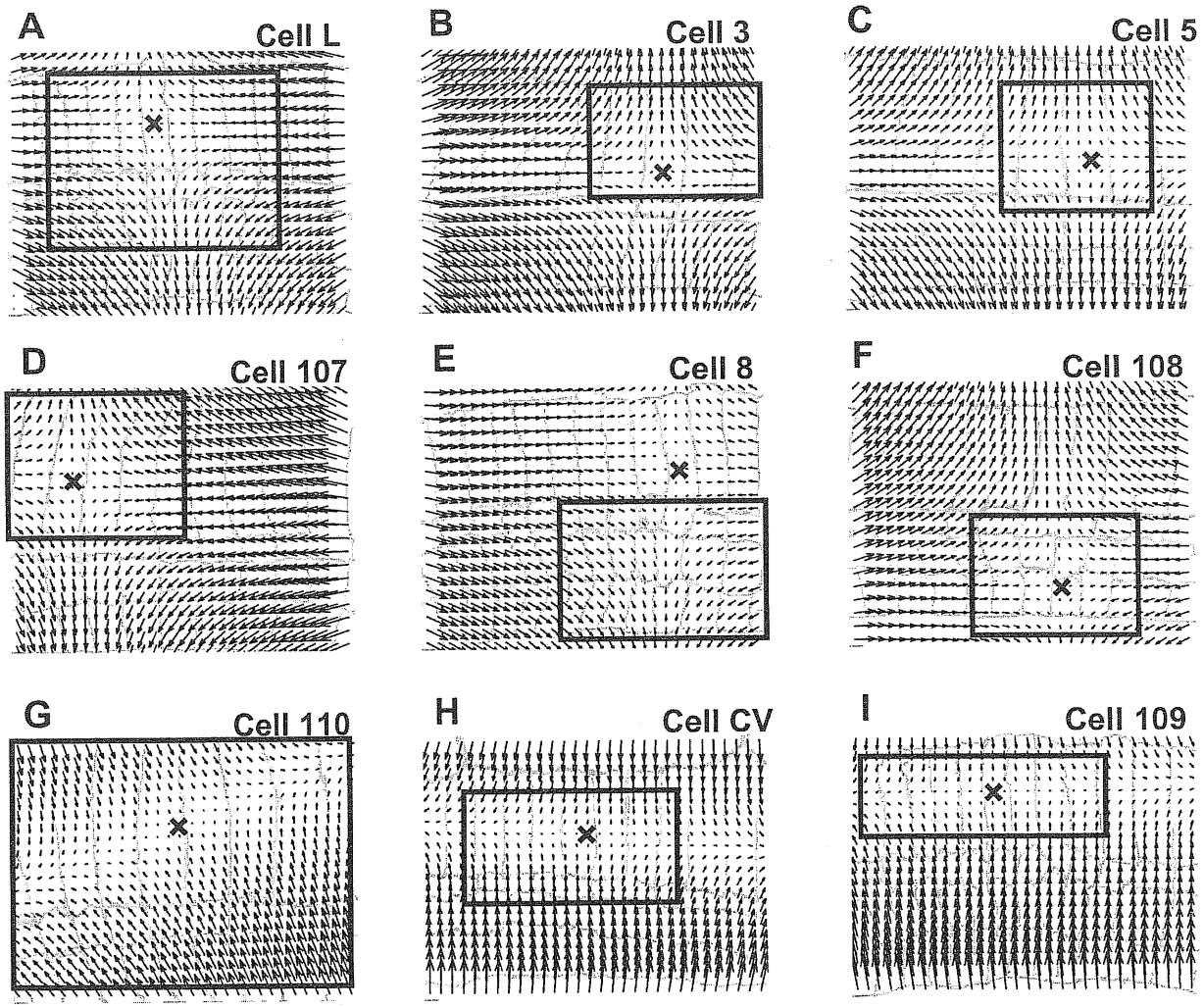

Figure 4.2 Linear approximations of the optical flows. Panels *A* to *I* show the vector fields obtained by linearly approximating the optical flows shown in the solid boxes in the corresponding panels of Fig. 4.1. In each panel the X indicates the position of the singular point. The drawings of the segment annuli are the same of Fig. 4.1. The agreement between the original optical flow (Fig. 4.1) and the linear approximation (Fig. 4.2) is good within the box and in the skin area mainly involved in the contraction and poor outside.

Note that the use of linear approximations in characterizing motoneuron contractions was primarily suggested by the finding that almost all optical flows induced by leech motoneurons had only one singular point, i.e. only one stationary point. This is the first requirement for a vector field to be linear (Sommerfeld, 1974). Indeed, all optical flows shown in **Fig. 4.1** and in the following figures have only one singular point. The only exception is the optical flow shown in **Fig. 4.1*D***, which has another singular point located in the ventral side of the skin (6^{th} annulus from left; the vector field rotates around it). This area, which is only passively moving, is not included in the linearization region (box in **Fig. 4.1*D*** and **Fig. 4.2*D***) for the reasons previously discussed. In characterizing the contraction the only relevant singular point is located inside the linearization region, in the dorsal side of the skin, where the deformation is large (X in **Fig. 4.2*D***).

Approximating skin deformations with linear vector fields is a powerful tool, because, as shown in Section 3.4, every planar linear field is uniquely characterized by a set of six parameters (Giachetti and Torre, 1996). These parameters are the coordinates p_x and p_y of the singular point and the four elementary deformations E, ω, S_1 and S_2, defined by Eq. (3.2). The computation of these six parameters allows a quantitative and reliable comparison among the deformations induced by different types of motoneurons in the same preparation and in segments dissected from different animals. The result of this comparison, for the 9 types of motoneurons previously analyzed in **Figs. 4.1** and **4.2**, is reported in **Figs. 4.3** and **4.4**.

Fig. 4.3 shows the singular point positions of the various motoneurons in different preparations. The gray background reproduces the annular margins of a representative body wall preparation; the central annulus is indicated by the arrow. Panel *A* shows the singular point positions for the contractions induced by longitudinal motoneurons 3, 5, 8, 107, 108 and L.

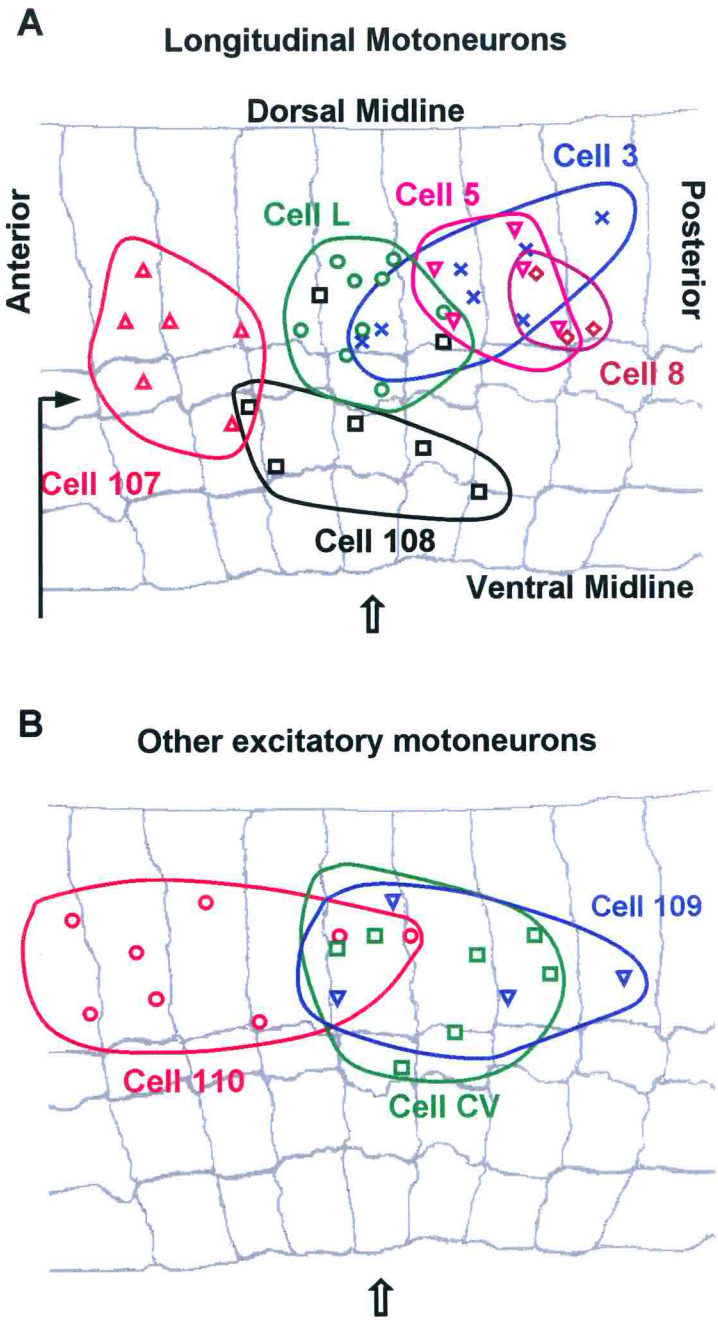

Figure 4.3 Distribution of the location of the singular points for the skin deformations induced by individual motoneurons in different preparations. *A*, The singular points of longitudinal motoneurons L (○), 3 (×), 5 (▽), 107 (△), 8 (◇) and 108 (□) in 9, 7, 5, 6, 3 and 7, different preparations, respectively. *B*, The singular points of the oblique motoneuron 110 (○), the circular motoneuron CV (□) and the flattener motoneuron 109 (▽) in 8, 7 and 4 different preparations, respectively. The gray background in panels *A* and *B* reproduces the annular margins of a representative body wall preparation; the arrow indicates the central annulus.

In panel *A* six specific regions, in which each motoneuron's singular points aggregate, are apparent. The size of these regions varies from 1.5 to 3 mm in the longitudinal direction (2 to 4 annuli) and from 1 to 2.5 mm in the transverse direction. As shown in panel *B*, singular points of oblique, circular and flattener motoneurons aggregate in clusters of slightly wider area (the singular points of motoneuron 110 span about five annuli).

Fig. 4.3 shows that the singular points of the contractions induced by the same motoneuron in different preparations tend to cluster in a specific skin area, although their exact location is rather variable from experiment to experiment. Part of this variability is likely an artifact due to small differences in the body-wall preparations I used. These differences can be produced by variations in the amount of body-wall removed from the leeches and by little damages to small nerve branches or muscle fibers during dissection. Another unavoidable source of variability is the location of the pins used to hold the preparation and the amount of tension they exert on the body-wall. Finally, it must be considered that, although the elementary deformations are very robust against variations of the selected linearization window (see comments on Section 3.4.4), the singular point location is, in general, much more sensitive to shape and size of the window in which linear approximation is computed. In conclusion, the previous considerations strongly support the idea that the observed variability in the singular point position is mainly due to artifacts introduced by the dissection procedure, the pinning and the linear approximation. In the present thesis I did not investigate how much of such variability is biological, i.e. due to properties of muscle activation or innervation by motoneurons. This is because the singular point position is only one of the parameters I used to classify the contractions induced by different motoneurons. This classification if mainly based on the computation of the elementary deformations that, as shown below, is highly reliable and robust against the sources of variability previously described.

Fig. 4.4 summarizes the relative weights of the four elementary deformations E, ω, S_1 and S_2, for the 9 motoneuron types shown in the previous figures. In each histogram, the gray bars are the mean relative weights of each elementary deformation (before being averaged, the elementary deformations were normalized to the absolute value of the largest of them). Negative longitudinal shear S_1 was the main deformation component in contractions induced by longitudinal motoneurons ($S_1 = -1$, with standard deviation = 0, for almost all of the longitudinal motoneurons analyzed in the figure). The other elementary deformation components were negligible. Their mean relative weight was usually lower than 0.15 (in absolute value) and if it reached higher values (as the rotation component $|\omega| > 0.25$ for motoneurons 3, 107 and 108) its uncertainty was large. Motoneurons inducing transverse contractions (cell CV and cell 109) were characterized by high positive longitudinal shear S_1 and high negative expansion E. The oblique motoneuron (cell 110) was characterized by high negative oblique shear S_2, high positive S_1, and high negative expansion E. For all motoneurons inducing longitudinal and transverse contractions, the main elementary deformation was $|S_1| = 1$ with no uncertainty, i.e. zero standard deviation. The only exception was cell 108, in which, in 1 out of 7 experiments, $|\omega|$ was bigger than $|S_1|$ and for this reason the uncertainty – and the standard deviation - on S_1 is not zero. The same consideration applies to cell 110, in which, in 1 out of 8 experiments, $|E|$ was bigger than the main elementary deformation $|S_2|$.

For each motoneuron included in the means shown in **Fig. 4.4**, I decided to normalize the elementary deformations to the largest of them, because I wanted to compare only the shapes of the contractions induced by the same kind of motoneuron in different preparations. The normalization I adopted allows for such a comparison, because it removes the variability in the intensity of the contractions that the same kind of motoneuron produces in different dissected preparations. In other words, this normalization

is essential for assessing how reliable is a classification of motoneuron contractions based on the relative weight of the elementary deformations. For this reason, **Fig. 4.4** is the only figure in which such normalization has been used. In all the other figures of the thesis the elementary deformations are not normalized, in such a way to allow for a comparison between both shape and intensity of the analyzed deformations (see, for example, **Figs. 4.6** and **4.7**).

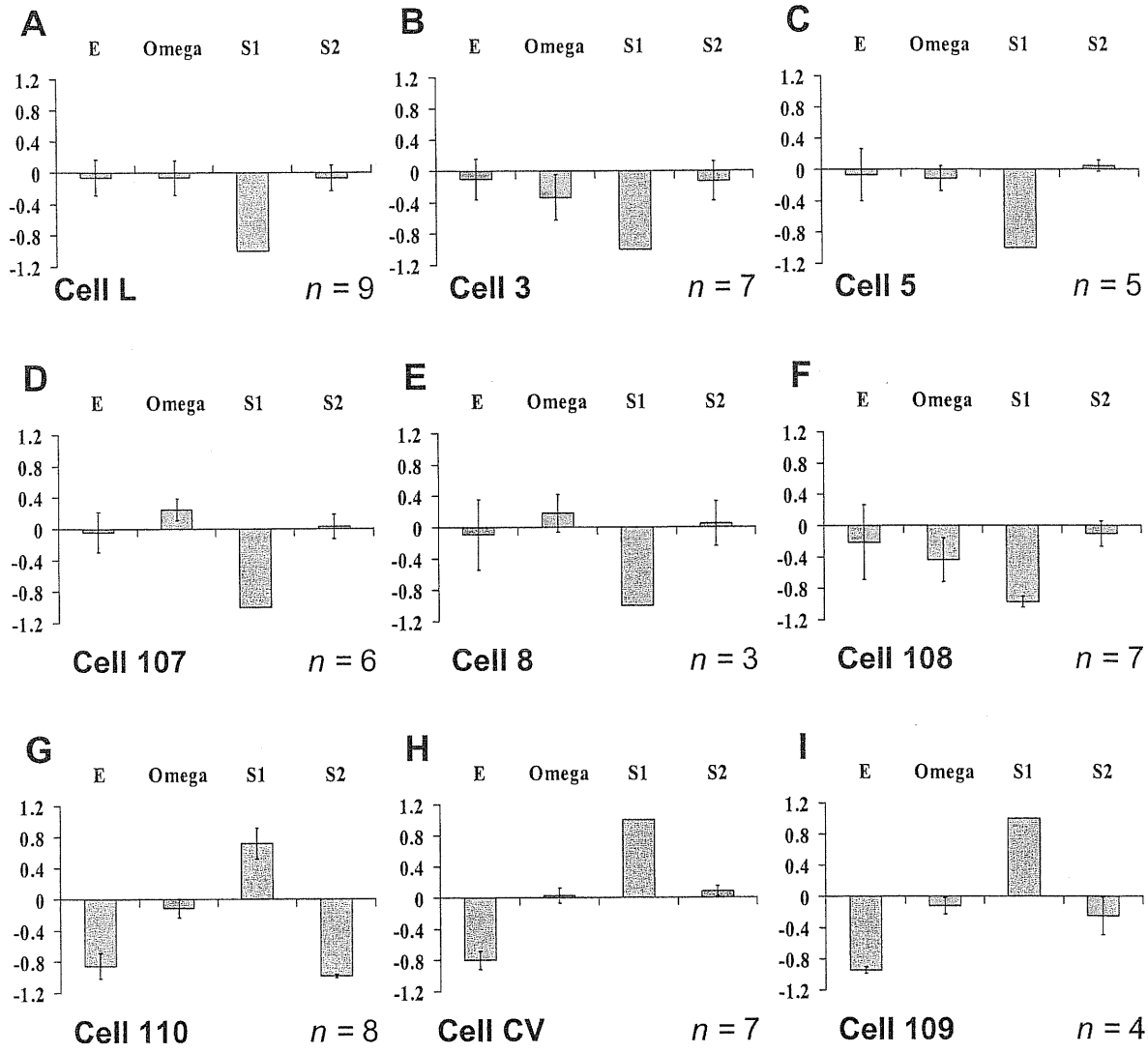

Figure 4.4 The average relative weights of the elementary deformations for different leech motoneurons. Panels *A* to *I* show the mean relative weight of expansion (E), rotation (ω), and the two shears S_1 and S_2 for the 9 motoneurons analyzed in Figs. 4.1 and 4.2. All components were normalized to the largest of them before averaging. The number of preparations used for each motoneuron is reported in the lower right corner of each panel. Error bars are the standard deviations of the mean.

Fig. 4.4 shows that the contractions induced by single motoneurons can be classified on the basis of their main elementary deformations. This classification is highly reliable because the uncertainty of the relative weight of the main elementary deformations is low (see the error bars in **Fig. 4.4**). Moreover, this classification is in strict agreement with the anatomical arrangement of the leech muscle fibers (Stuart, 1970): i) longitudinal (high $S_1 < 0$); ii) circular and flattener (high $S_1 > 0$ and $E < 0$); iii) oblique (high S_2, $S_1 > 0$ and $E < 0$). More precise classification of the contractions can be achieved by exploiting the differences in the location of the singular point for contractions induced by motoneurons belonging to the same class (see **Fig. 4.3**). Even finer classification can be obtained by looking at the region of the skin involved in the contraction, as originally done by visual inspection by Stuart (1970). For example, motoneurons L and 3 produce almost a pure negative longitudinal shear S_1 (**Fig. 4.4*A*** and ***B***) and the regions in which the singular points can be found are partially overlapping (**Fig. 4.3*A***). Nevertheless, the deformation induced by motoneuron 3 is restricted to the dorsal side of the skin (**Fig. 4.1*B***), while the contraction of motoneuron L affects both the ventral and dorsal part of the skin (**Fig. 4.1*A***). Similarly the motoneurons CV and 109 have similar elementary deformations (**Fig. 4.4*H*** and ***I***), but the contraction of motoneuron 109 is primarily evident in the dorsal part (**Fig. 4.1*I***), while that of the CV motoneuron is in the ventral part (**Fig. 4.1*H***).

Table 4.1 summarizes these properties for nearly all characterized excitatory motoneurons of the leech segmental ganglion. In addition to the 9 motoneurons previously described, the classification of the other longitudinal (cells 4 and 106), circular (cells 12 and 112), and oblique (cell 111) motoneurons is provided on the base of: i) the area of skin involved in the contraction; ii) the location of its singular point; iii) its major elementary deformations. The number of preparations used to validate the classification presented in **Table 4.1** ranges from 3 to 10, depending on the analyzed motoneuron.

Table 4.1 Properties of excitatory leech motoneurons

Motoneuron	Area of Contraction	Location of Singular Point	Major Components
3	Dorsal	Dorsal / Middle-Post.	$S_1 < 0$
4	Ventral	Dorsolateral / Post.	$S_1 < 0$
5	Dorsal	Dorsal / Post.	$S_1 < 0$
8	Ventral	Dorsal / Post.	$S_1 < 0$
12	Ventrolateral	Lateral / Middle	$S_1 > 0$; $E < 0$
106	Whole segment	Dorsolateral / Middle	$S_1 < 0$
107	Dorsal	Lateral / Ant.	$S_1 < 0$
108	Ventral	Ventrolateral / Middle	$S_1 < 0$
109	Dorsolateral	Dorsal / Middle-Post.	$S_1 > 0$; $E < 0$
110	Whole segment	Dorsal / Middle-Ant.	$S_2 < 0$; $S_1 > 0$; $E < 0$
111	Whole segment	Dorsal / Middle-Post.	$S_2 > 0$; $S_1 > 0$; $E < 0$
112	Dorsolateral	Dorsal / Middle-Post.	$S_1 > 0$; $E < 0$
CV	Ventrolateral	Dorsolateral / Middle-Post.	$S_1 > 0$; $E < 0$
L	Whole segment	Dorsolateral / Middle	$S_1 < 0$

Table 4.1 Properties of the excitatory leech motoneurons. Four classes of motoneurons are analyzed: i) longitudinal motoneurons 3, 4, 5, 8, 106, 107, 108, and L; ii) circular motoneurons 12, 112, and CV; iii) oblique motoneurons 110 and 111; and flattener motoneuron 109. The classification of the motoneurons is provided on the basis of: i) the area of skin involved in the contraction (from ventral to dorsal, along the transverse direction, parallel to the body annuli); ii) the location of its singular point (from ventral to dorsal, along the transverse direction and from anterior to posterior, along the longitudinal direction); iii) its major elementary deformations. The number of preparations used to validate the classification ranges from 3 to 10, depending on the analyzed motoneuron.

4.2.2 Time evolution of the contractions induced by single motoneurons

Fig. 4.5 shows the time evolution of the elementary deformations for the contractions induced by motoneurons 107 (panel *A*), 110 (panel *B*), and 12 (panel *C*), chosen as representative of the three possible classes of motoneuron contractions. I obtained the instantaneous values of the elementary deformations for cells 107 and 110 by computing and linearizing a sequence of 19 optical flows every 5 frames of the original image sequence (100 images). In the same way, I computed and linearized 9 optical flows from the sequence of 50 images describing the contraction induced by cell 12. The bar in the top of each panel gives the duration of the spike discharge induced in each motoneuron. Note that the ordinate values are velocities; these plots show how the rates of change of each elementary deformation proceed throughout the contraction that each motoneuron induces.

Motoneuron 107 is an excitor of the ventral longitudinal muscles. Its main elementary deformation was a negative longitudinal shear S_1 (**Fig. 4.4*D***). The contraction phase lasted from second 2 to second 6; the relaxation phase started at second 9, 2 seconds after the cessation of the stimulus. From second 7 to second 8 the skin reached a stationary phase with not appreciable movements. **Fig. 4.5** shows that the relative amplitude of the four elementary deformations did not appreciably change during the whole deformation. S_1 was consistently the main component of the deformation, simply reversing its sign in the transition from the contraction to the relaxation phase. **Fig. 4.5** also shows that, for cell 107, the contraction phase was much shorter and faster (high and narrow negative peak of S_1) than the relaxation phase (smaller and broader positive peak of S_1).

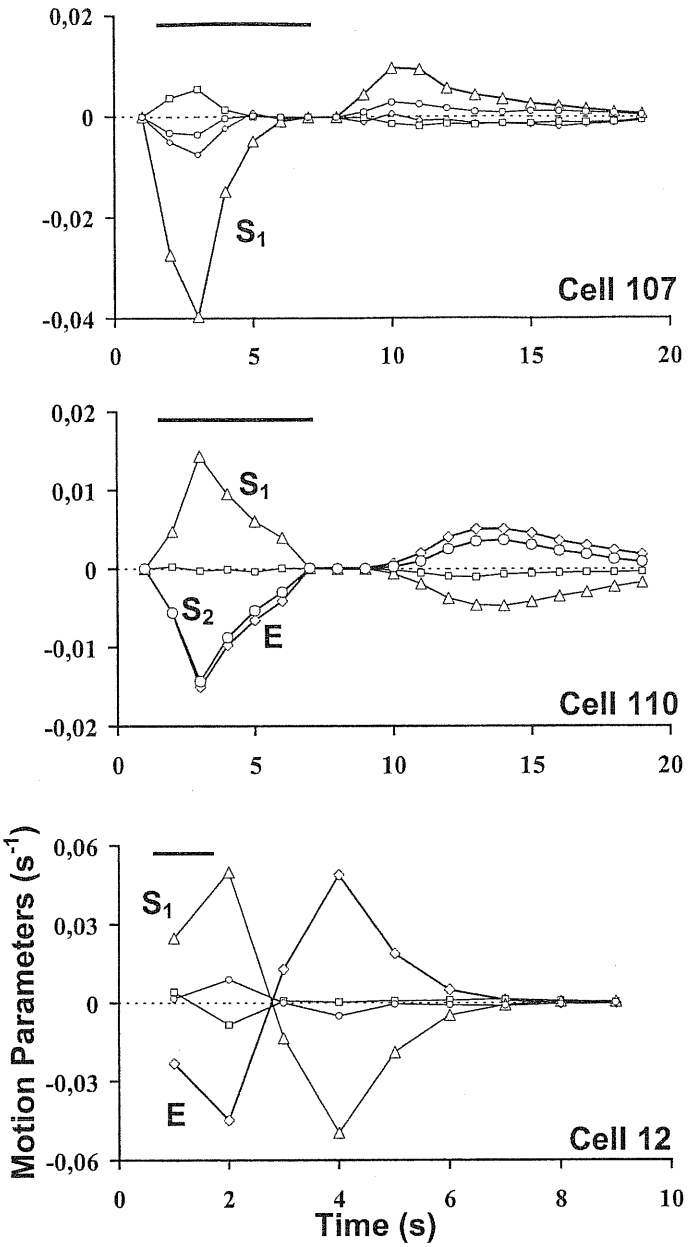

Figure 4.5 Dynamics of the deformations induced by three different classes of motoneurons. The time course of the elementary deformations for the contractions induced by motoneurons 107, 110 and 12 were obtained from the sequence of instantaneous optical flows. The motoneurons were stimulated to fire at a frequency between 20 and 40 Hz for 6 (cell 107 and 110) or 1 (cell 12) seconds. The bar at the top of each panel shows stimulation duration. The units in which the time varying deformations are expressed are s^{-1} because the data were calculated from every fifth image and the images were acquired at 5 Hz. Each panel shows the time evolution of expansion E (◇), rotation ω (□), longitudinal shear S_1 (△), and oblique shear S_2 (○).

The time course of motoneuron 110's deformation was similar; the deformation consisted of a short and rapid contraction, a stationary phase, and a long slow relaxation. The main elementary deformations (S_2, S_1 and E), had an almost identical time course.

Cell 12 (an excitor of the ventrolateral circular muscles) showed a similar time course of its main elementary deformations: S_1 and E. The main difference from the previous contractions was that the relaxation phase was shorter and faster: the peaks of S_1 and E in the relaxation phase were as large as their peaks in the contraction phase. As a general rule, contractions induced by the excitors of circular muscles always relaxed faster than the contractions induced by longitudinal and oblique motoneurons (data not shown).

The elementary deformations of the other longitudinal and circular motoneurons had similar time courses. For each motoneuron the relative amplitudes of the four elementary deformations did not appreciably change during the whole deformation. That is, although the amplitude of the vectors changed with time, according to the intensity of the contraction, the direction of the vectors was substantially constant, simply reversing sign from contraction to relaxation.

4.2.3 Combination of vector fields induced by single motoneurons

The characterization of skin deformations described in the previous sections was obtained when each motoneuron was stimulated individually. The next step of my project was to investigate how skin deformations induced by individual motoneurons add when two or more motoneurons are simultaneously activated.

Let us first consider the case when two longitudinal motoneurons, such as the L motoneuron and the dorsal longitudinal motoneuron 5, were coactivated. **Fig. 4.6*A*** and ***B*** show the optical flows induced by stimulation of motoneurons L and 5 individually. Panel ***C*** shows the optical flow induced by identical simultaneous stimulation of the two motoneurons. Panel ***D*** compares the vector field shown in ***C*** (black) to the vector field

obtained by linear superposition of the vector fields shown in ***A*** and ***B*** (red). The black and red vector fields are very similar, indicating a simple linear summation of the skin deformations induced by the individual motoneurons. Panel ***E*** shows the values of the elementary deformations for the contractions induced by the individual stimulation of cells L (gray histogram) and 5 (white histogram). Panel ***F*** shows: i) in gray, the elementary deformations for the contraction obtained by the simultaneous stimulation of the two motoneurons; ii) in red, the sum of the elementary deformations obtained for the individual stimulation of the two neurons (each red bar in ***F*** is the sum of the corresponding gray and white bars in ***E***). Panels ***E*** and ***F*** show that all three vector fields drawn in ***A***, ***B*** and ***C*** are characterized by a large negative value of S_1 and negligible values of E, S_2, and ω, showing that the contraction resulting from the simultaneous activation of two longitudinal motoneurons is still an almost pure negative longitudinal shear. Moreover the gray and red bars in panel ***F*** are almost identical, indicating that also the elementary deformations add linearly.

Let us now consider the case when two motoneurons innervating different muscle fibers are simultaneously stimulated. **Fig. 4.7*A*** and ***B*** show the optical flows induced by individual stimulation of circular motoneuron 112 and of longitudinal motoneuron 5. Panel ***C*** shows the optical flow obtained by identical simultaneous stimulation of the two motoneurons. Panel ***D*** compares the vector field shown in ***C*** (black) to the linear superposition of the vector fields shown in ***A*** and ***B*** (red). The black and red vector fields in ***D*** are very similar, indicating that simultaneous activation of cells 5 and 112 induces a skin deformation that is an almost perfect linear summation of the deformations the individual motoneurons induced.

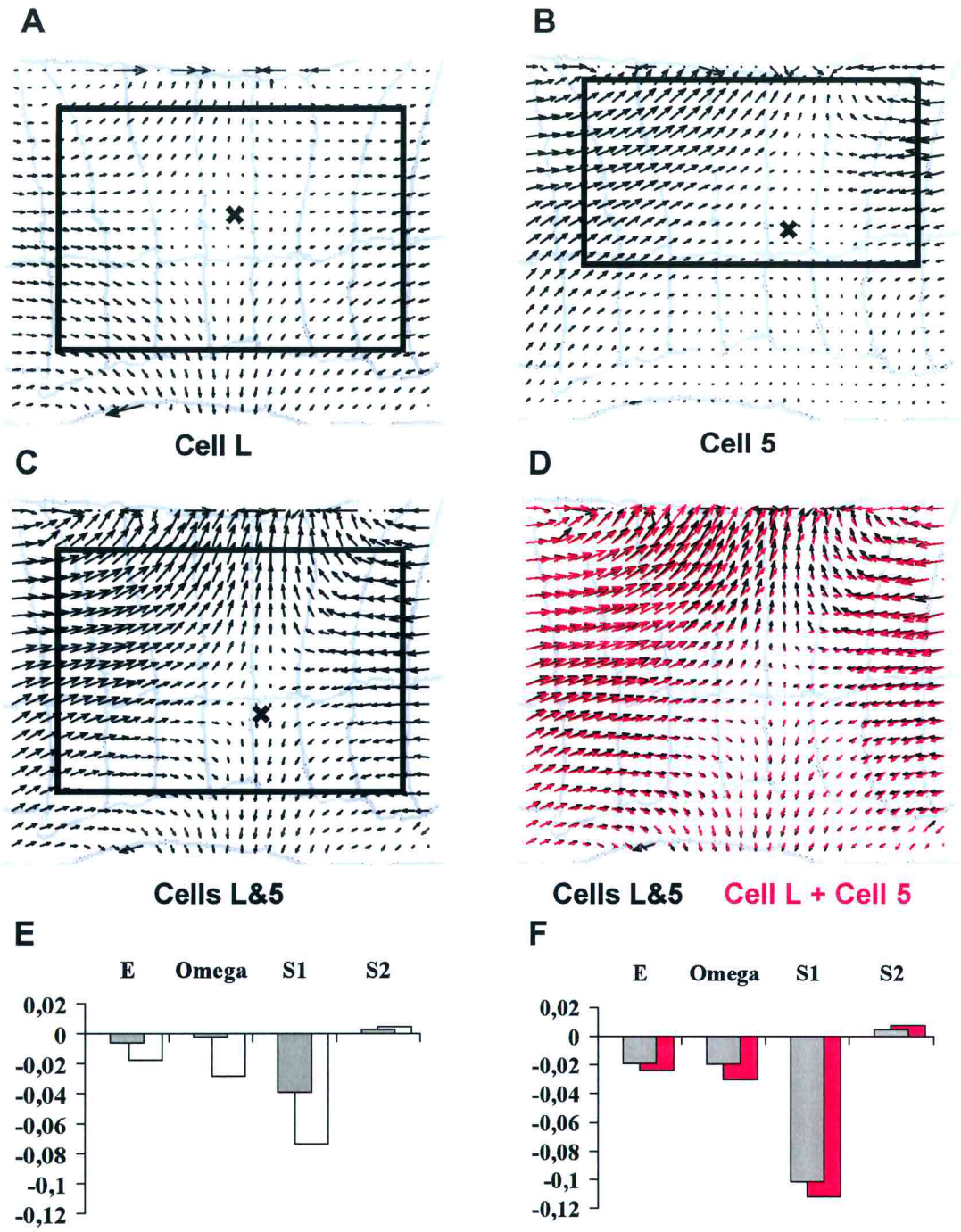

Figure 4.6 Superposition of the deformations evoked by motoneurons innervating the same class of muscle fibers. *A*, Optical flow following longitudinal motoneuron L stimulation with a current pulse lasting 5 seconds and evoking a spike discharge of about 14 Hz. *B*, Optical flow following longitudinal motoneuron 5 stimulation with a current pulse lasting 5 seconds and evoking a spike discharge of about 34 Hz. *C*, Optical flow following identical simultaneous stimulations of both longitudinal motoneurons *D*, Sum of the optical flows shown in *A* and *B* (red) compared to the optical flow shown in *C* (black). *E*, Elementary deformations of the optical flows shown in *A* and *B* (L, gray bars; 5, white bars). *F*, Sum of the elementary deformations of motoneurons L and 5 (red bars) compared to the elementary deformations of the optical flow shown in *C* (gray bars). The width of the annuli in panels *A*, *B*, *C*, *D* is about 0.8 mm. Same scale in *E* and *F*.

The analysis of the elementary deformations shows that the combination of a longitudinal and of a circular motoneuron leads to a vector field characterized by a large negative value of E as the main deformation component. In the following, I will refer to this kind of skin deformation (characterized by large negative E and smaller values of S_1, S_2, and ω) as a *pure compression*. **Fig. 4.7*E*** reports the values of the elementary deformations induced by individual stimulation of cells 112 (gray histogram) and 5 (white histogram). As expected, the contraction induced by the longitudinal motoneuron is almost entirely characterized by a large negative value of S_1, while that induced by the circular motoneuron by a large positive value of S_1 and a large negative value of E. **Fig. 4.7*D*** shows the elementary deformations induced by simultaneous stimulation of the two motoneurons (gray bars) and the sum of the elementary deformations induced by individual stimulation of the two neurons (red bars). The gray and red bars in ***F*** are almost identical, indicating that the elementary deformations add linearly. Because of this linear summation, when a longitudinal and a circular motoneuron are simultaneously activated the resulting vector field has a small value of S_1 but a significant negative value of E, corresponding to a local pure compression. This suggests that a pure compression requires the simultaneous activation of at least one longitudinal and one circular motoneuron.

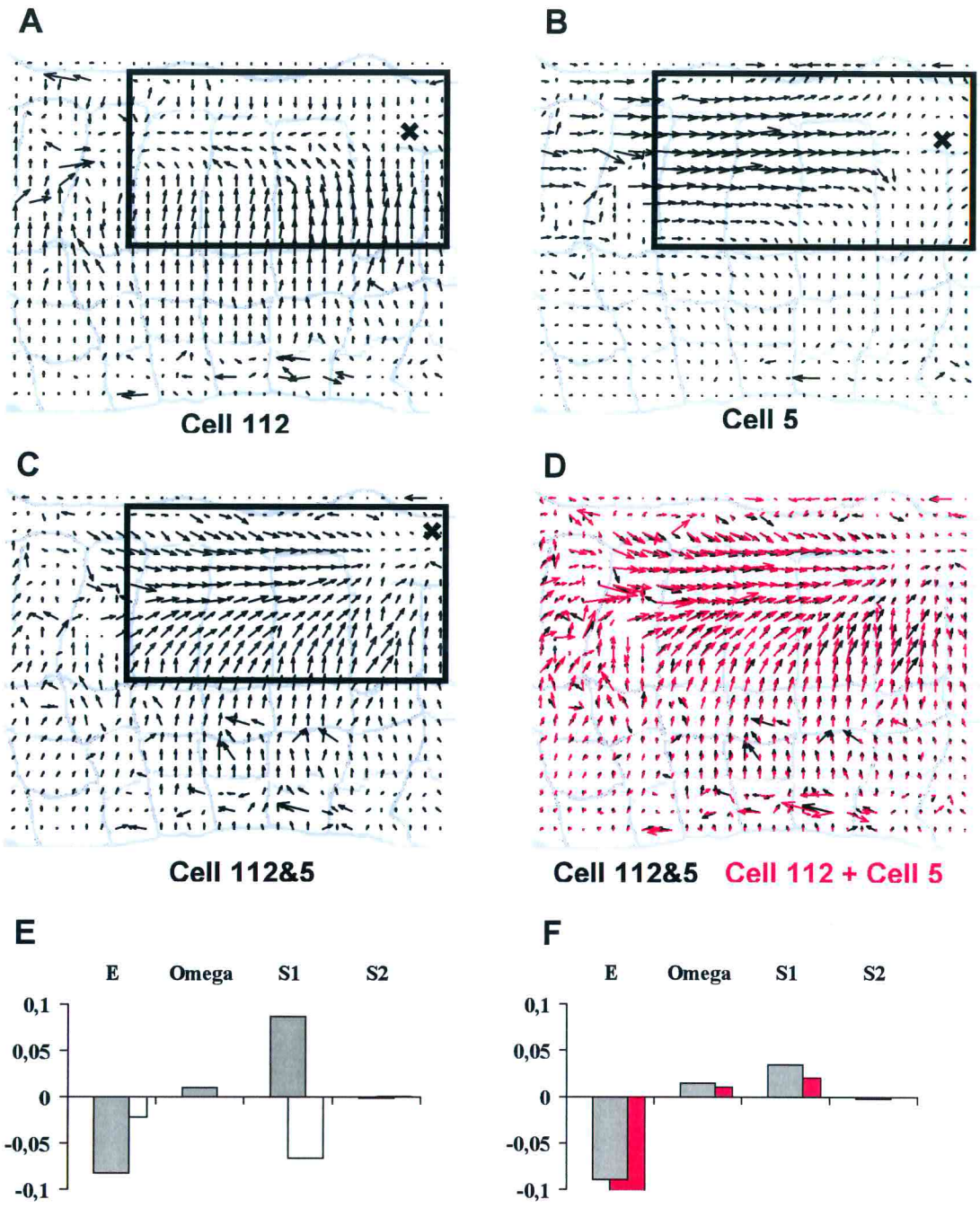

Figure 4.7 Superposition of the deformations evoked by motoneurons innervating different muscle fiber classes. *A*, Optical flow following circular motoneuron 112 stimulation with a current pulse lasting 5 seconds and evoking a spike discharge of about 28 Hz. *B*, Optical flow following longitudinal motoneuron 5 stimulation with a current pulse lasting 5 seconds and evoking a spike discharge of about 42 Hz. *C*, Optical flow following identical simultaneous stimulation of both motoneurons. *D*, Sum of the optical flows shown in *A* and *B* (red) compared to the optical flow shown in *C* (black). *E*, Elementary deformations computed for the optical flows shown in *A* and *B* (112, gray bars; 5, white bars). *F*, Sum of the elementary deformations of motoneurons 112 and 5 (red bars) compared to the elementary deformations of the optical flow shown in *C* (gray bars). The width of the annuli in panels *A*, *B*, *C*, *D* is about 1 mm. Same scale in *E* and *F*.

This deduction was supported by simultaneous recordings from different pairs of longitudinal and circular (or flattener) motoneurons, such as: motoneurons 3 and 112 (not shown); motoneurons 108 and 12 (not shown); motoneurons L and 109 (not shown). These experiments clearly showed that when a longitudinal and a circular (or flattener) motoneuron were coactivated, the resulting skin deformation was a pure compression. Similarly, simultaneous recordings from different pairs of longitudinal motoneurons confirmed the result shown in **Fig. 4.6**: when two longitudinal motoneurons were simultaneously stimulated, the resulting skin deformation was an almost pure negative longitudinal shear. This was true also for longitudinal motoneurons innervating not overlapping regions of the body-walls. This is shown in **Fig. 4.8**, in which the linear superimposition of skin deformations induced by motoneurons 8 and 3 is reported (panel ***D***). The elementary deformations of the contraction (panel ***C***) resulting from simultaneous stimulation of these motoneurons clearly indicate that such a contraction is an almost pure longitudinal shear (panel ***F***), as expected for longitudinal motoneurons (see **Fig. 4.4**).

When motoneurons innervating oblique muscles, such as motoneurons 110 or 111, and a longitudinal or circular motoneuron were simultaneously activated by depolarizing current, vector fields induced on the leech skin similarly added linearly. This is shown in **Fig. 4.9**, in which the linear superimposition of skin deformations induced by motoneurons 110 and 5 is reported. The optical flows induced by these motoneurons added linearly (panel ***D***) and the resulting deformation field (panel ***C***) had elementary deformations (panel ***F***) characterized by high negative E and S_2 and much smaller positive S_1. This was expected because of the opposite sign of S_1 for the contractions induce individually by motoneurons 110 and 5 (panel ***E***).

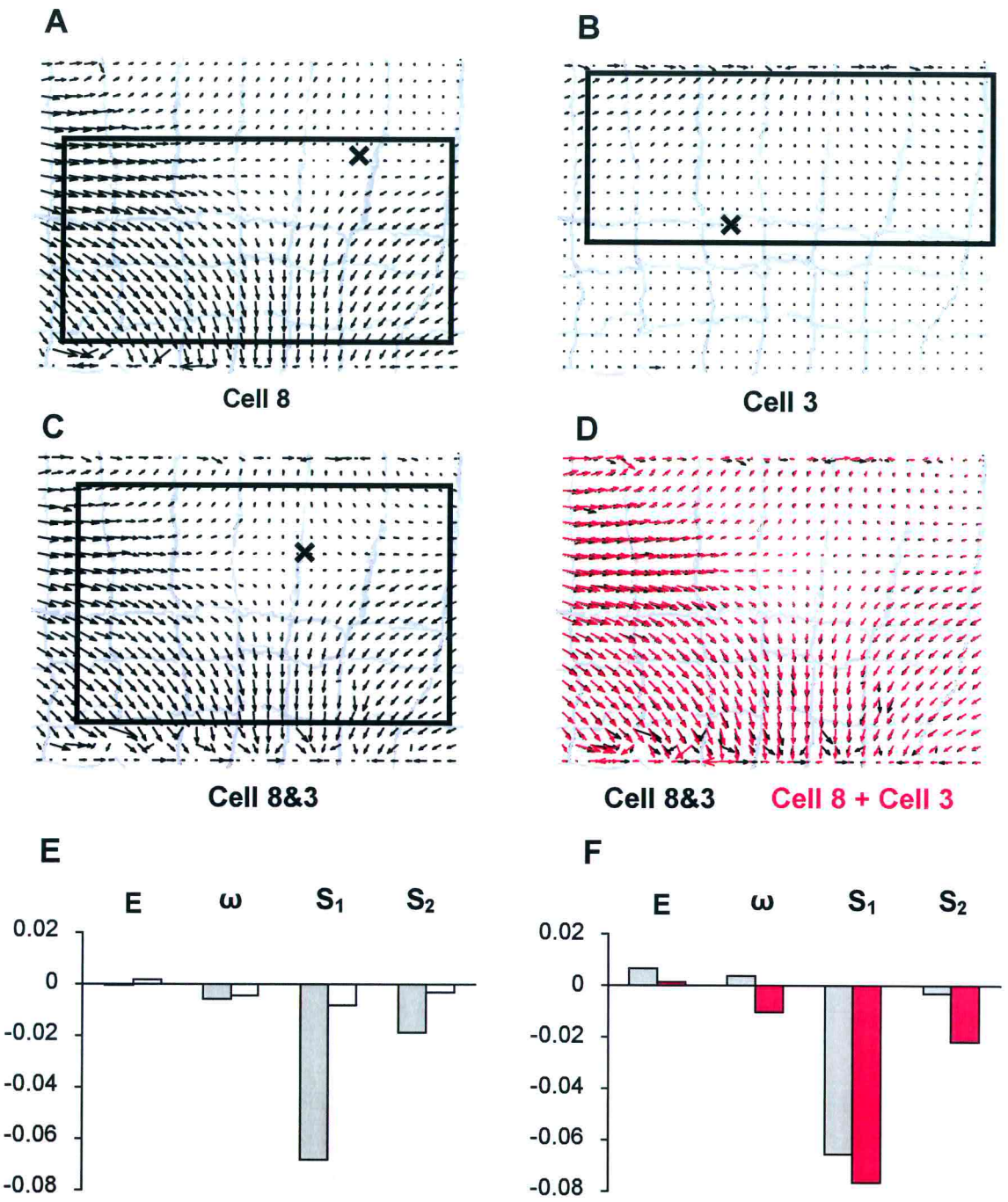

Figure 4.8 Superposition of the deformations evoked by a pairs of longitudinal motoneurons innervating not overlapping body-wall regions. *A*, Optical flow induced by activation of motoneuron 8. *B*, Optical flow induced by activation of motoneuron 3. *C*, Optical flow induced by simultaneous activation of both motoneurons. *D*, Sum of the optical flows shown in *A* and *B* (red) compared to the optical flow shown in *C* (black). *E*, Elementary deformations computed for the optical flows shown in *A* and *B* (8, gray bars; 3, white bars). *F*, Sum of the elementary deformations of motoneurons 8 and 3 (red bars) compared to the elementary deformations of the optical flow shown in *C* (gray bars). The width of the annuli in panels *A*, *B*, *C*, *D* is about 1 mm. Equal normalization in *E* and *F*.

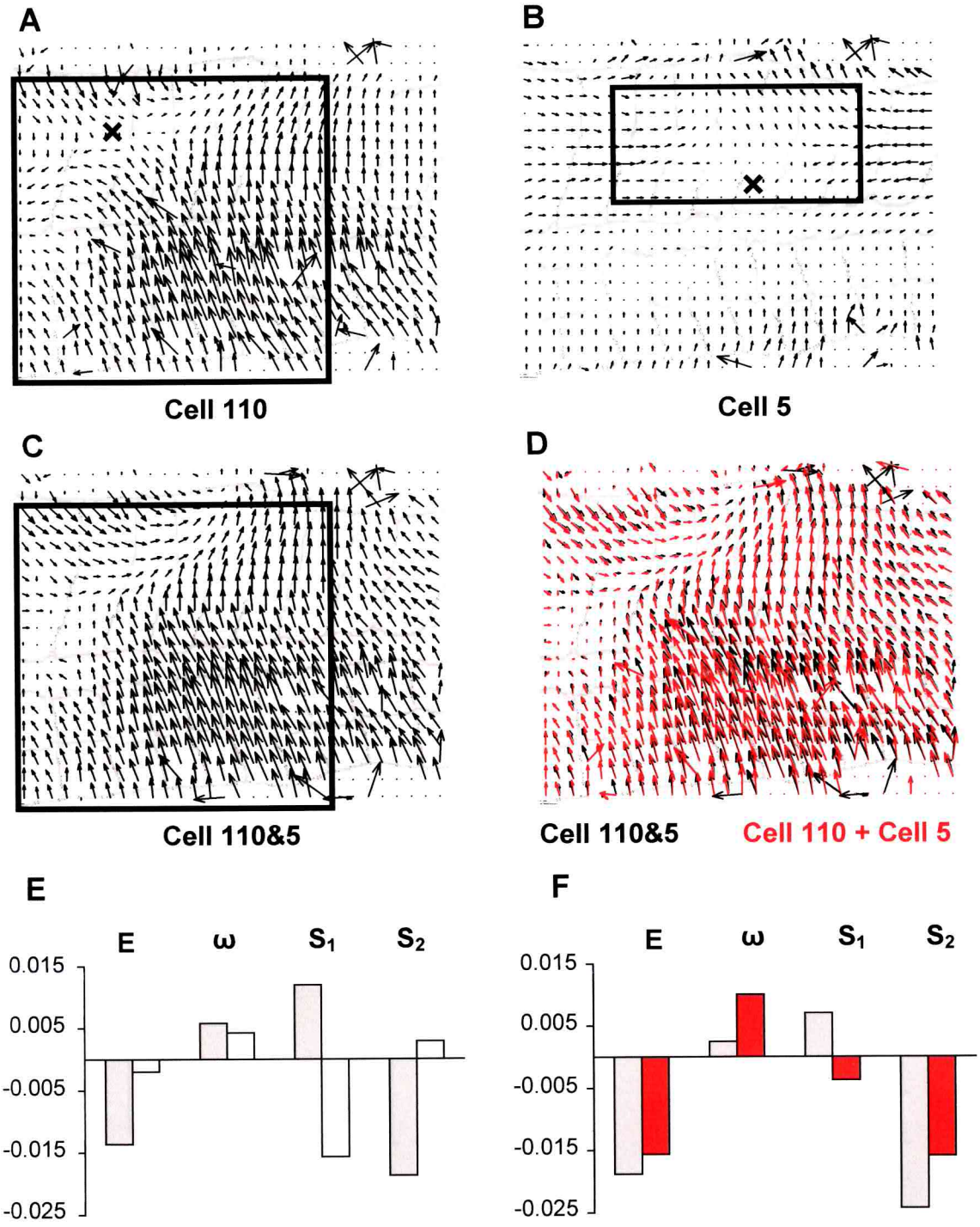

Figure 4.9 Superposition of the deformations evoked by motoneurons innervating different oblique and longitudinal muscles. *A*, Optical flow induced by activation of motoneuron 110. *B*, Optical flow induced by activation of motoneuron 5. *C*, Optical flow induced by simultaneous activation of both motoneurons. *D*, Sum of the optical flows shown in *A* and *B* (red) compared to the optical flow shown in *C* (black). *E*, Elementary deformations computed for the optical flows shown in *A* and *B* (110, gray bars; 5, white bars). *F*, Sum of the elementary deformations of motoneurons 110 and 5 (red bars) compared to the elementary deformations of the optical flow shown in *C* (gray bars). The width of the annuli in panels *A*, *B*, *C*, *D* is about 0.7 mm. Same scale in *E* and *F*.

In summary, these experiments strongly support the hypothesis that skin deformations induced by different motoneurons, during a light or moderate mechanical stimulation, sum linearly as a general rule. In turn this property of linear superposition enables complex deformations to be decomposed into the muscle types sustaining them. For example, when a skin deformation caused by a mechanical stimulation is indeed a local pure compression, characterized by a large value of E without a simultaneous large S_1 or/and S_2, it can be inferred that longitudinal and circular fibers are coactivated.

Note that real skin deformations sum linearly, but in general this is not the true for their linear approximations. The linear sum of linear approximations only holds for pairs of motoneurons innervating skin areas that are at least partially overlapping and which have linearization window and singular point located in similar positions. This is the case for cells 112 and 5, both innervating dorsal muscles, and cells 5 and L, whose deformations overlap in a wide dorsal area of the skin (**Figs. 4.7*F*** and **4.6*F***). In particular, the case shown in **Fig. 4.7** is the ideal one for linear sum of elementary deformation: the activated motoneurons innervated almost exactly the same region of body-wall, so that the same linearization window was chosen for both cells and the resulting singular point positions were almost coincident. Also for the motoneuron pair shown in **Fig. 4.6**, the elementary deformations added almost linearly, because the linearization regions were overlapping in a wide area and the resulting singular point were in similar positions. On the contrary, when two motoneurons innervating non-overlapping skin regions are coactivated, in general, their elementary deformations do not add linearly. This is the case of **Fig. 4.8**, in which the component S_1 is smaller, for the simultaneous stimulation of cells 8 and 3 (panel *F*), than that expected from the linear summation of elementary deformations of individual motoneurons (panel *E*). Similarly, in **Fig. 4.9**, there are relevant deviations from the linear sum of the elementary deformations. In particular, S_1 (panel *F*) has opposite sign and is

much bigger than what expected for linear sum of elementary deformations of cells 110 and 5 (panel *E*). This is because the contractions induced by motoneurons 110 and 5 overlap only in a small skin area and their linearization windows and singular point positions are significantly different. Nevertheless, it is important to note that, even in the case in which the elementary deformations of a pair of coactivated motoneurons do not sum linearly, the contraction resulting from their coactivation is still generally linear around the singular point. And, more important, the elementary deformations of this resulting contraction are strictly related to those of individual motoneurons, so that it is still easy to infer which classes of motoneurons sustain the contraction. This is clearly shown in **Fig. 4.9*F***, in which the value of S_1 for the contraction induced by simultaneous activation of cells 110 and 5 is less than half the value of S_2. The relative weight of S_1 and S_2 is not compatible with a pure oblique contraction (see **Fig. 4.4*G***) and clearly indicates the coactivation of cell 110 and a longitudinal motoneuron. Similarly, the value of S1 resulting from simultaneous activation of cells 8 and 5 (**Fig. 4.8*G***) clearly indicates that the undergoing body-wall contraction is a pure longitudinal deformation sustained only by longitudinal motoneurons. These results support the idea that identification of specific classes of motoneurons sustaining a deformation characterized by specific values of its elementary components is a robust and reliable procedure.

4.2.4 Comparison of skin deformations caused by mechanical stimulation and electrical excitation of mechanosensory neurons

As a further example of the ability of optical flow analysis in neurobiology, I analyzed the optical flows induced by mechanical stimulation of the leech skin to identify which muscle fibers are primarily activated and which mechanosensory neurons mediate that activation. In these experiments I inserted an intracellular electrode into an identified mechanosensory neuron to: i) measure the number of spikes the mechanical stimulation induced in that

neuron, ii) characterize the vector fields induced by a controlled number of spikes elicited in the mechanosensory neuron.

Ventral and dorsal P cells

Fig. 4.10 shows data obtained from a preparation in which both the ventral (***A*** and ***B***) and dorsal (***C*** and ***D***) P cells were impaled. Mechanical stimulation of the skin in the ventral side, exerting a force of about 20 mN for 300 ms (touch location is indicated by the circle in panel ***A***), induced 12 ventral P cell spikes (lower trace in panel ***A***) and the vector field of skin deformations shown in the upper part of panel ***A***. Induction of similar P cell firing by current injection (lower trace in panel ***B***), induced a very similar vector field and singular point location (top part, panel ***B***; singular points are indicated by the X's in ***A*** and ***B***). Both vector fields have the characteristic shape of a ventral pure compression with the arrows pointing towards the center of the deformation. This qualitative observation was confirmed by computing their elementary deformations (**Fig. 4.11*A***, ***B***); both vector fields have similar large negative E values. On the base of the considerations reported in the previous section (see **Fig. 4.7*C***) I concluded that both deformations were sustained by simultaneous activation of longitudinal and circular muscles.

Mechanical stimulation in the dorsal side of the skin (circle) induced the vector field and dorsal P cell firing shown in **Fig. 4.10*C***. Induction of similar P cell firing induced a very similar vector field and singular point location (**Fig. 4.10*D***; singular points marked by X's). Both contractions are characterized by a similar high negative value of the expansion E (**Fig. 4.11*C*** and ***D***). The higher values of E and S_1 in **Fig. 4.11*C*** in comparison to those in **Fig. 4.11*D***, indicate that the pure compression induced by the mechanical stimulation was slightly stronger than that induced by dorsal P cell intracellular stimulation, in accordance with the higher number of spikes elicited by the mechanical stimulus.

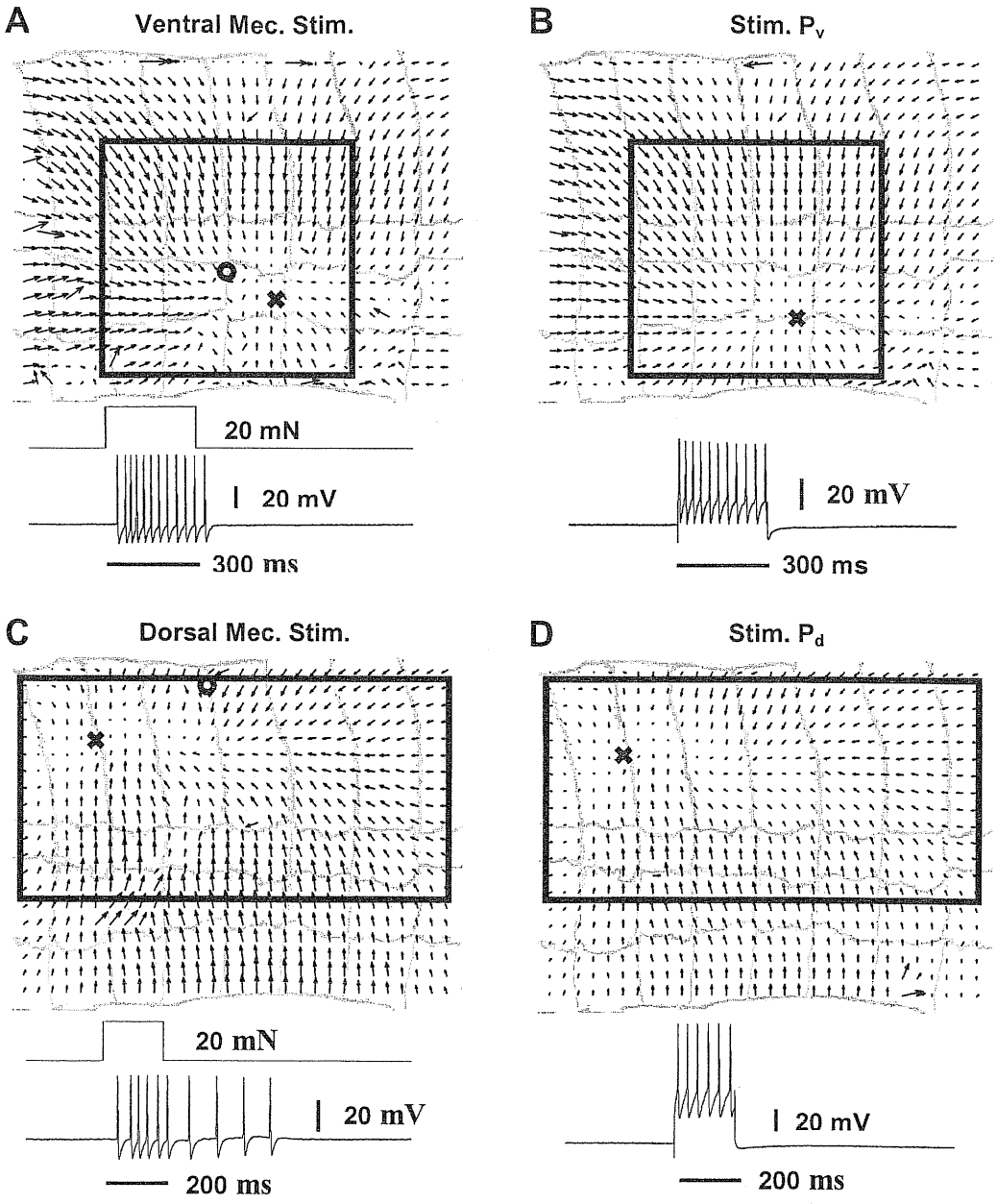

Figure 4.10 Skin deformations caused by mechanical stimulation and P cell intracellular stimulation. *A*, Optical flow induced by mechanical stimulation (20 mN for 300 ms, circle) in the ventral side of the segment. The X is the location of the singular point. The bottom traces show stimulus duration and the ventral P cell response. *B*, Optical flow induced by ventral P cell intracellular stimulation; note marked similarity. *C*, Optical flow and dorsal P cell response induced by mechanical stimulation (20 mN for 200 ms) in the dorsal side of the segment. Symbols as in *A*. *D*, Optical flow induced by dorsal P cell intracellular stimulation; note marked similarity. The width of the annuli is about 0.9 mm.

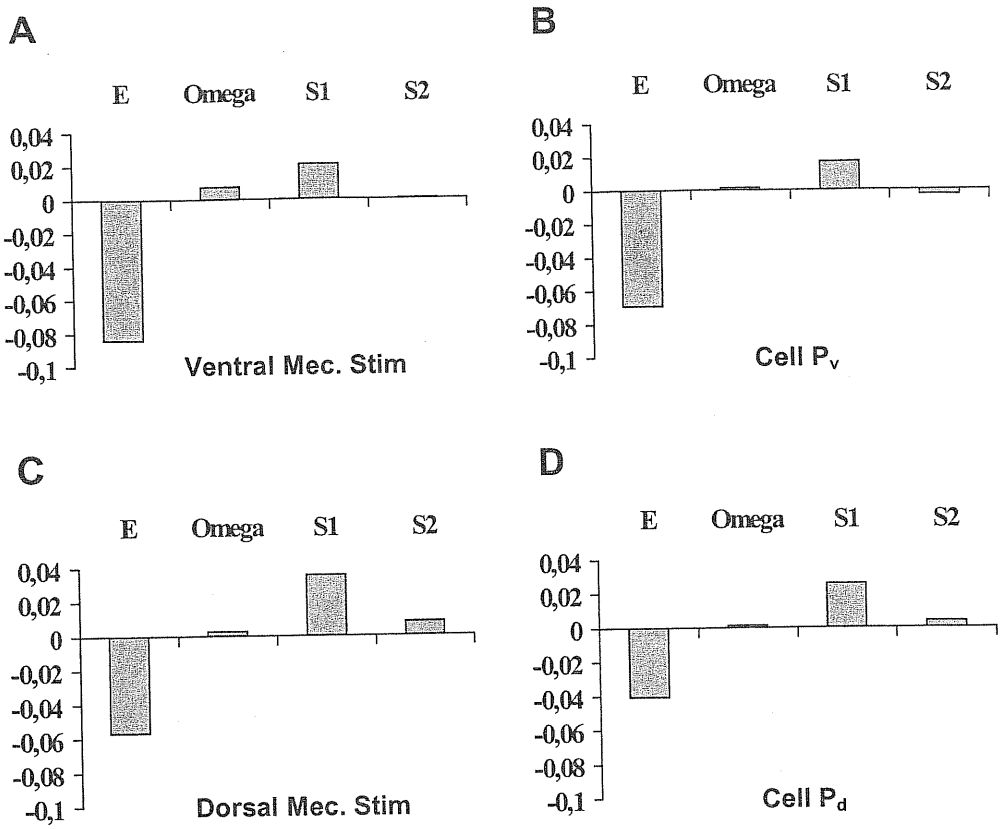

Figure 4.11 The elementary deformations induced by mechanical stimulation and intracellular P cell stimulation. *A* to *D* show the elementary deformations of the optical flows in the corresponding panels of Fig. 4.10. The elementary deformations were computed by linearizing the optical flows shown in Fig. 4.10 in the regions indicated by the solid boxes. Same scale in all panels.

Monitoring T cells

Fig. 4.12 shows the results obtained when a dorsal T cell was impaled. Mechanical stimulation of the dorsal skin (circle, panel *A*) induced an ON discharge of about 4 spikes in the T cell followed by an OFF response of more than 10 spikes (lower trace in *A*). The induced vector field on the leech skin was again a pure compression, characterized by a high negative value of the expansion *E*, as is shown in panel *C*, which plots the elementary deformations for the optical flow in panel *A*. When the same T cell was forced to fire similarly by successive depolarizing current pulses the induced vector field was

qualitatively different and of much smaller amplitude (**Fig. 4.10*B***; note that the magnification-gain is 5-fold greater in this panel than in *A*). The large difference in optical flow induced by mechanical stimulation and T cell stimulation is also apparent in the elementary deformation plots (**Fig. 4.12*C*, *D***).

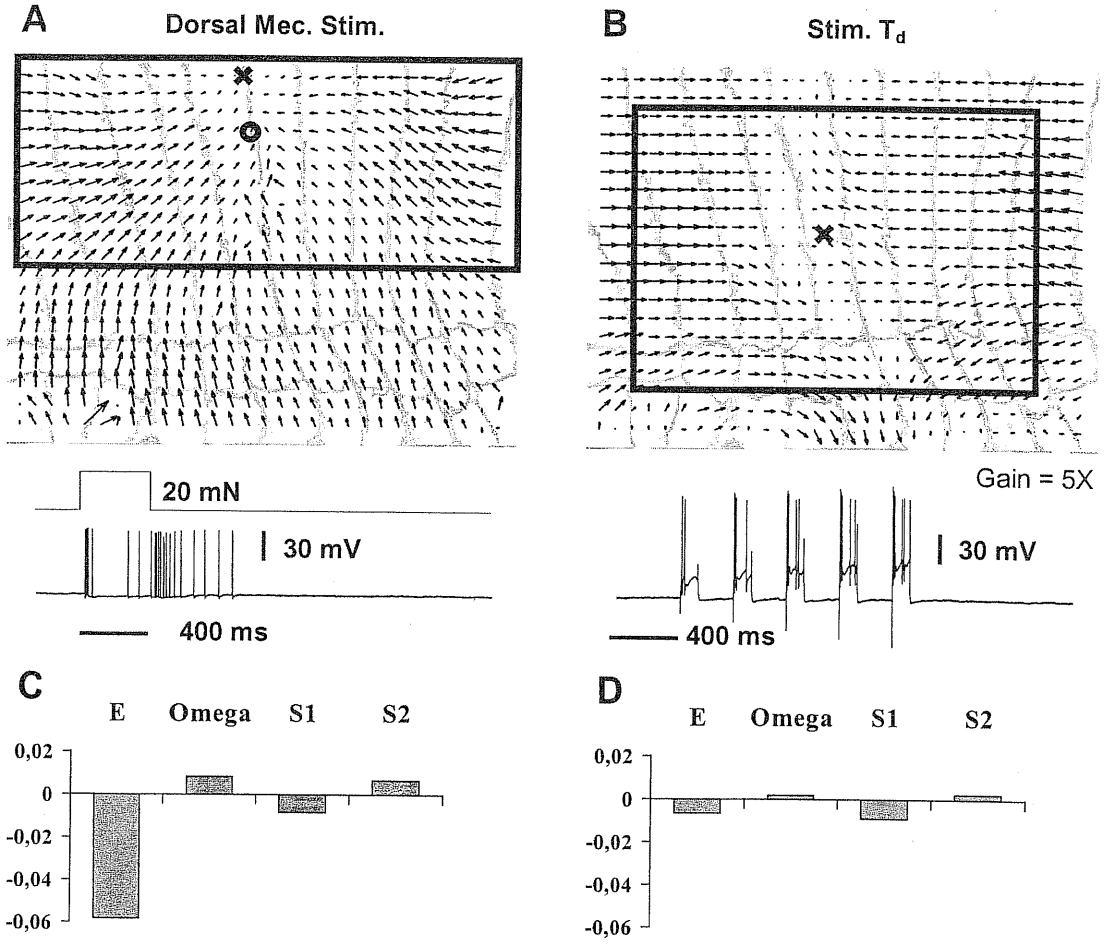

Figure 4.12 T cell contribution to motor response. *A*, Optical flow induced by mechanical stimulation (20 mN for 400 ms) in the dorsal side of the segment. Symbols as in Fig. 4.8. The bottom traces show the duration of the stimulus and the spikes that it evoked in the dorsal T cell. *B*, Optical flow induced by intracellular dorsal T stimulation cell with successive depolarizing current pulses (bottom trace). *C*, Elementary deformations computed for the vector field shown in *A*. *D*, Elementary deformations computed for the vector field shown in *B*. The boxes in *A* and *B* are linearization regions for the corresponding optical flows. The width of the annuli in *A* and *B* is about 0.6 mm. Same scale in panels *C* and *D*.

Relative contribution of P and T cells

The data presented so far clearly show that motor responses initiated by a localized mechanical stimulation are primarily mediated by P cells. This result is in agreement with previous studies (Kristan, 1982; Lockery and Kristan, 1990a; Wittenberg and Kristan, 1992a) and extends their findings to the global shape of the field of deformations. One of these studies (Kristan, 1982), however, reported data showing: i) response to skin stimulation about 4-fold greater than response to individual stimulation of P cell; ii) large contribution of T cells in mediating the reflex when coactivated simultaneously to P cells. I addressed these two points in a series of experiments.

Skin deformation induced by intracellular stimulation of ventral or dorsal P cell was compared to deformation induced by mechanical stimulation of the skin in several different preparations. In 15 out of 17 preparations the shape of the optical flow and the relative weight of the elementary deformations were almost identical for contractions induced by P cell and mechanical stimulation. Alternatively, each T cell stimulation (7/7) evoked a vector field of deformation with a structure significantly different from that obtained by mechanical stimulation.

An exact comparison between the intensities of deformations induced by mechanical stimulation of the skin or electrical stimulation of a P cell requires evoking the same number of spikes in the P cell in both stimulations. In these cases (5 experiments) the contraction induced by mechanical stimulation was only slightly stronger than that evoked by P cell stimulation (usually 1.1 to 1.5-fold larger; compare **Fig 4.11*A*** and ***B***).

The role of T cells was further investigated by experiments in which a T and a P cell were first alternatively and then simultaneously stimulated. Collected data exhibited some variability: 4 out of 7 experiments clearly showed that the individual stimulation of T cells was only slightly effective (see **Fig. 4.12**), but the coactivation of T and P cells was

able to induce a contraction 1.5 to 2-fold greater than the contraction induced by individual stimulation of P cells.

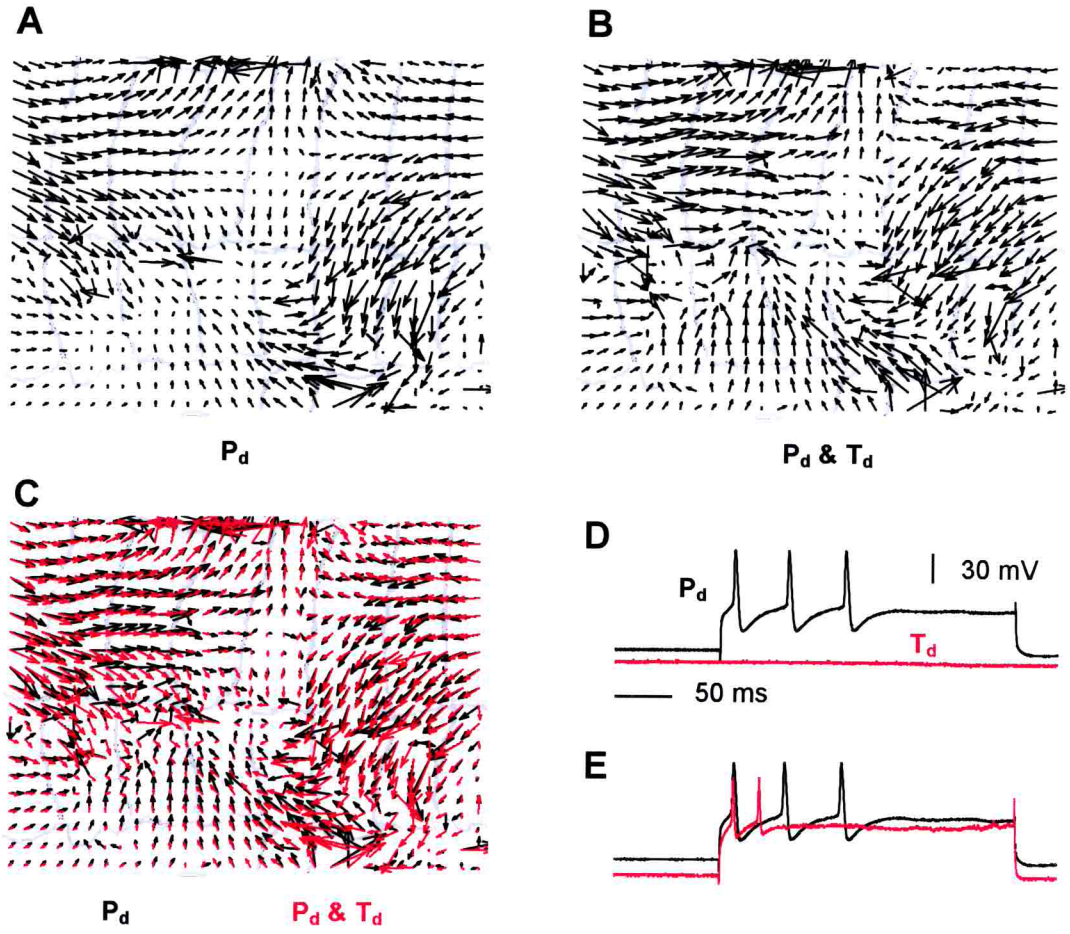

Figure 4.13 Contribution of T cells to sensory-motor response. *A*, Contraction induced by evoking three action potentials in the cell P_d (black trace in *D*). *B*, Contraction induced by simultaneously evoking three spikes in the cell P_d (black trace in *E*) and two spikes in the cell T_d (red trace in *E*). *C*, The optical flows drawn in *A* and *B* are shown in the same panel to allow for a better comparison between their amplitudes. *D* and *E*, Firing pattern of the dorsal P and T cells underlying the contractions shown respectively in *A* and *B*. The width of the annuli in *A*, *B* and *C* is about 0.8 mm. The optical flows are drawn with a magnification 2×.

One of these experiments is shown in **Fig. 4.13**, in which the deformations induced by individual firing of the dorsal P cell (panel *A*) and by simultaneous firing of the dorsal P and T cells (panel *B*) are drawn. The comparison between these two optical flows (panel *C*) shows that activation of T_d during P_d firing did not change significantly the shape of the deformation field but potentiated its strength up to 2-fold, depending on the field area considered (the optical flows in **Fig. 4.13** *A* and *B* were compared by computing the ratio between the length of their arrows in different positions). In 3 out of 7 experiments the skin deformations elicited by electrical stimulation of the P cell or of the same P cell and another T cell were identical.

Experiments in which P and T cells were alternatively hyperpolarized during mechanical stimulation were also performed. Hyperpolarization of the P cell was able to reduce the strength of the contraction - without changing its shape - in proportion to the reduction in the number of evoked spikes. Hyperpolarization of T cells had a much lower effect on the contraction strength. One of these experiments is shown in **Fig. 4.14**. Panel *A* reports the contraction obtained by inducing cell P_v to fire five spikes. The resulting deformation is almost identical to that obtained by mechanical stimulation of the skin evoking the same number of spikes in cell P_v (panel *B*). This indicates that the contraction was mainly mediated by activation of cell P_v. This was confirmed by the fact that strong hyperpolarization of cell P_v was able to drastically reduce the contraction strength during mechanical stimulation of the skin (panel *C*). The role of T cells was assessed by impaling cell T_v. First of all, I verified that mechanical stimulation of the skin evoked in cell T_v a spike train of five action potentials (bottom trace in panel *D*) and that the resulting deformation field was identical to that drawn in panel *B* (data not shown). Then, I hyperpolarized cell T_v during mechanical stimulation of the skin. The cell fired only two spikes (middle trace in panel *D*) and the resulting field (panel *D*) was only slightly smaller of that obtained without hyperpolarizing the cell (panel *B*).

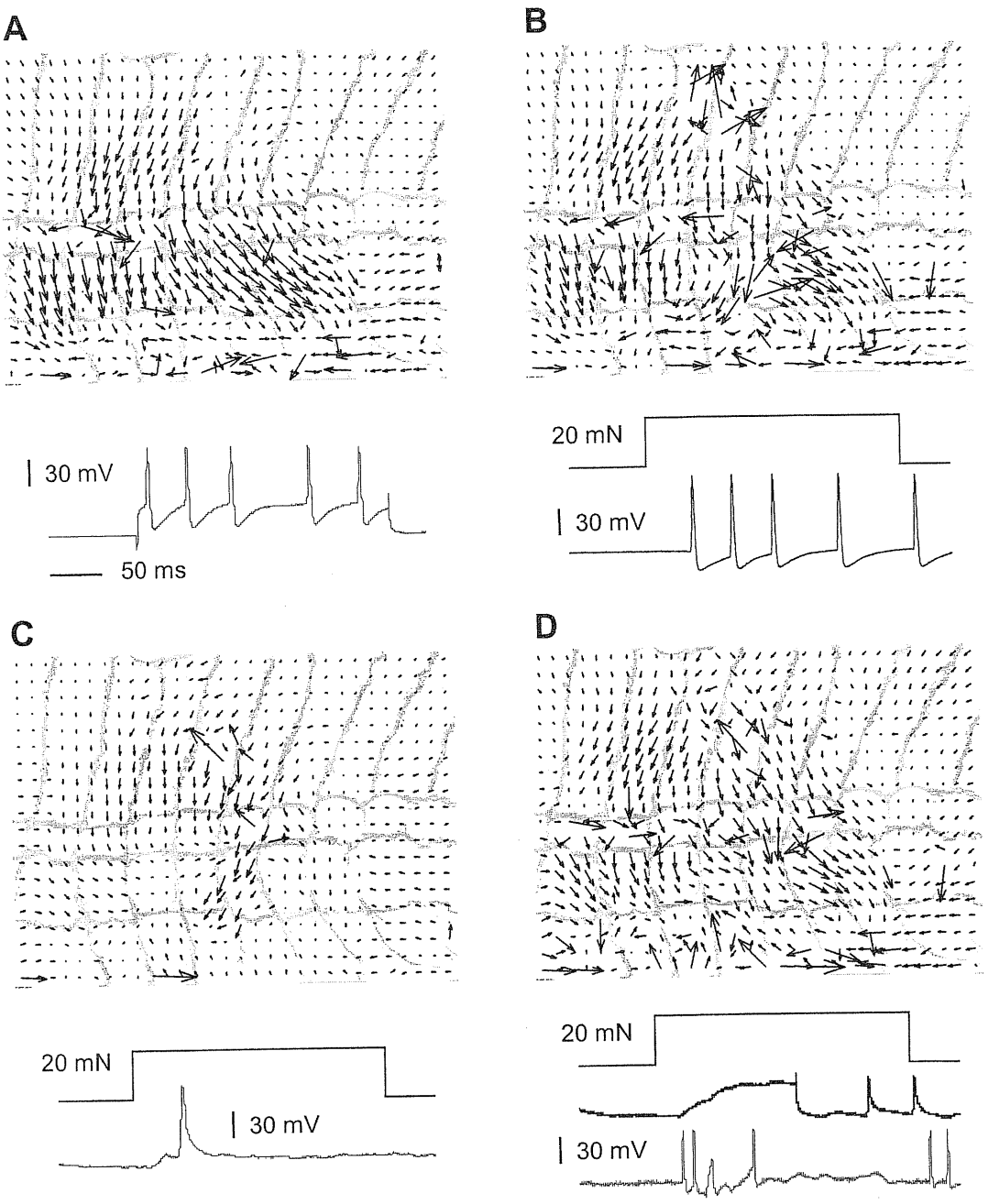

Figure 4.14 Role of P and T cells in mediating sensory-motor responses. *A*, Contraction induced by evoking five action potentials (bottom trace) in the cell P_v. *B*, Contraction and ventral P cell response induced by mechanical stimulation (20 mN for 200 ms) in the ventral side of the skin. *C*, Contraction and ventral P cell response induced by similar mechanical stimulation of the skin. Cell P_v was kept hyperpolarized during the stimulation and fired only one spike. *D*, Contraction induced by similar mechanical stimulation of the skin during hyperpolarization of cell T_v, which fired two spikes near the end of the mechanical stimulus (middle trace). The natural (without hyperpolarization) firing pattern of cell T_v following mechanical stimulation is shown in the bottom trace. In *B*, *C* and *D* the squared pulse indicates the stimulus duration. The width of the annuli is about 0.7 mm. In the central area of the skin the optical flow is rather irregular, due to the shadow of the nylon filament used for the mechanical stimulation.

Monitoring N cells

Fig. 4.15 shows data obtained when the medial N cell was impaled. Mechanical stimulation (circle, panel ***A***) induced in the medial N cell just 1 or 2 spikes or no spikes at all (lower trace in panel ***A***). Measurable skin deformation could only be evoked firing at least 6 spikes in the medial N cell (9 spikes were elicited in the experiment shown in panel ***B***). Despite this increase in the N cell activity, the deformation vector field induced by N cell firing was much smaller (note magnification change in panel ***B***) and qualitatively different from that induced by the mechanical stimulation (panel ***A***). Panels ***C*** and ***D***, which report the elementary deformations for the optical flows drawn in panels ***A*** and ***B***, support the qualitative data shown in **Figs. 4.15*A*** and ***B***; mechanical stimulation induced a large negative E and a slightly smaller positive S_1, but N cell stimulation evoked equally small negative E and S_1. Similar results were obtained by impaling the lateral N cell.

Mechanical stimulation in more intact preparations and in intact leech

The experimental results presented so far were obtained in isolated leech segments. Some of these results, such as the major contribution of the P cells to the motor responses induced by mechanical stimulation, confirm and extend the classical descriptions of the local reflexes in the leech (Kristan, 1982; Lockery and Kristan, 1990a; Wittenberg and Kristan, 1992a). In particular, coactivation of longitudinal and circular muscles following mechanical stimulation (see **Figs. 4.10*A***, **4.10*B***, **4.12*A*** and **4.15*A***) has not previously been reported and suggests a more complex pattern of activation for motoneurons and interneurons involved in such reflexes (Lockery and Kristan, 1990a, b; Wittenberg and Kristan, 1992a, b). To verify these data, I repeated these mechanical stimulations in more intact preparations.

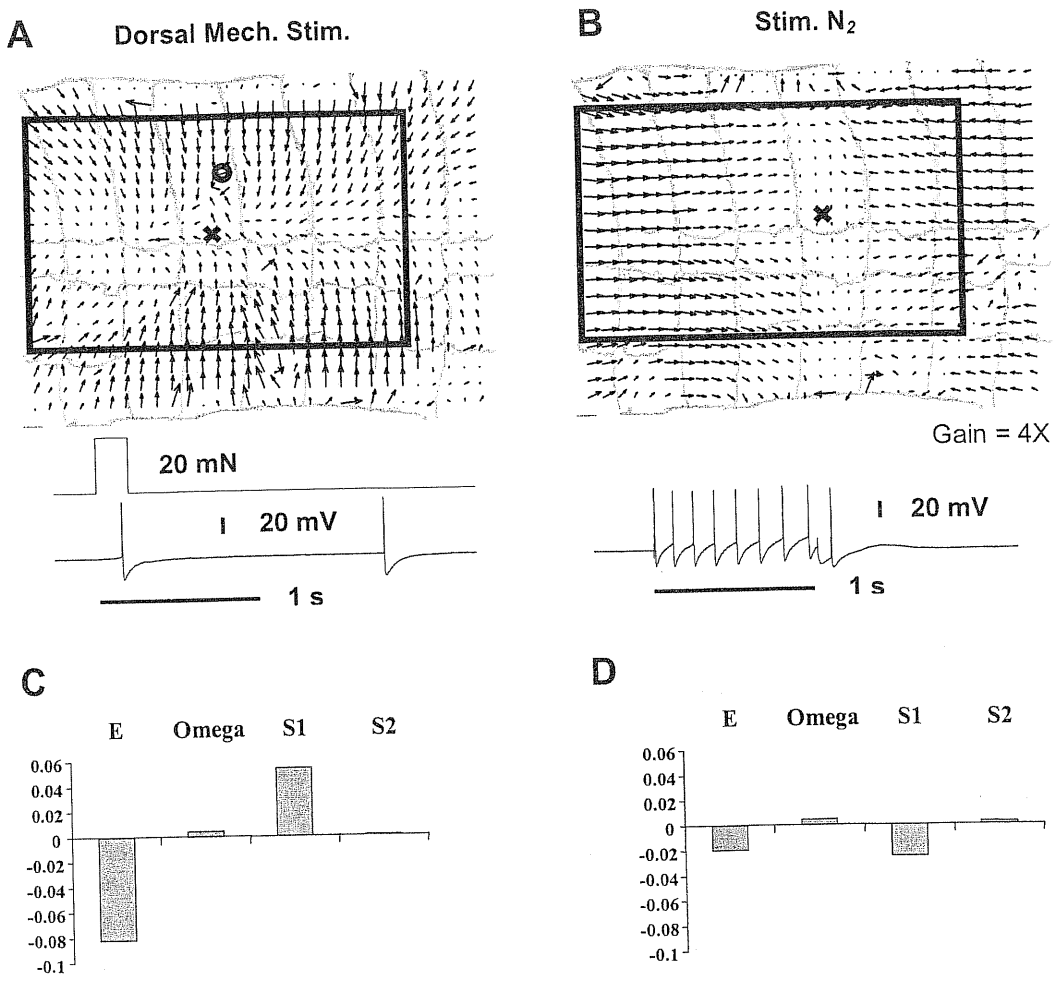

Figure 4.15 N cell contribution to motor response. *A*, Optical flow induced by mechanical stimulation (20 mN for 200 ms) in the dorsal side of the segment. Symbols as in Fig. 4.8. *B*, Optical flow induced by intracellular medial N cell stimulation. *C*, Elementary deformations computed for the vector field shown in *A*. *D*, Elementary deformations computed for the vector field shown in *B*. The boxes in *A* and *B* are the linearization regions for the corresponding optical flows. The width of the annuli in *A* and *B* is about 0.8 mm. Same scale in panels *C* and *D*.

I used the intact body-wall preparation described in Section 2.1.3 (an intact hemisection of body wall in which the ganglion and the roots were not exposed and cleaned) to verify coactivation of longitudinal and circular muscles by moderate mechanical stimulation of leech skin. In the great majority of intact body-wall preparations (4/5), I consistently observed vector fields similar to those shown in **Figs. 4.10*A*, 4.10*B***,

4.12*A* and 4.15*A*, i.e. pure compressions with high negative values of the expansion E as main elementary deformation. The location of the singular point followed approximately the location of the mechanical stimulus. In a few preparations, I observed almost pure transverse (high positive S_1 and high negative E) or longitudinal (high negative S_1) contractions, indicating some degree of variability in motoneuron activation in different preparations. A possible explanation to this variability is suggested by three preparations that were kept under observation for several hours, in which variability in the response to the same mechanical stimulation, repeated at intervals of 30 minutes, was observed. In these preparations, the transverse component of the deformation, sustained by the circular muscles, decreased with time so that only the longitudinal component was visible at the end of the experimental session (after 3 or 4 hours). This is likely attributable to a faster deterioration of circular muscle fibers in comparison to the longitudinal muscle fibers.

Analysis of the vector fields induced by mechanical stimulation was also repeated in intact leeches in which two or three segments were secured to the sylgard dish with 4 pins (see Section 2.1.3). In intact leeches, the mechanical stimulations used in the experiments shown in **Figs 4.10**, **4.12** and **4.15** induced optical flows similar to those obtained in isolated segments. However, while results in isolated segments were reproducible (except for the slow run-down of circular muscle response), in intact leeches the effect of mechanical stimulations was more variable. Often the same mechanical stimulation evoked a clear local pure compression in some trials but a longitudinal or a transverse deformation in others. This variability in the intact leech may arise from the greater complexity of the whole animal and the presence of feedback from other segments and input from the head and tail brains.

4.2.5 Time evolution of the contraction caused by mechanical stimulation

As shown in the previous section, mechanical stimulation can evoke a complex pattern of skin deformations in which different classes of motoneurons and muscles are involved.

The dynamics of this complex deformation, i.e. the timing with which different sets of muscles are recruited, can again be described by analyzing the sequence of instantaneous optical flows $\vec{O}_i$ computed for each video frame.

Fig. 4.16 shows the dynamics of a deformation induced by touching the skin in the lateral side (the location of the touch is indicated by the circle in panel *A*). Every fifth frame of the original image sequence (50 images) acquired at 5 Hz was selected and a sequence of 9 instantaneous optical flows was obtained. Panels ***A*** to ***C*** show the instantaneous vector fields at three different times during the skin contraction. Panel ***D*** shows the time course of the elementary deformations during the first 9 seconds of the deformation. The thick horizontal bars on the top of panel ***D*** indicate the time intervals in which longitudinal and circular muscles are supposed to contract (gray) or relax (white). The thin black bar indicates the duration of the mechanical stimulus (20 mN for 200 ms).

Direct observation of the shape of the vector fields reveals at least three different phases of the deformation. The initial phase shown in panel ***A*** is a dorsal pure compression. The successive phase (***B***) is a ventral longitudinal shear. The third phase (***C***), computed several seconds later when the deformation is in the relaxation phase, looks like a longitudinal shear, but the parallel direction of the arrows suggests the presence also of a strong expansion component. These qualitative observations are confirmed by the time course of the elementary deformations (***D***). In the initial phase of the contraction, from second 0 to second 2, the main component of the deformation was the negative expansion E. I concluded that in this phase the longitudinal and circular muscles were coactivated to produce the dorsal pure compression drawn in panel A. Immediately after (from seconds 2 to 4) the expansion coefficient vanished and the contraction was sustained by only negative longitudinal shear S_1 (panel ***B***). Presumably in this phase circular muscles had ceased contracting and the deformation was driven only by the longitudinal muscles. At second 5 the circular muscles started to relax. The expansion coefficient E became positive and

increased until it reached the same magnitude as S_1, but with opposite sign (compare to the transverse relaxation in panel *C*). The longitudinal relaxation began later, after the termination of the acquired image sequence.

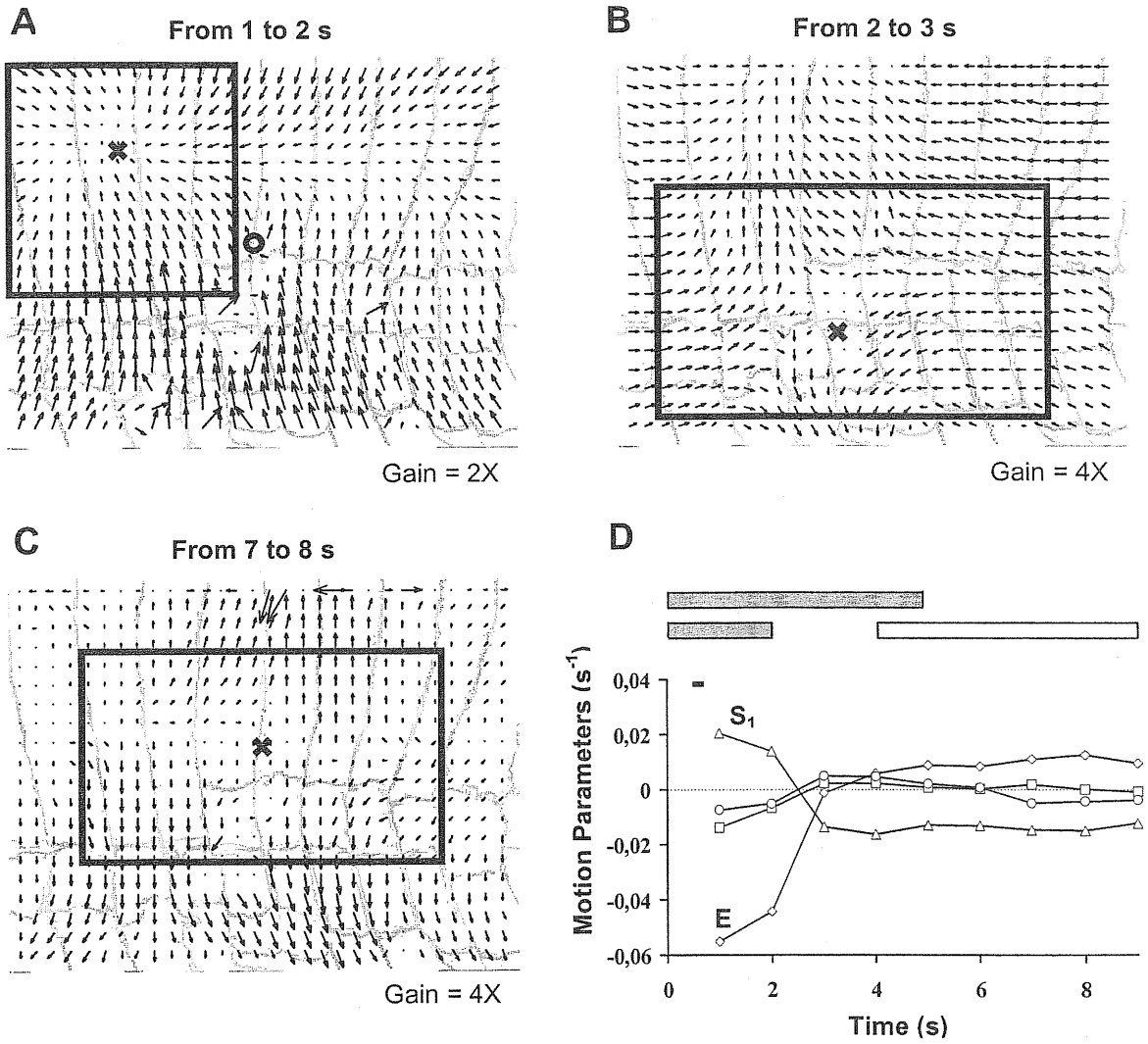

Figure 4.16 Dynamics of a complex contraction induced by a mechanical stimulation. Panels *A* to *C* show the instantaneous vector fields at three different times during skin contraction. The location of the mechanical stimulus is indicated in *A* by the circle. The Xs represent the positions of singular points. The time interval during which each flow occurred is shown in the top of each panel. Panel *D* shows the time course of the elementary deformations - expansion E (◇), rotation ω (□), longitudinal shear S_1 (△), and oblique shear S_2 (○) - during the first 9 seconds of the deformation. The thick horizontal bars on the top of panel D indicate the time intervals in which longitudinal and circular muscles are presumed to contract (gray) or relax (white). The thin bar indicates the duration of the mechanical stimulus (20 mN for 200 ms). The boxes in *A*, *B*, and *C* are the linearization regions for the corresponding optical flows. The width of the annuli in *A*, *B* and *C* is about 0.7 mm.

Fig. 4.16 shows that the dynamics of a deformation induced by a mechanical stimulation can be complex. The dynamics exhibited some variability from preparation to preparation, but in the same preparation were usually reproducible over 30 – 40 minutes. Sometimes (12 cases over a total of 46 different stimulations of the skin in various zones and of P cells in 17 different preparations) longitudinal and circular muscles seemed to contract and relax in clearly distinct phases, as for the experiment described in **Fig. 4.16**, but most of the times (34/46) the longitudinal and circular muscles seemed to contract and relax simultaneously.

4.3 Discussion

Results presented in Section 4.2 show that, by using the technique described in Chapter 3, based on the computation of optical flow, a more accurate classification of the contraction different muscles induce, and a better characterization of sensory-motor responses in the leech body-wall preparation can be obtained. Using this technique it is possible to infer which muscles are activated by mechanical stimuli and to identify which mechanosensory neurons primarily mediate these local reflexes.

4.3.1 Motoneuron classification and optical flow

Table 4.1 and **Figs. 4.3** and **4.4** show that by analyzing the optical flow of contracting pieces of skin it is possible to more completely characterize leech excitatory motoneuron actions. This is possible because optical flow provides a two dimensional characterization of muscle contraction, which cannot be adequately measured by conventional force transducers, which measure only scalar quantities. Quantitative properties of the optical flow - i.e., the location of the singular point and its elementary deformations - produced by the excitation of a given motoneuron were highly reproducible in different leech segments and in different leeches. This quantitative two-dimensional description represents a new and more complete characterization of leech excitatory motoneuron actions.

All longitudinal motoneurons induce vector fields with a large negative S_1, circular motoneurons induce fields with a large positive S_1 and a negative E, and oblique muscles induce fields with a large negative S_2. Different longitudinal and circular muscles, however, produce distinct vector fields in specific skin areas due to the characteristic location of their singular points.

4.3.2 Validity of linear approximations

All quantitative analysis reported in the present work are based on computation of the elementary deformations, used to characterize contractions induced by single motoneurons (**Figs. 4.2, 4.3**) as well as by local mechanosensory stimulation (**Figs. 4.10-4.16**). The computation of these deformations requires approximating the real vector field with a linear vector field. It is well known that all smooth, i.e. regular, vector fields can be locally approximated by linear vector fields (Sommerfeld, 1974). Linear vector fields are characterized by the presence of just one singular point, i.e. of an immobile point. Indeed all vector fields with just one singular point can usually be well approximated by linear vector fields. All vector fields analyzed in this Chapter, evoked by a single mechanical stimulation and by the electrical stimulation of one or pairs of motoneurons, had only one singular point within the area where the skin contracted. Therefore, I adopted a linear approximation in order to provide a simple and compact description of the analyzed contraction.

It is probable that different patterns of motoneuron activation evoked by more complex mechanical stimulation produce non-linear patterns of skin deformations, with more than one singular point in the optical flow. In this case, however, a piecewise linear approximation can be used (Campani and Verri, 1992): separate linear approximations can be computed in distinct windows around each singular point.

4.3.3 Linear summation and motoneuron identification

Sensory motor responses are not mediated by single motoneurons (Lockery and Kristan, 1990a; Wittenberg and Kristan, 1992a; Shaw and Kristan, 1995; Arisi et al., 2001) and it is therefore important to establish the relevance of the proposed motoneuron characterization when motoneurons are coactivated. I investigated this issue by simultaneously impaling pairs of motoneurons innervating the same (**Fig. 4.6**) or different (**Figs. 4.7**, **4.8** and **4.9**) muscle fibers and applying an electrical stimulation evoking a contraction not larger than that evoked by a light or moderate mechanical stimulation (i.e. exerting a force not greater than 50 mN).

In all experiments (9/9) I performed the deformations produced by pairs of impaled motoneurons added almost linearly (**Figs. 4.6 - 4.9**). Even though all-possible motoneuron pairs were not examined and no triplets or larger groups of motoneurons were simultaneously stimulated, collected data strongly supports the linear superposition of skin deformations as a general rule for light and moderate stimulations. I cannot exclude that, for some pairs of motoneurons, the sum of deformations might not be perfectly linear. Nevertheless, I expect that possible deviations from linearity will mainly affect the strength of a contraction sustained by coactivated motoneurons but not its global shape and the relative weight of its elementary deformations. Similarly, I expect that coactivation of several longitudinal motoneurons during performance of a local motor reflex (see next Chapter) could produce a saturation of the intensity of the contraction resulting from the combination of their individual deformation fields. However, this kind of non-linear effect would not change significantly the shape of the resulting deformation, which would be easily recognizable as sustained by a pool of longitudinal motoneurons. On the other hand, the experiments I performed (see **Figs. 4.6** and **4.8**) lead me to exclude the possibility that such a multiple coactivation of longitudinal motoneurons could result in a highly non-linear superimposition of their deformation fields, able to change significantly the relative

weight of the elementary deformations expected for a longitudinal contraction. There are not theoretical (possible local linear sums, with or without saturation), anatomical (the arrangement of the longitudinal fibers) and experimental (the data shown in Section 4.2.3) reasons to expect that such a non-linear superimposition could take place. Based on these considerations, it is extremely unlikely that a pure compression (i.e. a deformation with large $E < 0$ and relatively low values of the remaining elementary deformations), such as that produced by mechanical stimulation of the leech skin or P cell stimulation (see **Figs. 4.10** and **4.11**), could simply be accounted by coactivation of longitudinal motoneurons. Given that similar considerations can be applied to all other classes of motoneurons (see **Figs. 4.7** and **4.9**), the only reasonable way to explain the origin of pure compressions, observed during local sensory-motor responses, is to hypothesize that they are sustained by the coactivation of longitudinal and circular muscles so that the large negative S_1 value associated with longitudinal motoneurons is balanced by the large positive S_1 value associated with circular motoneurons (see **Table 4.1** and **Fig. 4.7**). This conclusion, although not fully proofed by data collected so far, is strongly supported by the experiments and by the theoretical considerations described in the present Chapter. It also supported by data reported for other neuromuscular systems, such as that of the frog, in which similar linear sum of force fields produced by muscle activation has been observed (d'Avella and Bizzi, 1998; Bizzi et al., 2000).

The linear sum of skin deformations can be also used to infer which classes of muscle fibers are activated during different kinds of mechanosensory stimulation. As previously discussed, P cell firing induces a pure compression that can be explained by the simultaneous recruitment of longitudinal and circular fibers almost equally activated. Alternatively, when T or N cells are forced to fire, the induced vector field in the skin has large negative values of both S_1 and E. This deformation can be explained as again being

due to longitudinal and circular fibers coactivation, but with circular fibers being activated to a lesser degree than before.

The proposed approach thus seems adequate to identify which muscle classes (longitudinal, circular and oblique) are activated during skin deformations, but cannot identify which specific longitudinal or circular motoneuron is activated.

4.3.4 Motoneuron activation in sensory motor responses

The analysis of deformations induced on the leech skin by a brief mechanical stimulation in isolated segments indicated coactivation of both longitudinal and circular motoneurons (**Figs. 4.10**, **4.12*A***, **4.15*A***). Analysis of elementary deformations supported this conclusion (**Figs. 4.11**, **4.12*C***, **4.15*C***, **4.16*D***). Also in intact leeches longitudinal and circular motoneurons seemed to be coactivated, but the degree of contraction of longitudinal and circular fibers was more variable.

These results indicate that during local bending, a local withdrawal reflex of the leech (Kristan, 1982; Lockery and Kristan, 1990a, b; Lewis and Kristan, 1998b), circular motoneurons are activated. This extends the classical description of this reflex, which has before this work been considered to arise from contraction of longitudinal muscles at the stimulated site and relaxation of those on the opposite side of the body (Kristan, 1982; Lockery and Kristan, 1990a, b). **Figs. 4.10**, **4.12** and **4.15** suggest a slightly different paradigm in which circular muscles are also activated to withdraw the body from the stimulus site. This response is reminiscent of *circumferential indentation*, a reflex induced by moderate mechanical stimulation, observed in young leech embryos by Reynolds et al. (1998). This reflex, presumably mediated by activation of the segment circular muscles, wanes in late embryos and is replaced in adults by local bending. The results presented here show that circular muscle activation is maintained in adult animals as a fundamental component of the local bending. The experiments performed in intact animals suggest an involvement of circular muscles in other local reflexes such as local shortening, a

defensive reflex involving several segments anterior and posterior to the stimulus usually paired with local bending (Wittenberg and Kristan, 1992a, b).

The analysis of the dynamics of the motor responses (**Fig. 4.16**) shows that distinct muscles can be recruited in different phases of the response, suggesting a selective activation of the corresponding pools of motoneurons at specific times.

4.3.5 Role of mechanosensory neurons in local motor responses

The results shown in **Fig. 4.10** clearly show that motor responses evoked by mechanical stimulation are primarily mediated by P cells. In almost all tested preparations, the field of deformation induced by touching the skin dorsally or ventrally had the same shape as the field induced by intracellular stimulation of dorsal or ventral P cells. The relative weight of the elementary deformations was the same in both kinds of stimulation, indicating that the structure of this local motor reflex is almost exclusively mediated by P cells. In comparison to mechanical stimulation, the strength of the motor response was slightly weaker when induced by P cell firing, suggesting an involvement of T cells in enhancing the response. T cells, when individually activated, gave a poor and often negligible contribution to skin contraction (**Fig. 4.12**), but when they were forced to fire simultaneously with P cells, the resulting contraction could potentiate up to 2-fold in comparison to individual P cell stimulation (**Fig. 4.13**).

These results confirm the role of T cells in potentiating contractions when coactivated together with P cells, but to a more minor extent than previously reported (Kristan, 1982). I never observed deformations induced by skin stimulation up to 4-fold greater than P induced deformations (Kristan, 1982). This discrepancy is probably due to the different stimulation protocols used in the present work and by Kristan. He delivered a train of 10 electrical pulses at 10 Hz to the skin, inducing a persistent P and T cell firing at about 10 Hz for 1 s. My mechanical stimuli were much shorter (200 to 400 ms) and induced a persistent high frequency firing in the P cell (**Figs. 4.10** and **4.14*B***) and a

transient ON and OFF high frequency firing in the T cell (**Figs. 4.11** and **4.14*D***). During high frequency P cell firing the transient activation of T cell is probably less effective than during the sustained low frequency firing of both cells.

The N cells are not activated by light mechanical stimulation and do not contribute to these motor responses (**Fig. 4.15**), as expected by previous reports (Kristan, 1982).

5 Highly variable spike trains underlie reproducible sensory-motor responses in the medicinal leech

Once analyzed the processing of a sensory-motor response (local bending) at the level of muscle activation in a leech body-segment (see previous Chapter), the next step in investigating distributed motor behavior in the leech was to characterize the pattern of activity of motoneurons coactivated during such reflexive behavior. More precisely, the part of my Ph.D. project described in this Chapter aimed at investigating the variability of the bending reflex at different levels of processing: mechanosensory neurons, motoneurons, muscle activation and behavior. The major aim of this study was to understand if local bending is mediated by a population code at the level of motoneurons, which can account for its reproducibility.

5.1 Introduction

As recalled in the introductory chapter, the nervous system of the leech is a particularly suitable model to investigate neural coding of sensory-motor responses because it allows both observation of behavior and the simultaneous measurement of a large fraction of its underlying neuronal activity. This Chapter describes the coding of local-bending reflex (see Section 1.2.2) at the level of the output stage of the leech central nervous system (CNS): the motoneurons. The local bending is initiated by a moderate mechanical stimulation of the leech skin and is primarily mediated by mechanosensory pressure (P) cells (see Section 1.2.2 and Results of the previous Chapter, namely Section 4.2.4), whose firing is highly reproducible (Pinato and Torre, 2000). The purpose of the experiments described in this Chapter was to investigate: i) how reproducible is the local bending; ii) how reproducible is its neural coding at the level of motoneurons.

The local bending was quantitatively characterized by computing the optical flow, as described in Chapter 3. The firing activity of a large fraction of motoneurons involved in the behavior was measured by combining parallel extracellular recordings from the roots and spike sorting techniques, as described in Methods (Sections 2.2.1 and 2.5.1).

The results of my experiments show that the firing pattern of individual motoneurons is highly variable from trial to trial and that local bending is mediated by the coactivation of a population of motoneurons firing in a statistically independent way. Because of statistical independence the electrical activity of the motoneuron population becomes less variable. In addition, the time course of muscle contraction primarily depends on the number of incoming motoneuron spikes and not on their exact timing. These mechanisms are the basis of motor output reproducibility in leech local bending.

This Chapter shows that reproducible motor output does not require reproducible firing of individual motoneurons, and illustrate the biophysical mechanisms that allow a reproducible motor output to be driven by highly variable spike trains. These properties, here demonstrated in the leech nervous system, are likely to be general features of neural computation, and widely present across nervous systems.

5.2 Results

5.2.1 Reproducibility of the local bending

I studied the firing pattern of mechanosensory neurons and the reproducibility of the local bending by using a body-wall preparation, in which a leech body wall segment was flattened over a piece of Sylgard while ganglion innervation was maintained (see Section 2.1.2).

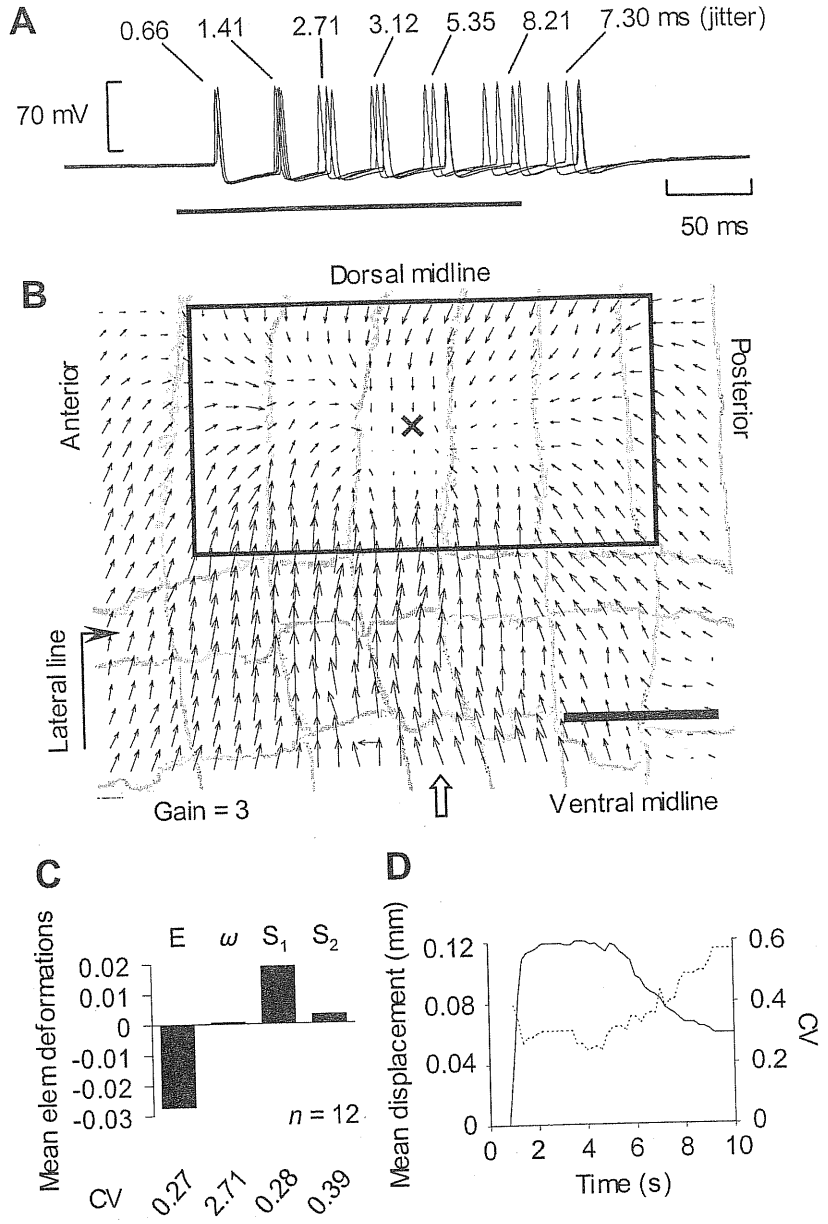

Figure 5.1 Reproducibility of local bending. *A*, Four superimposed intracellular recordings from dorsal P cell following identical mechanical stimulation (20 mN) of the dorsal leech skin. The thick bar indicates the stimulus duration (200 ms). The jitter of each spike is reported in ms. *B*, Optical flow describing the maximal skin deformation induced by evoking two action potentials in the P_d. The gray background shows the shape of the preparation. The central annulus of the innervated segment is indicated by the white arrow. The X indicates the singular point. The window is the linearization region, where the elementary deformations shown in *C* were computed. Arrow magnification 3 ×. *C*, Decomposition of the optical flow in the solid box of *B* into the four elementary deformations: expansion *E*, rotation ω, and two shear components S_1 and S_2. The mean values of the elementary deformations over 12 trials of the same stimulation are drawn. Their coefficient of variation (CV) is shown at the bottom of the panel. *D*, Time evolution of the displacement (solid line) and of the corresponding CV (dotted line) of a representative point on the leech skin during the same trials of *C*.

Fig. 5.1*A* shows the typical firing pattern of a dorsal P cell (P_d), following mechanical stimulation of the dorsal body wall. When the skin was touched with a nylon filament, the cell P_d quickly responded with a highly reproducible firing. In fact both the number of spikes and their timing were highly reproducible, with a jitter ranging from less than 100 μs to less than 4 ms for the first four spikes fired by the neuron (Pinato and Torre, 2000). These data and those reported by Pinato and Torre (2000) suggest that the coefficient of variation of the number of spikes fired by P cell following mechanical stimulation is near 0, i.e. much smaller than the value (around 0.19) previously reported by Lewis and Kristan (1998). However, it must be considered that the spike trains shown in **Fig. 5.1** were induced by a stimulus (200 ms) much shorter than that used by Lewis and Kristan (500 ms), which counted the spikes in a still larger time window (700 ms) after the stimulus onset. Since the variability of the firing pattern of P cells progressively increases with the stimulus duration (Pinato and Torre, 2000), the higher variability reported by Lewis and Kristan can be easily explained in terms of duration of the applied stimulus and of the time window chosen to count the spikes.

The firing of mechanosensory neurons made muscle fibers contract and initiate local bending. As shown in Section 4.2.4, the intensity and shape of local bending is almost completely determined by the P cells (Kristan, 1982). Therefore, the motor response evoked by a controlled number of spikes in one of the P cells was studied. The associated maximal skin deformation was quantitatively characterized by computing the optical flow, which is a two-dimensional vector field that describes the point displacements on the skin and provides a complete characterization of the motor response (see Chapter 3).

Fig. 5.1*B* shows the optical flow induced on the leech skin by evoking two spikes in the cell P_d. The flow is drawn on a gray background, showing the annular margins of the imaged skin preparation. The local structure of the optical flow can be analyzed by

computing its best linear approximation in a region (the window in **Fig. 5.1*B***) around its stationary point (the X in **Fig. 5.1*B***). The linear approximation is completely characterized by six parameters: the coordinates of the stationary point and the four elementary deformations: rotation (ω), expansion (E), horizontal (S_1), and oblique (S_2) shear (see Chapter 3, namely Section 3.4). The flow shown in **Fig. 5.1*B*** is a dorsal compression, sustained by coactivation of longitudinal and circular muscles (see Chapter 4, namely Section 4.2.4) and characterized by a high negative expansion (E) and a significant positive shear (S_1) (**Fig. 5.1*C***). I quantified the reproducibility of this motor response by computing the coefficient of variation (CV) of its significant elementary deformations (E and S_1), which was around 0.3 (bottom of **Fig. 5.1*C***). The variability of the motor response was also quantified by measuring the displacement of selected points on the leech skin and by measuring their CV (**Fig. 5.1*D***). These points were usually selected at the edge of the region chosen to compute the linearization (the window in **Fig. 5.1*B***). On average, the CV of the point displacements was between 0.2 and 0.3. These results were confirmed by experiments repeated on 7 different preparations, in which the dorsal and the ventral P cells were alternatively stimulated and the skin was touched. All these experiments showed that the pattern of skin deformation during local bending is characterized by a CV between 0.2 and 0.3 in both its global shape and the displacement of single points on the skin surface.

5.2.2 Timing of motoneuron spike trains and low-pass filter properties of muscle fibers

Having assessed the reproducibility of the local bending (**Fig. 5.1*C*** and ***D***) and of its coding at the level of mechanosensory neurons (see **Fig. 5.1*A***) (Pinato and Torre, 2000), the next step of my analysis was to investigate the reproducibility of spike trains in motoneurons, i.e. in the ganglion output.

The firing pattern of motoneurons following P cell stimulation was studied in the isolated leech ganglion. By using extracellular suction pipettes it was possible to record voltage signals from fine roots ipsilateral to the stimulated P cell and to precisely characterize the variability of motoneuron spike trains involved in local bending (see Sections 2.2.1 and 2.5.1).

Fig. 5.2*A* shows three extracellular recordings from the DP:B2 bifurcation, obtained during identical repeated stimulation of the dorsal P cell (intracellular recording from P cell shown at the bottom of **Fig. 5.2*A***). Spikes fired by three identified motoneurons are indicated by rows of dots of different colors: green, motoneuron 6; blue, motoneuron L; red, motoneuron 3. These are all excitatory motoneurons innervating longitudinal muscle fiber, responsible for the shortening of the leech body during local bending. These motoneurons fired in a rather irregular way among different trials and this result is emphasized by the comparison with the precise timing of the spikes fired by P cell (black dots). **Fig. 5.2*B*** shows the jitter of the first spike evoked in these motoneurons and in other five longitudinal excitatory motoneurons (blue circles), simultaneously recorded from the other roots. Data from similar experiments performed on other two preparations are also shown (red squares and green triangles). In every experiment, the firing pattern of all coactivated motoneurons was much more variable than the firing activity of mechanosensory neurons (compare **Fig. 5.1*A***). The first spikes occurred with a jitter usually higher than 10 ms (2^{nd} exp: motoneuron 5 ~ 6 ms, motoneuron 107 ~ 8 ms; 1^{st} and 2^{nd} exp: motoneuron 3 ~ 19 ms; motoneuron 6 ~ 12 ms) and often of the order of 50-100 ms. For some motoneurons the jitter was higher than 200 ms (1^{st} exp: motoneurons 4 and 8 – data not shown). The second spikes had a still higher jitter, while the third, fourth and fifth spikes had jitters ranging from several hundred milliseconds to more than 1000 ms (data not shown).

These experiments were repeated in five different preparations (data from three of them shown in **Fig. 5.2*B***), in which the dorsal and the ventral P cells were alternatively stimulated. As shown in **Fig. 5.2*B***, for some motoneurons the value of the jitter of the first and consecutive spikes had a large variability from preparation to preparation.

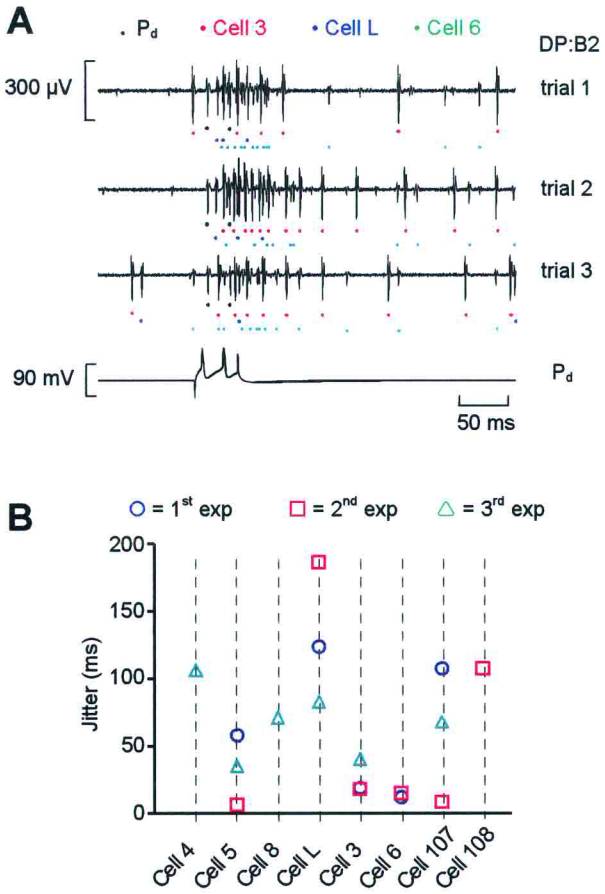

Figure 5.2 Variability of motoneuron spike trains during local bending. *A*, Three extracellular voltage recordings from the DP:B2 root during identical intracellular stimulation of a P cell with two spikes (lowest trace). In the extracellular recordings the spikes from P cell and from motoneurons 3, L and 6 are indicated by black, red, blue and green dots respectively. *B*, Blue circles: jitter of the first spike of the motoneurons shown in *A* and of other five motoneurons, simultaneously recorded from the AA, MA, PP and DP:B1 roots. Red squares and green triangles: similar data obtained from identical experiments repeated in other two preparations. In all three experiment considered, spike discharges in motoneurons were evoked by intracellular stimulation of a dorsal P cell with two spikes. Jitter was computed from 76, 85 and 44 repetitions of the same stimulation for respectively experiments 1 (blue circles), 2 (red squares) and 3 (green triangles). Motoneurons 4, 5, 8, L, 3, 6, 107 and 108 are all excitors of longitudinal muscles.

In summary, all these experiments clearly showed that the precise time coding of the stimulus in mechanosensory neurons is not preserved at the level of the motoneurons. Nevertheless the motor response elicited by local mechanical stimulation of the leech skin is significantly reproducible (**Fig. 5.1*C*** and ***D***).

One of the biophysical mechanisms that can account for the reproducibility of the local bending is the low-pass filtering property of the muscles. Leech muscles (Mason and Kristan, 1982), as some muscles of other invertebrates and lower vertebrates (Morris and Hooper, 1997; Morris and Hooper, 1998) contract very slowly and integrate the incoming spike trains over a very long time window (several hundred milliseconds). This suggests that the time course of the muscle contraction primarily depends on the number of spikes fired by the activated motoneurons (Mason and Kristan, 1982; Morris and Hooper, 1997) and not on their exact timing.

I verified this integration property of the leech muscles in a series of experiments in which the spike timing of a single motoneuron was changed by applying depolarizing current steps of different duration and intensity but which all evoked the same total number of action potentials. **Fig. 5.3*A*** shows the time course of the displacement of a selected point on the leech skin, when spike trains of different duration and frequency were evoked in motoneuron 3, an excitor of longitudinal muscles. The displacements indicated by the red and the black traces of **Fig. 5.3*A*** were induced by the spike discharges shown respectively in **Figs. 5.3*B*** (*first* stimulation protocol) and ***C*** (*second* stimulation protocol). The total number of spikes evoked by these two intracellular stimuli was the same (37) but their time distribution was completely different. Nevertheless, the resulting displacements were almost identical. Note that muscle contraction has an intrinsic high variability, so that, when a spike train identical to that shown in **Fig. 5.3*B*** was again evoked, the corresponding displacement (blue line in **Fig. 5.3*A***) differed from the red trace more than the black trace did (this property will be discussed in the next section).

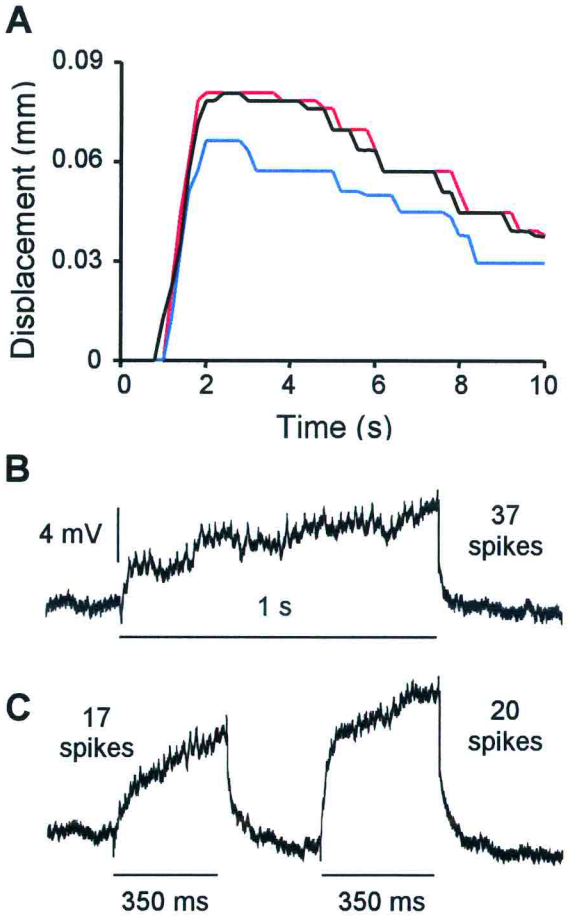

Figure 5.3 Low-pass filter properties of muscle fibers. *A*, Time course of the displacement of a selected point on the leech skin, when motoneuron 3 was forced to fire a controlled number of spikes (37) in three different stimulations. The displacements indicated by the red and the black traces were induced by the spike discharges shown respectively in panels *B* and *C*. The displacement indicated by the blue trace was evoked by a spike discharge similar to that shown in *B*. *B*, Spike train evoked in motoneuron 3 by a single depolarizing current step of 0.7 nA lasting 1 s (total number of evoked spikes = 37). *C*, Spike train evoked in motoneuron 3 by two consecutive depolarizing current steps of 1 nA lasting 350 ms each (total numb7er of evoked spikes = 37).

Data presented in **Fig. 5.3** show that contractions induced by the second protocols do not differ from contractions induced by the first one more than what would be expected from the natural variability of muscle contraction evoked by a fixed number of spikes (see

Fig. 5.5). Similar stimulation protocols, applied to five different motoneurons in three different preparations, confirmed the results shown in **Fig. 5.3**. In all experiments, skin displacements evoked by the second protocol were always statistically indistinguishable by those evoked by the first one: 1) the second protocol produced displacements which were always within 1 standard deviation (STD) from the mean displacement induced by the first stimulation protocol; 2) including data from the second protocol in the computation of mean and STD for the first one, did not significantly change the value of the mean nor increase the STD.

5.2.3 Reproducibility of motoneuron firing

Having assessed that muscle contraction primarily depends on the number of spikes fired by activated motoneurons, I investigated the reproducibility of motoneuron firing following mechanical stimulation. As shown in **Fig. 5.3**, the contraction of leech muscles is not sensitive to the jitter of the motoneuron spikes, but muscle contraction may be sensitive to the number of the incoming spikes in the time window over which spikes are integrated. In fact, **Fig. 5.2*A*** shows that not only the spike timing of coactivated motoneurons is significantly variable, but the spike number too.

I quantified the statistical properties of motoneuron firing by computing the average firing rate (AFR) and its CV for all identified motoneurons coactivated during local bending. I used a 200 ms time bin, because this is large enough to observe a noticeable skin contraction when single motoneurons are induced to fire at physiological rate. Moreover, in the experiments performed to study local bending, muscle contraction developed after 200 ms following mechanosensory stimulation and reached its peak in about 1 s (see **Fig. 5.1*D***). Therefore, muscle fibers integrate motoneuron spikes over an effective time window of about 200-400 ms.

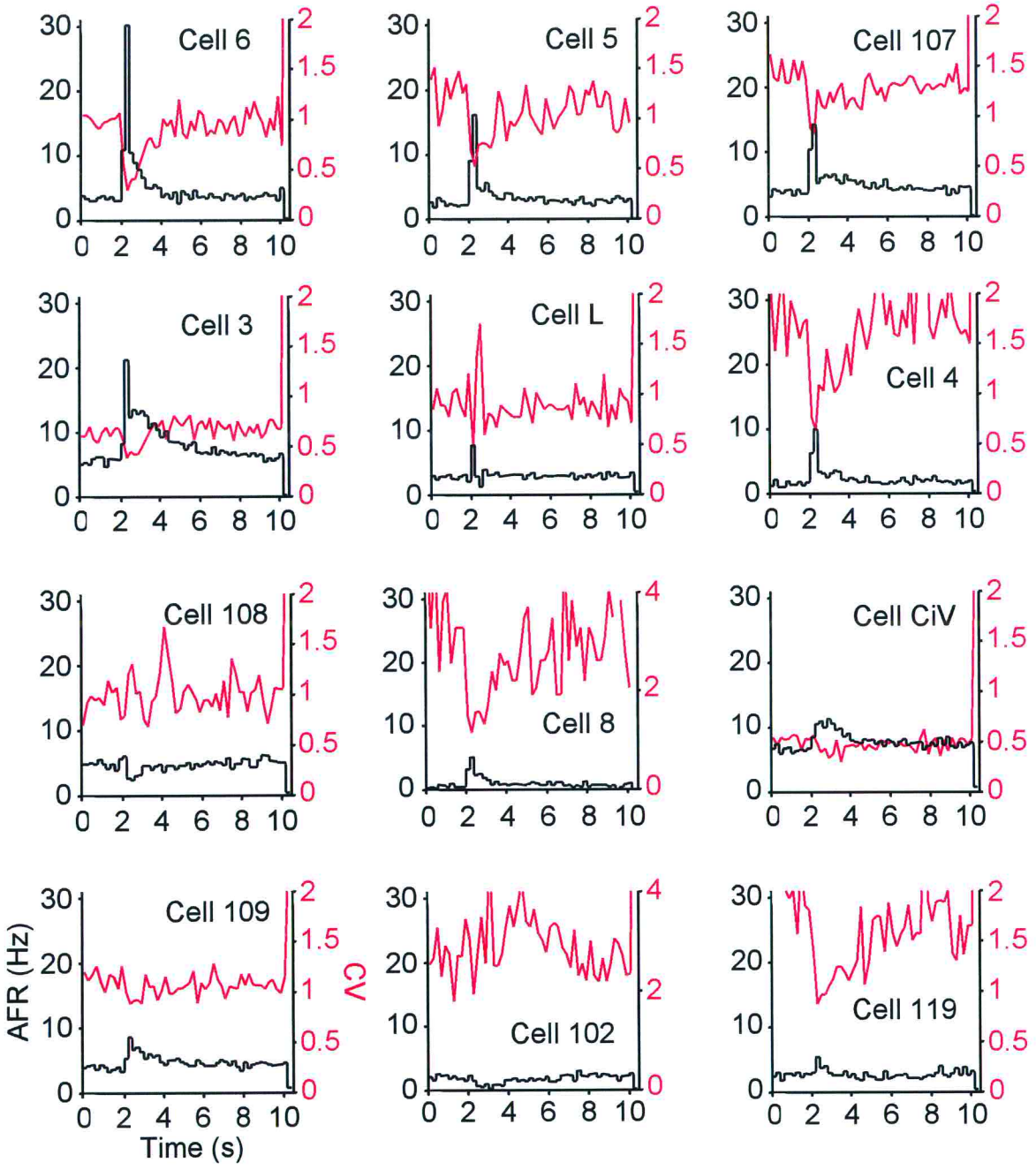

Figure 5.4 First order statistics of motoneuron spike trains. Average firing rate (black lines) and coefficient of variation (red lines) of the activity of twelve coactivated motoneurons during local bending. Motoneurons from the same experiment analyzed in Figs. 5.2*A* and *B* (blues circles). Local bending was elicited by inducing dorsal P cell to fire two spikes. Data obtained from 76 different trials. Binwidth 200 ms.

Fig. 5.4 shows the AFR (black line) and the CV (red line) for all identified motoneurons from the experiment already shown in **Figs. 5.2*A*** and ***B*** (blue circles). In the experiment, two spikes were evoked in the cell P_d. All motoneuron bursts were recorded from roots ipsilateral to the stimulated cell P_d. This means that the innervation fields of the recorded motoneurons were all ipsilateral to the receptive field of the cell P_d (controlateral motoneurons were not recorded in the present study). As expected (Lockery and Kristan, 1990a), all the identified dorsal excitors (DEs), i.e., the excitatory motoneurons of dorsal longitudinal muscles, were activated by the stimulus. The firing rate of these motoneurons (cells 6, 5, 107 and 3) increased to 15-30 Hz after 30-60 ms (mean latency of the first spike) from the stimulus onset, with a CV transiently decreasing from about 1 to a value between 0.3 and 0.5 at the peak of the response. Other identified motoneurons were coactivated by the stimulus: cell L, excitor of all longitudinal muscles; cell 4 and 8, ventral excitors (VI); cell CiV, an excitor of ventral circular muscles; cell 109, an excitor of flattener muscles (FE); cell 119, a ventral inhibitor (VI). These neurons were activated at lower rate (5-10 Hz) with a CV at the peak of the response just lower than 1 for most of them. Other motoneurons were inhibited: cell 108, a VE; cell 102, a dorsal inhibitor (DI).

This pattern of activation of motoneurons is consistent with the classical description of the dorsal local bending: activation of all DEs and cell L, activation of VI and inhibition of DI and VE (Lockery and Kristan, 1990a). It also confirms the involvement of motoneurons inducing transverse contractions (CiV and FE) in the local bending (see previous Chapter, namely Section 4.2.4). **Fig. 5.4** shows that also some VEs, as cell 4 and 8, were excited. These neurons were activated at a low rate by the P_d firing (5-10 Hz), while P_v firing activated them at much higher rate (20-30 Hz - data not shown). As general trend, in all experiments performed (five), I observed that: 1) DEs and VEs were always strongly activated by, respectively, P_d and P_v firing; 2) some VEs and some DEs

could be activated at low rate by, respectively, P_d and P_v firing. These results suggest that some VEs and some DEs can be recruited during the stimulation of, respectively, dorsal and ventral P cells, in a rather variable way from preparation to preparation. This is consistent with the execution of lateral bending, which is usually elicited by simultaneous activation of both dorsal and ventral P cells on the same side of the ganglion (Lockery and Kristan, 1990a; Lockery and Kristan, 1990b; Kristan et al., 1995).

Fig. 5.4 shows that the CV of the firing activity of individual motoneurons coactivated during local bending is rather high. All activated motoneurons have a CV between 0.4 and 1 at the peak of the response, with the only exception of cell 6 (CV ~ 0.3). Similar results were obtained in all five tested preparations, in which the dorsal and ventral P cells were alternatively stimulated. In every experiment between 8 and 12 motoneurons were simultaneously recorded and identified and their AFR and CV were computed. Almost all recorded motoneurons had a CV between 0.4 and 1 at the peak of the AFR. No more than one dorsal or ventral excitor per experiment had a CV ~ 0.3, following stimulation, respectively, of the dorsal or ventral P cell. To test if such variable firing rates in individual motoneurons can sustain the reproducible motor responses observed during local bending (see **Fig. 5.1*C*** and ***D***), I investigated the reproducibility of the contractions induced by single motoneuron firing.

5.2.4 Variability of muscle contraction

The variability of the motor response depends on the variability of the motoneuron firing pattern as well as on the variability of the muscle contraction. This, in turn, can be due to the variability in the neurotransmitter release at the neuromuscular junction and/or to spike conduction failure at some axonal branches of the innervating motoneuron, in the case of multiple branches innervation of the muscle (Stuart, 1970; Hoover et al., 2002).

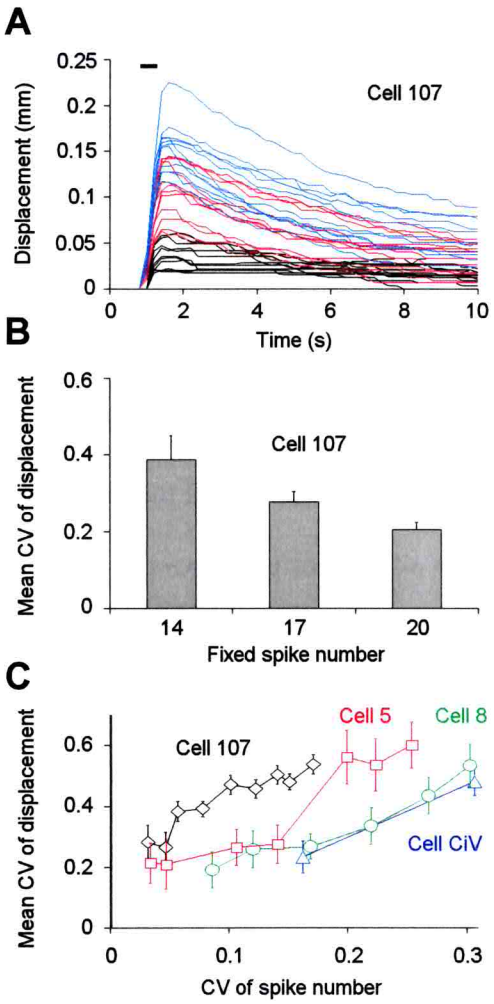

Figure 5.5 Variability of muscle contraction. *A*, Displacements of a selected point on the leech skin during the repetitive stimulation of motoneuron 107 with depolarizing current steps of increasing size lasting 400 ms (horizontal bar) and evoking a controlled number of spikes in the neuron. 11 trials (black lines) with 14 spikes, 12 trials (red lines) with 17 spikes and 11 trials (blue lines) with 20 spikes were recorded. *B*, Mean CV of the maximum displacement of 6 selected points, when a fixed number of spikes was evoked in motoneuron 107 in different repetitions. 11, 12 and 11 repetitions with 14, 17 and 20 spikes respectively were considered. *C*, Relation between the mean CV of the maximum displacement of 6 selected points and the CV of the spike number for motoneurons 107 (black ◊), 5 (red □) , 8 (green ○) and CiV (blue Δ) impaled in four different preparations.

I studied the variability of muscle contraction by impaling individual motoneurons with a sharp intracellular electrode and by evoking a controlled number of spikes. I followed the displacement of a representative point on the skin when 14 (black traces), 17 (red traces) or 20 spikes (blue traces) were evoked within 400 msec in motoneuron 107 (**Fig. 5.5*A***) by depolarizing current steps of increasing size. The CV of the associated displacement for a fixed number of spikes was around 0.4 for 17 spikes and decreased to around 0.2 for 20 or more spikes (**Fig. 5.5*B***). When the number of spikes of the motoneuron was allowed to vary, the CV of the skin displacement increased almost linearly with the CV of the motoneuron firing, as shown in **Fig. 5.5*C*** (black line). **Fig. 5.5*C*** also shows a similar trend for three other motoneurons in three different preparations: cell 5 (red line), cell 8 (green line) and cell CiV (blue line). These results, repeated in four different preparations, show that the CV measured for the local bending, between 0.2 and 0.3 (see **Fig. 5.1*C*** and ***D***), is just larger than the CV of the skin deformation evoked by a single motoneuron firing with a CV of almost 0, i.e. with almost perfect reproducibility (**Fig. 5.5*B***). From the data shown in **Fig. 5.5*C*** I expect that a CV of the skin displacement between 0.2 and 0.5 should be produced by a single motoneuron firing with a CV varying between 0.1 and 0.2. Single motoneurons whose firing rate has a CV ≥ 0.3 cannot induce skin deformations with a CV lower than 0.5.

Fig. 5.4 suggests that the CV of the firing rate of coactivated motoneurons, at the peak of the response, is too high to account for the reproducibility of local bending. However, for slow-contracting, non-spiking muscles, such as those of the leech, the contraction amplitude primarily depends on the number of spikes in the motoneuron burst induced by mechanosensory stimulation rather than on the firing frequency of motoneurons (Morris and Hooper, 1997). **Fig. 5.6** shows the CV of the spike number, in time bins of increasing size following P_d firing, for the first eight motoneurons analyzed in

Fig. 5.4. The time bin varies from 200 ms (the same of **Fig. 5.4**) to 1 s, because local bending reached its peak in about 1 s by the onset of the P cell stimulation (see **Fig. 5.1*D***) and the more active motoneurons (first four panels in **Fig. 5.4**) fired at sustained rate for about 1 – 1.2 s. Counting spikes in time windows of increasing size slightly reduced the variability in the number of spikes fired by activated motoneurons (**Fig. 5.6**). Nevertheless, even when very long time window (1s) were taken into account, the CV of the spike number of just one motoneuron (cell 6) reached a value as low as 0.2. All other motoneuron bursts had a CV ≥ 0.3 : cell 3 and L ~ 0.3; cell 5 ~ 0.35; cell 4 ~ 0.5; cells 108, 107 and 8 > 0.7.

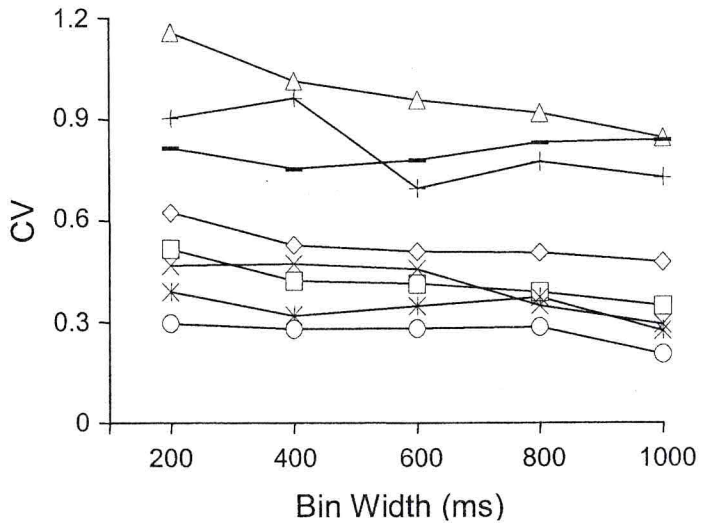

Figure 5.6 Variability of spike number in motoneuron bursts. Coefficient of variation of the spike number, in time bins of increasing size following P_d firing, for motoneurons 6 (○), 3 (✻), L (×), 5 (□), 4 (◇), 108 (+), 107 (−) and 8 (△) (same data of Fig. 5.4).

Data presented in **Figs. 5.4**, **5.5** and **5.6** clearly show that the reproducibility of the local bending cannot be exclusively explained by the low-pass filtering properties of the leech muscles (see **Fig. 5.3**). Although muscle fibers are not sensitive to the timing of the

incoming spikes, muscle contractions are rather sensitive to variations in the spike number (**Fig. 5.5*C***). The AFR of individual motoneurons, coactivated during local bending (**Fig. 5.4**), is definitely too variable to account for this reproducible behavior. Moreover, the number of spikes in motoneuron bursts lasting up to 1 s, is also too variable to explain the reproducibility of the local bending (**Fig. 5.6**). Some other mechanism should take place to reduce variability of the motor output.

5.2.5 Distributed organization of the motor output

A biophysical mechanism that can explain such a low variability of the local bending is the distributed organization of the firing activity sustaining it, at the level of the motoneurons. **Fig. 5.7** shows the second order statistics for the activity of some motoneurons whose AFR and CV were reported in **Fig. 5.4**. As described in Section 2.5.3, the second order statistics was characterized by computing, for each pair of coactivated motoneurons, the joint probability p_{ij} that both motoneurons fire one spike, and H_{ij}, the joint entropy of their firing activity (Pinato et al., 2000). For all pairs of motoneurons shown in **Fig. 5.7** (the most strongly activated during local bending - see **Fig. 5.4**), p_{ij} was almost equal to $p_i\, p_j$ and H_{ij} was identical to $H_i + H_j$ (see Section 2.5.3). Thus, the firing of these motoneurons, co-activated during local bending, was pair-wise statistically independent. I found similar results for every pair of motoneurons shown in **Fig. 5.4** and for every pair of motoneurons recorded in the other five experiments I performed.

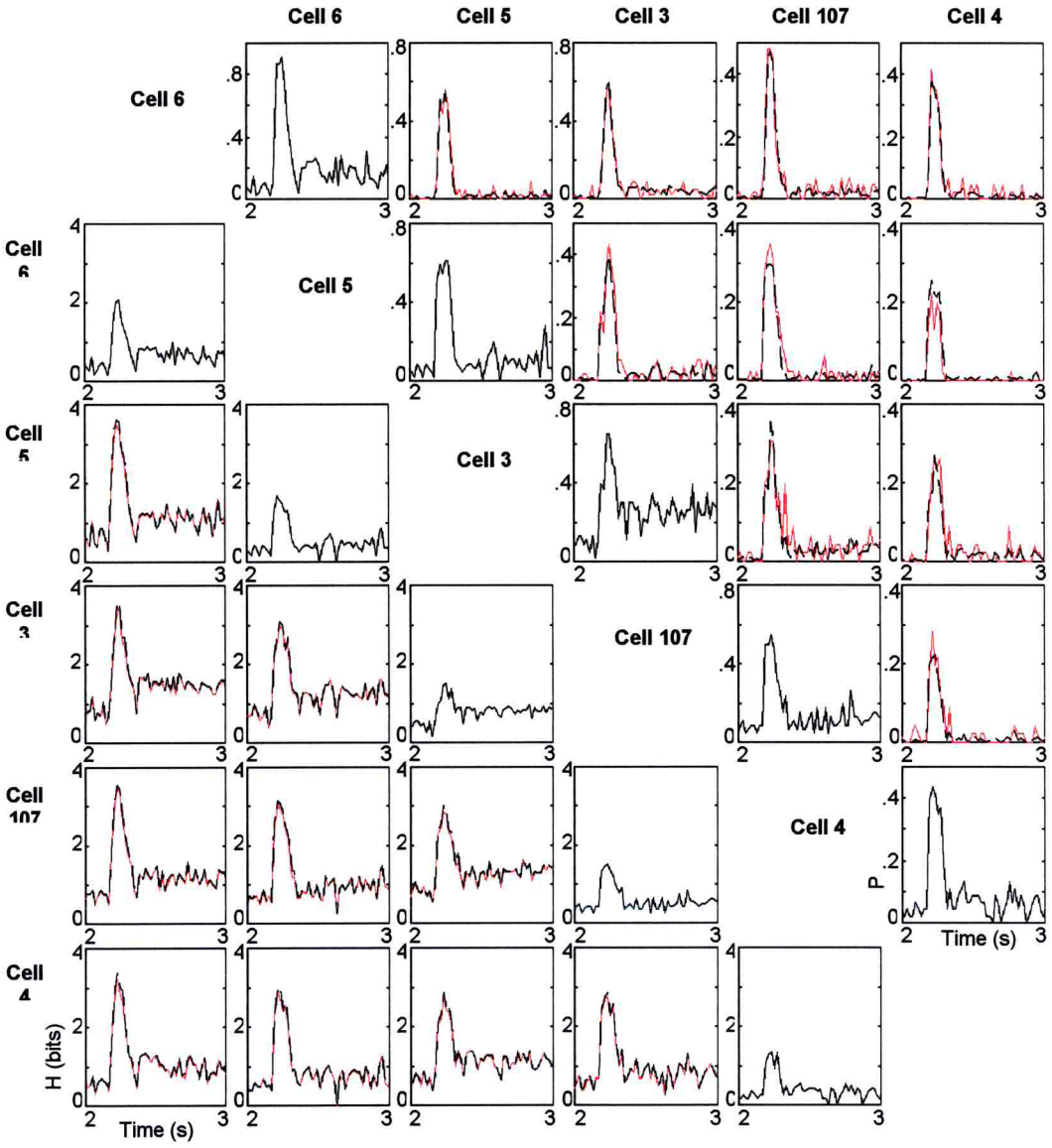

Figure 5.7 Second order statistics of motoneuron spike trains. Second order statistics for motoneurons 6, 5, 3, 107 and 4, whose AFR and CV are shown in Fig. 5.4. Upper right panels: for each pair of motoneurons i and j, the joint probability of fire p_{ij} (red line) is compared to the product of individual probabilities $p_i\ p_j$ (black dashed line). Lower left panels: the joint entropy H_{ij} (red line) is compared to the sum of individual entropies H_i+H_j (black dashed line). Binwidth 20 ms.

These observations suggest that the motor response analyzed in **Fig. 5.1** has a distributed organization (Tsau et al., 1994; Wu et al., 1994; Lewis and Kristan, 1998; Pinato et al., 2000): it is produced by the coactivation of a population of motoneurons and its low variability is the result of the underlying neuron pooling. This is supported by **Fig. 5.8*A***, where the CVs of the firing rates of all identified longitudinal motoneurons activated during local bending (first eigth neurons of **Fig. 5.4**) are drawn (dashed lined) together with the CV of their ensemble activity (solid line). **Fig. 5.8*A*** clearly shows that the CV of each individual motoneuron in the pool is significantly higher than that of the pooled activity (rarely over 0.5 and close to 0.2 at the peak of the response). A similar result was obtained when the number of spikes in motoneuron bursts was counted and its CV was computed (see **Fig. 5.6**). The number of spikes of the population of coactivated motoneurons had a CV always close to 0.2 for every selected time window (from 200 ms up to 1 s, in steps of 200 ms). This increase in reproducibility of the population firing is a consequence of the statistical independence illustrated in **Fig. 5.7** (Pinato et al., 2000). The pattern of activation of motoneurons following dorsal and ventral P cell firing was analyzed in five different preparations. All these experiments gave results similar to those shown in **Figs. 5.4**, **5.7** and **5.8*A***: motoneurons fired quite irregularly from trial to trial, but the CV of their pooled activity had a minimum lower than 0.2 because of their statistical independence. On the basis of data shown in **Fig. 5.5**, this CV is small enough to guarantee a motor response as reproducible as that shown in **Fig. 5.1**.

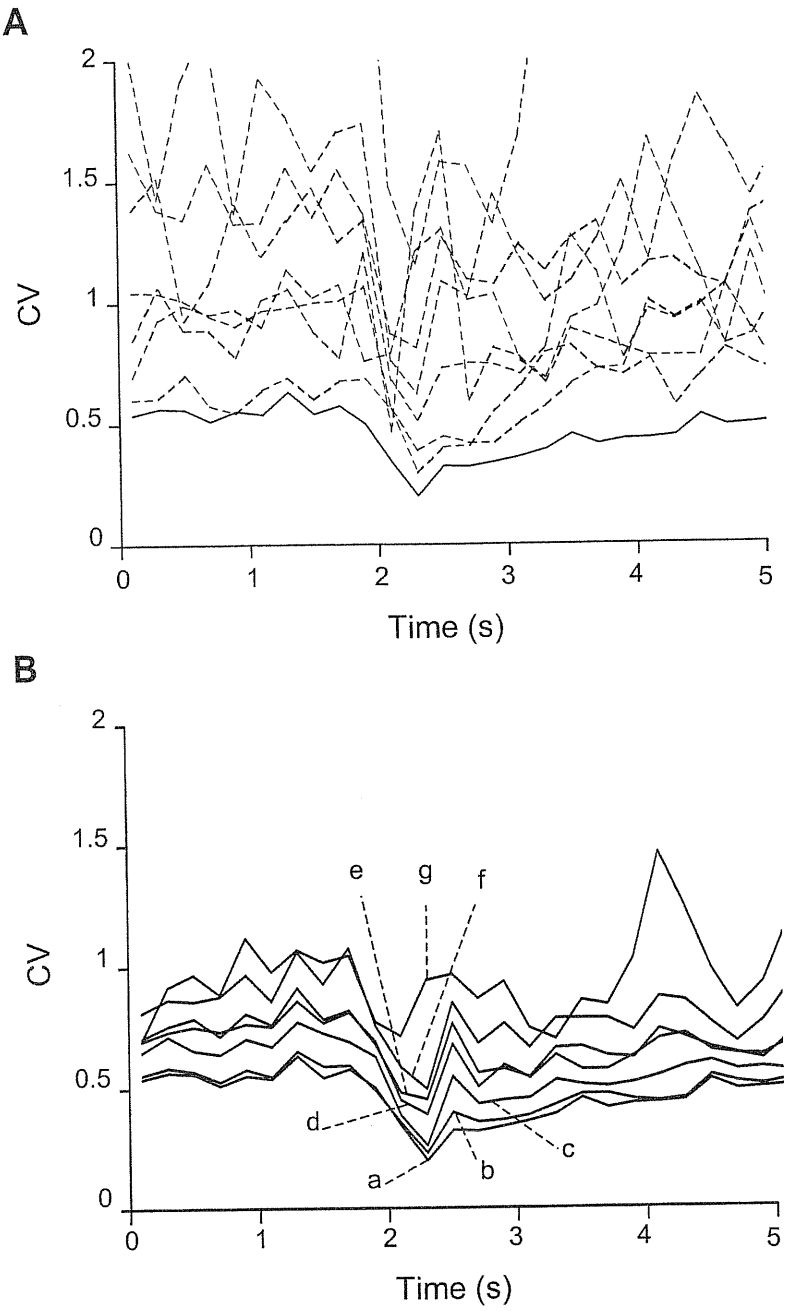

Figure 5.8 Pooling variability of coactivated motoneurons. *A*, The CV of 8 longitudinal motoneurons (cells 6, 5, 107, 3, L, 4, 108 and 8) coactivated during local bending (dashed lines) is compared to the CV (solid line) of their pooled activity. Motoneurons from the same experiment analyzed in Figs. 5.2, 5.4 and 5.6. *B*, The CV of the pooled activity of the same motoneurons is computed by removing individual motoneurons one at the time from the pool. The lower trace (a) is the CV computed for the whole population of motoneurons (cells 6, 5, 107, 3, L, 4, 108 and 8) and corresponds to the solid line of *A*. The other six traces are the CVs obtained by removing from the starting population the following motoneurons: cell 6 (b); cells 6 and 3 (c); cells 6, 3 and 5 (d); cells 6, 3, 5 and 4 (e); cells 6, 3, 5, 4 and L (f); cells 6, 3, 5, 4, L and 107 (g).

This distributed coding across a population of independent motoneurons not only assures reliability of the motor response but also allows graceful degradation of performance with damage to individual motoneurons. We tested robustness of population coding by computing the CV of the pooled activity of the motoneuron population from which data of single motoneurons were removed one at the time. The result is shown in **Fig. 5.8*B***. The CV increased in little steps, while removing individual motoneurons from the pool. This guarantees gradual decrease in reliability of motor output in case of damage to individual motoneurons. Note, in particular, that even the removal from pooling of motoneurons with more reproducible firing (cells 6 and 3) did not remarkably increased the variability of the population firing that still had a CV with a minimum lower than 0.25 (see legend for details).

5.2.6 Local bending is sustained by the coactivation of several motoneurons

Given that local bending is sustained by the coactivation of a population of motoneurons (**Fig. 5.4**), and that skin deformations induced by pairs of motoneurons superimpose linearly (see Section 4.2.3), I tested whether local bending can be approximated by the linear sum of an ensemble of skin deformations induced by individual motoneurons. I addressed this issue in a series of experiments in which I impaled and stimulated the P cells and as many motoneurons as possible in the same skin preparation.

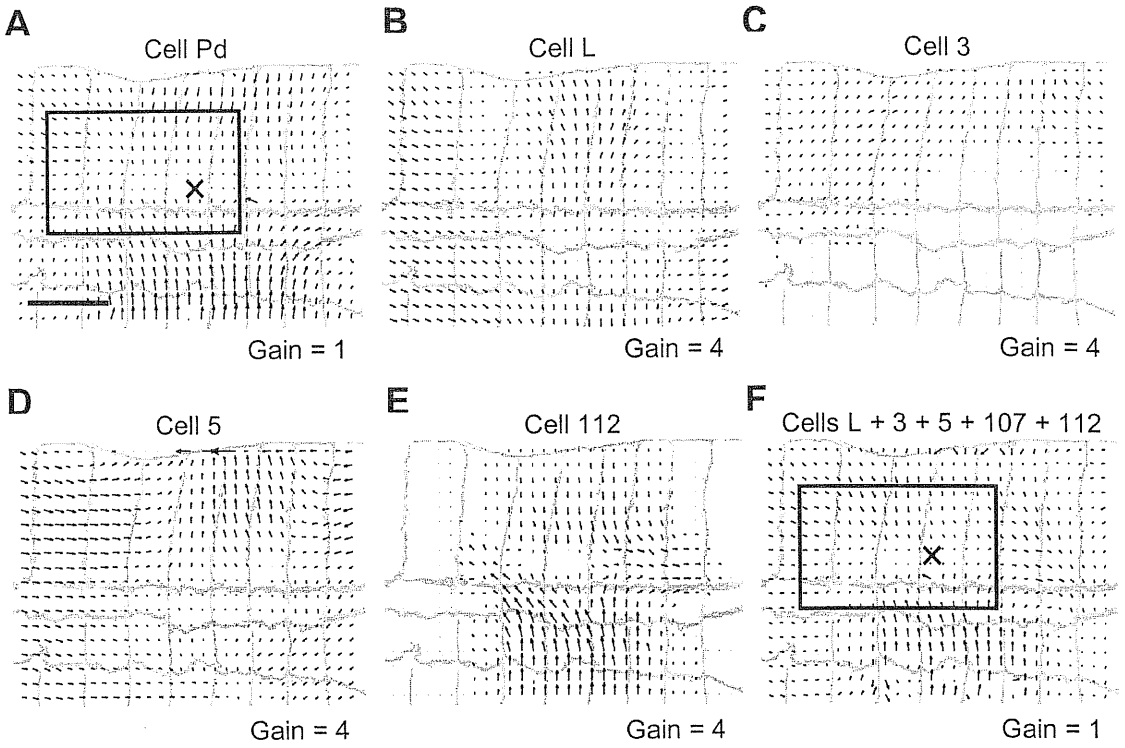

Figure 5.9 Distributed motor output. *A*, Optical flow describing the maximal skin contraction evoked by the firing of two spikes by a dorsal P cell. *B*, *C*, *D* and *E* Optical flows describing the maximal skin contractions induced by the firing of motoneurons L, 3, 5 and 112 respectively at ~ 10-20 Hz in the same preparation. *F*, The linear superposition of the optical flows in *B*, *C*, *D* and *E*. The gain of the optical flow in *A* and *F* is 1, but otherwise is 4. The windows in *A* and *F* are the linearization regions used to compute the stationary point position (Xs) and the elementary deformations shown in Fig. 5.10.

Fig. 5.9 summarizes the results of one of these experiments. **Fig. 5.9*A*** shows the optical flow induced by firing two spikes in a dorsal P cell. In the same preparation motoneurons L, 3, 5, 112 and 107 were impaled. The corresponding optical flows are drawn in **Figs. 5.9*B-E*** (optical flow of cell 107 not shown). These optical flows were obtained by inducing the impaled motoneurons to fire a burst of action potentials at 15 -20 Hz for 400 ms to evoke firing patterns similar to those recorded during P_d stimulation (see **Fig. 5.4**). **Fig. 5.9*F*** shows the linear superposition of these optical flows induced by individual motoneurons. Since most excitors of longitudinal muscles were included in the

sum, a marked similarity between the intensity and shape of the local bending (**Fig. 5.9*A***), and those of the linear sum of the impaled motoneurons (**Fig. 5.9*F***), is apparent. This was confirmed by calculating the elementary deformations of the two fields drawn in **Figs. 5.9*A*** and ***F***. As shown in **Fig. 5.10**, the main elementary deformations (E and S_1) of these two optical flows differ for less than 5%. These results confirm that the local bending cannot be accounted by the activation of just one motoneuron: it is necessary to consider the optical flows associated to a large number of motoneurons to obtain a good approximation of its shape and intensity. Specifically, **Fig. 5.9** shows that the coactivation of several motoneurons, not only assures the reproducibility of the local bending (**Fig. 5.8**) but also its strength (note that the optical flows induced by motoneurons are shown with a magnification four times larger than the optical flow associated with the local bending). These results were confirmed in two other experiments in which a P cell and 3-4 motoneurons were impaled in the same preparation.

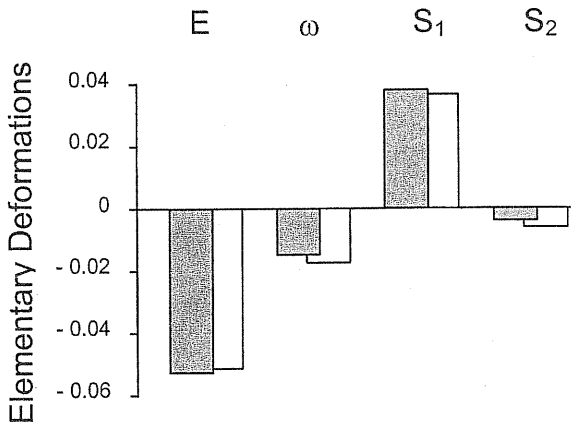

Figure 5.10 Accuracy of the linear superposition. Elementary deformations for the optical flows shown in Figs. 5.9A (gray bars) and F (white bars).

5.3 Discussion

The data presented in this Chapter show that local bending (a simple sensory-motor response of the leech) is rather reproducible (**Fig. 5.1**), but the firing of the motoneurons that sustains it, is much more variable (**Fig. 5.2** and **5.4**). Since it was possible to record simultaneously from the majority of motoneurons involved in the motor response (**Fig. 5.4**) the existence of hidden motoneurons firing in a highly reproducible way is unlikely. Therefore, my conclusion is that highly reproducible spike trains are not necessary for highly reproducible motor responses.

5.3.1 Temporal averaging

Reliability of the behavior is obtained by temporal and ensemble averaging. Temporal averaging is guaranteed by the low pass filtering properties of the leech muscle fibers, which integrate motoneuron spikes within an effective time window of about 200 ms. As shown in **Fig. 5.3**, the low pass properties of muscle fibers make the time course of a contraction relatively insensitive to the jitter of motoneuron spikes.

Muscle contractions produced by individual motoneurons show significant variability even when driven by perfectly reliable spike trains (**Fig. 5.5*B***). When spike trains in a motoneuron have a CV of about 0.25, the resulting muscle contraction has a CV around or greater than 0.5, i.e., significantly higher than the CV of the movements observed during local bending (compare **Figs. 5.1** and **5.5**). Therefore, reliability of local bending cannot be accounted only by the low pass properties of muscle contraction and an additional ensemble averaging is necessary.

5.3.2 Ensemble averaging

The motor response is mediated by coactivation of an ensemble of distinct motoneurons (see **Figs. 5.4**, **5.7** and **5.8**), which fire in an almost statistically independent way (**Fig. 5.7**). Statistical independence compensates for the fluctuations (see **Figs. 5.4** and **5.6**) in the firing of individual motoneurons and thus the ensemble firing of the motoneuron population becomes less variable (**Fig. 5.8**). In addition, fluctuations of muscle contraction evoked by individual motoneurons (see **Fig. 5.5**) will probably be compensated and averaged by statistical independence (Hoover et al., 2002).

Fig. 5.11 shows a simple scheme, indicating where, in the reflex pathway, variability is introduced and which biophysical mechanisms counteract it. The first spikes in the mechanosensory P cell are remarkably reproducible (**Fig. 5.1*A***), often with a jitter of less than 100 μsec (Pinato and Torre, 2000). In a leech ganglion, neural signals from sensory neurons reach motoneurons through monosynaptic and polysynaptic pathways (Muller et al., 1981; Lockery and Kristan, 1990b; Wittenberg and Kristan, 1992). Polysynaptic pathways introduce a significant variability and the first spikes in motoneurons occur with a jitter higher than 10 ms and often of the order of 100 msec (1000 times larger than in mechanosensory neurons). Given these biophysical constraints, reliability of the motor response in the leech is achieved by integrating spikes over a time window of several hundreds of ms and over a population of some dozens of motoneurons. Therefore, population coding in the leech is not only used for interpolation between neurons with different receptive fields (Lewis and Kristan, 1998) or for population vector code (Georgopoulos et al., 1986; Lewis and Kristan, 1998; Georgopoulos, 2000), but also for increasing reliability of the behavior. Indeed, if local bending were not mediated by a motoneuron population, but only by a single motoneuron, given the high variability of individual motoneuron firing (**Fig. 5.4**) and the variability of muscle contraction (**Fig. 5.5**), the resulting motor response would have a CV of around 0.6-0.7, approximately three

times that observed (**Fig. 5.1**). Since we are recording from the majority of leech motoneurons it is highly unlikely that there is an undetected mechanism with more precise spikes.

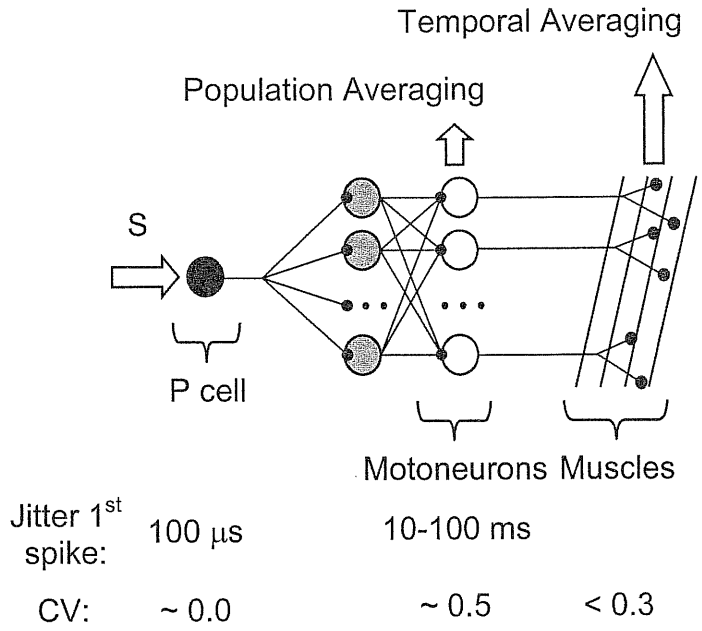

Figure 5.11 Proposed scheme of the neuronal network mediating local bending reflex. Mechanosensory stimuli (S) are coded by precise firing of a pressure P cell (black unit). Then, neural signals cross one layer of interneurons (gray units) to reach motoneurons (white units) that, in turn, innervate muscle fibers. The jitter of the first spike for the P cell and the motoneurons is shown at the bottom of the figure together with the CV of: P cell firing, individual motoneuron firing; amplitude of the motor response. Reliability of the motor response is achieved by integrating spikes over a population of some dozens of motoneurons and over a time window of several hundreds of ms.

5.3.3 Comparison to earlier studies

A number of studies focused on reliability of neural firing in invertebrate (Bialek and Rieke, 1992; de Ruyter van Steveninck RR et al., 1997; Warzecha and Egelhaaf, 1999; Warzecha et al., 2000; Hoover et al., 2002) and mammalian (Shadlen and Newsome, 1994; Mainen and Sejnowski, 1995; Shadlen and Newsome, 1998; Stevens and Zador, 1998;

Kara et al., 2000; Lestienne, 2001) nervous systems, as well as on population coding (Georgopoulos et al., 1986; Lewis and Kristan, 1998; Georgopoulos, 2000), correlated/uncorrelated firing (Zohary et al., 1994; Alonso et al., 1996; Raz et al., 1996; Bergman et al., 1998; Bair et al., 2001; Goldberg et al., 2002), and distributed organization of the neural response (Tsau et al., 1994; Wu et al., 1994; Middlebrooks et al., 1998). The present work describes, for the first time to my knowledge, how the reliability of the spike trains degrades crossing consecutive stages of a nervous system during the execution of a simple behavior, and which biophysical mechanisms the nervous system uses to obtain global reliability with unreliable components. The stimulus is coded by precisely timed spikes in sensory neurons of the input stage but the associated motor response is mediated by a rate code distributed across a population of statistically independent output units. This distributed rate code not only increases reliability of the behavior but also offers several other advantages. It can stabilize the dynamics of the motor response and can assure its robustness, allowing graceful degradation of performance with damage of individual motoneurons (see **Fig. 5.8*B***).

Two recent studies require a more accurate comparison with the present contribution.

The cat visual system

A similar attempt to track variability at different neural stages has recently been performed in the cat visual system by Kara et al. (2000). They recorded simultaneously from three different stages of the cat nervous system and showed that trial-by-trial response variability of visual cells becomes higher at each consecutive visual stage. The present work and that by Kara et al. (2000) substantially differ in the choice of the model nervous system studied (invertebrate versus mammal) and of the investigated neural process (coding of sensory-motor responses versus representation of visual stimuli). Nevertheless, the results reported in the two studies are in general agreement, since both

works show that neural responses become more variable as they cross consecutive synaptic levels.

The stomatogastric neuromuscular system of the lobster

A recent paper by Hoover et al. (2002) is more strictly related to the present work. Hoover et al. recorded simultaneously: 1) the extrajunctional potentials (EJPs) evoked in the pyloric muscles of the lobster stomatogastric neuromuscular system by motor nerve stimulation; and 2) the amplitude of the pyloric muscle contraction. They found high variability in EJP amplitude whereas the contraction of the corresponding pyloric muscle was highly deterministic. The issue they investigated, i.e., how electrical responses with large amplitude variation give rise to deterministic muscle output, is clearly related to the subject of the present Chapter. However, several points make my work and that by Hoover et al. significantly different. They studied the contraction of an individual muscle induced by stimulation of an individual motor nerve, while I investigated neural coding of a sensory-motor response by a population of coactivated sensory and motor neurons. The electrical responses they measured are EJPs in an activated muscle, while I recorded the firing pattern of tens of coactivated motoneurons, each innervating specific muscle fibers. In brief, the results obtained by Hoover et al. can be properly compared only to the results showing variability of the contraction induced by single leech motoneuron firing, as reported in **Fig. 5.5** of the present work. This comparison suggests that variability in the amplitude of EJPs could play similar roles in leech muscles (Stuart, 1970) and in lobster pyloric muscles and be responsible for the variability of the contraction produced by reliable firing of single leech motoneurons (**Fig. 5.5**). Another mechanism proposed by Hoover et al. to reduce pyloric contraction variability – combinatorial averaging of EJPs in individual muscle fibers – could play a similar role in the leech muscles. This is suggested by the reduction in variability I observed when the number of spikes in the burst fired by a single motoneuron was increased (**Fig. 5.5*B***). Finally, averaging across muscle fibers

whose electrical responses are uncorrelated – the second mechanism proposed by Hoover et al. to reduce pyloric contraction variability – supports the idea that statistical independence in the electrical response of coactivated motoneurons (present work) and/or individual muscle fibers (Hoover et al., 2002) is a powerful mean to enhance reliability and stability of muscle contraction.

5.3.4 Conclusions

Averaging action potentials over an ensemble of neurons and over an appropriate time window is a likely mechanism for nervous systems to achieve high reproducibility despite using poorly reliable components such as neurons, synapses, and muscles. The extent of ensemble and time averaging, however, will be constrained by the task to be performed and by the biophysical properties of the specific neurons involved. The precision of spike occurrence depends on the requirements of the action or output: in the present case a significant jitter (even of about 100 ms) and a CV of about 0.4 in individual motoneurons is tolerated. Several tasks performed by the auditory system (Heil and Irvine, 1997; Heil, 1997; Middlebrooks et al., 1998; Furukawa and Middlebrooks, 2002) requires very precise timing among spikes with a jitter of less than 100 μsec. These data suggest that neurons are reliable on the time scale needed to attain the observed behavioral criteria. Therefore, any analysis of reliability of spike trains in a neuron or a population of neurons has to take into account the precision requirements imposed by the action or output to be produced.

Conclusions and perspectives

The experiments described in this thesis aimed at investigating the distributed motor pattern underlying reflexive behavior in the medicinal leech. My major research findings concern the computational role of motoneurons and muscles in mediating leech sensory-motor motor responses, and can be summarized in three main achievements.

First, I developed a new method for quantifying the pattern of deformation induced by muscle contraction on the leech body walls. This method consists in acquiring image sequences of the contracting tissue and then analyzing them, by computing the optical flow, i.e. the two-dimensional vector field describing the point displacements on the imaged tissue. This approach is highly innovative and is superior, for many aspects, to the classical way of quantifying tissue deformations by means of a force or displacement transducer, because it provides a two-dimensional representation of the field of deformation. Moreover, this method, which I demonstrated by analyzing muscle contractions in the leech body-wall, has a general relevance, because it can be applied to characterize every kind of deformation in almost flat tissues with enough texture.

My second major achievement was to successfully apply such method to the analysis of leech sensory-motor responses elicited by local mechanical stimulation of the leech body-wall. In particular, I studied the motor pattern underlying local bending, a motor response caused by moderate mechanical stimulation of the leech skin. In this way, I found out that: 1) all leech motoneurons can be classified according to the field of deformation they elicit on the leech body walls; 2) deformations induced by individual motoneurons sum linearly when pairs of motoneurons are coactivated; and 3) local bending, is sustained by coactivation of two distinct classes of motoneurons (circular and longitudinal) and is almost entirely mediated by one class of mechanosensory neurons (pressure P cells). These results revealed the distributed processing underlying leech

reflexive behavior at the level of muscle activation and motoneuron recruitment, showing that complex motor responses result from the linear sum of a small number of basic behavioral units. These behavioral units correspond to the functional patterns of deformation that activation of different sets of motoneurons and muscles induces on the leech body-wall.

The third major achievement of my Ph.D. project consists in the study of neural coding of leech sensory-motor responses. In particular, I investigated the reproducibility of local bending and that of neural activity sustaining it. My experiments confirmed that local bending is coded by precisely timed spike trains in mechanosensory neurons of the input stage of the leech CNS. On the other side, I found that the firing of individual motoneurons, the output units of the leech CNS, is highly variable. Nevertheless, the pattern of body-wall deformation produced by local bending is much more reproducible than motoneuron firing sustaining it. I verified that reliability of local bending cannot be accounted only by the low pass filtering properties of leech muscles that integrate incoming spikes from motoneurons over large time windows and therefore are poorly sensitive to their timing. The key mechanism able to explain reproducibility of local bending is the finding that this motor response is mediated by a rate code distributed across a population of motoneurons firing in a statistically independent way. Such statistical independence reduces the variability of the population firing and increases reliability of the motor behavior. Therefore, local bending is mediated by a population code at the level of motoneurons, which accounts for its reproducibility.

The research findings described above show the utility of an experimental approach combining quantitative analysis of behavior with electrophysiological recording in a simple invertebrate system such as the medicinal leech. The long-term objective in our lab is to extensively apply the method based on the computation of the optical flow to characterize different kinds of leech motor behavior. In particular, in the near future, we

will investigate the role of inhibitory motoneurons in mediating local bending and the behavioral response produced by activation of controlateral P cells. We expect that firing of controlateral P cells will produce in a body-wall preparation a pattern of relaxation, which should be accounted by activation of ipsilateral inhibitory motoneurons. We will also explore different combinations of simultaneous stimulation of P cell pairs. These experiments will provide a complete behavioral analysis of all possible kinds of local bending in a single segment of leech body-wall.

The next step in analyzing leech reflexive behavior will be investigating the sensory-motor responses in more intact preparations. The first preparation we plan to use will be a whole single segment of leech body-wall. This preparation should allow us to verify how contraction and relaxation can combine in an intact piece of body wall in which local bending can be elicited in a specific region. The second preparation we are planning to use is a piece of body wall composed by multiple body segments kept innervated by the corresponding chain on segmental ganglia. Two or three segments could be used to monitor local motor responses involving more than one segment. For instance, the interaction between local bending and local shortening could be studied at the level of behavioral output and motoneuron activation. The coding of stimulus location along the longitudinal direction of the leech body could also be investigated using this kind of preparation.

A different project, which already started in our lab, is again about the study of leech behavior, but its aims and the experimental approach to achieve them are rather different from those described above. Instead of studying local reflexive behavior in reduced preparations, we started by investigating the explorative behavior of intact and semi-intact leeches. The animals, pinned by the caudal region on the recording chamber, are free to move the anterior part of their body to explore the environment. Colored bins glued on the surface of the leech body are tracked on-line by an imaging system that can

acquire their positions for several hours. The goal of this project is to understand if such explorative movements, apparently random, have any dynamical structure and what can be its functional role. Semi-intact preparations will also be imaged, simultaneously recording the activity of motoneurons in a selected body segment. This will allow us to understand how this explorative behavior can be related to neural activity mediating it.

References

Aggarwal JK, Nandhakumar N (1988) On the computation of motion from sequences of images - A review. Proc IEEE 76: 917-935.

Allen C, Stevens CS (1994) An evaluation of causes for unreliability of synaptic transmission. Proc Natl Acad Sci USA 91:10380-10383.

Alonso JM, Usrey WM, Reid RC (1996) Precisely correlated firing in cells of the lateral geniculate nucleus. Nature 383: 815-819.

Anadan P (1989) A computational framework and an algorithm for the measurement of visual motion. Int J Comput Vision 3: 283-310.

Arisi I, Zoccolan D and Torre V (2001) Distributed motor pattern underlying whole-body shortening in the medicinal leech. J Neurophysiol 86:2475-2488.

Aschwanden P, Guggenbuhl W (1992) Experimental results from a comparative study on correlation-type registration algorithms. In: Robust Computer Vision (Forster, Ruwiedel, eds), pp 268-287. Wichmann.

Baader AP, Kristan WB, Jr. (1995) Parallel pathways coordinate crawling in the medicinal leech, Hirudo medicinalis. J Comp Physiol [A] 176: 715-726.

Baader AP, Bachtold D (1997) Temporal correlation between neuronal tail ganglion activity and locomotion in the leech, Hirudo medicinalis. Invert Neurosci 2: 245-251.

Baader AP (1997) Interneuronal and motor patterns during crawling behavior of semi-intact leeches. J Exp Biol 200: 1369-1381.

Bair W, Zohary E, Newsome WT (2001) Correlated firing in macaque visual area MT: time scales and relationship to behavior. J Neurosci 21: 1676-1697.

Bergman H, Feingold A, Nini A, Raz A, Slovin H, Abeles M, Vaadia E (1998) Physiological aspects of information processing in the basal ganglia of normal and parkinsonian primates. Trends Neurosci 21: 32-38.

Bertero M, Poggio T, Torre V (1988) Ill-posed problems in early vision. Proc IEEE 76: 869-889.

Bialek W, Rieke F, de Ruyter van Steveninck RR, Warland D (1991) Reading a neural code. Science 252: 1854-1857.

Bialek W, Rieke F (1992) Reliability and information transmission in spiking neurons. Trends Neurosci 15: 428-434.

Bizzi E, Tresch MC, Saltiel P, d'Avella A (2000) New perspectives on spinal motor systems. Nat Rev Neurosci 1: 101-108.

Blackshaw SE (1981) Morphology and distribution of touch cell terminals in the skin of the leech. J Physiol 320:219-28.: 219-228.

Blackshaw SE, Nicholls JG, Parnas I (1982) Physiological responses, receptive fields and terminal arborizations of nociceptive cells in the leech. J Physiol 326:251-60.: 251-260.

Blackshaw SE (1993) Stretch receptors and body wall muscle in leeches. Comp Biochem Physiol Comp Physiol 105: 643-652.

Blackshaw SE, Nicholls JG (1995) Neurobiology and development of the leech. J Neurobiol 27: 267-276.

Boulis NM, Sahley CL (1988) A behavioral analysis of habituation and sensitization of shortening in the semi-intact leech. J Neurosci 8: 4621-4627.

Brodfuehrer PD, Friesen WO (1986) Initiation of swimming activity by trigger neurons in the leech subesophageal ganglion. I. Output connections of Tr1 and Tr2. J Comp Physiol [A] 159: 489-502.

Brodfuehrer PD, Debski EA, O'Gara BA, Friesen WO (1995) Neuronal control of leech swimming. J Neurobiol 27: 403-418.

Brodfuehrer PD, Parker HJ, Burns A, Berg M (1995) Regulation of the segmental swim-generating system by a pair of identified interneurons in the leech head ganglion. J Neurophysiol 73: 983-992.

Brodfuehrer PD, Thorogood MS (2001) Identified neurons and leech swimming behavior. Prog Neurobiol 63: 371-381.

Burke RE, Rudomin P, Zajac FE (1970) Catch property in single mammalian motor units. Science 168: 122-124.

Cacciatore TW, Rozenshteyn R, Kristan WB, Jr. (2000) Kinematics and modeling of leech crawling: evidence for an oscillatory behavior produced by propagating waves of excitation. J Neurosci 20: 1643-1655.

Calabrese RL, Nadim F, Olsen OH (1995) Heartbeat control in the medicinal leech: a model system for understanding the origin, coordination, and modulation of rhythmic motor patterns. J Neurobiol 27: 390-402.

Calabrese RL (1995) Oscillation in motor pattern-generating networks. Curr Opin Neurobiol 5: 816-823.

Camhi JM (1988) Escape behavior in the cockroach: distributed neural processing. Experientia 44: 401-408.

Campani M, Verri A (1992) Motion Analysis from first-order properties of optical flow. CVGIP: Image Understanding 56:90-107.

Cang J, Friesen WO (2000) Sensory modification of leech swimming: rhythmic activity of ventral stretch receptors can change intersegmental phase relationships. J Neurosci 20: 7822-7829.

Cang J, Yu X, Friesen WO (2001) Sensory modification of leech swimming: interactions between ventral stretch receptors and swim-related neurons. J Comp Physiol [A] 187: 569-579.

Cang J, Friesen WO (2002) Model for intersegmental coordination of leech swimming: central and sensory mechanisms. J Neurophysiol 87: 2760-2769.

Carlton T, McVean A (1993) A comparison of the performance of two sensory systems in host detection and location in the medicinal leech Hirudo medicinalis. Comp Biochem Physiol Comp Physiol 104: 273-277.

Castellucci VF, Kandel ER (1974) A quantal analysis of the synaptic depression underlying habituation of the gill-withdrawal reflex in Aplysia. Proc Natl Acad Sci U S A 71: 5004-5008.

d'Avella A, Bizzi E (1998) Low dimensionality of supraspinally induced force fields. Proc Natl Acad Sci U S A 95: 7711-7714.

Dan Y, Alonso JM, Usrey WM, Reid RC (1998) Coding of visual information by precisely correlated spikes in the lateral geniculate nucleus. Nat Neurosci 1: 501-507.

De Luca CJ, Erim Z (1994) Common drive of motor units in regulation of muscle force. Trends Neurosci 17: 299-305.

de Ruyter van Steveninck RR, Lewen GD, Strong SP, Koberle R, Bialek W (1997) Reproducibility and variability in neural spike trains. Science 275: 1805-1808.

Eisenhart FJ, Cacciatore TW, Kristan WB, Jr. (2000) A central pattern generator underlies crawling in the medicinal leech. J Comp Physiol [A] 186: 631-643.

Friesen WO, Poon M, Stent GS (1976) An oscillatory neuronal circuit generating a locomotory rhythm. Proc Natl Acad Sci U S A 73: 3734-3738.

Frost WN, Kandel ER (1995) Structure of the network mediating siphon-elicited siphon withdrawal in Aplysia. J Neurophysiol 73: 2413-2427.

Furukawa S, Middlebrooks JC (2002) Cortical representation of auditory space: information-bearing features of spike patterns. J Neurophysiol 87: 1749-1762.

Galbraith JA, Thibault LE, Matteson DR (1993) Mechanical and electrical responses of the squid giant axon to simple elongation. J Biomech Eng 115: 13-22.

Gardner CR, Walker RJ (1982) The roles of putative neurotransmitters and neuromodulators in annelids and related invertebrates. Prog Neurobiol 18: 81-120.

Georgopoulos AP, Schwartz AB, Kettner RE (1986) Neuronal population coding of movement direction. Science 233: 1416-1419.

Georgopoulos AP (2000) Neural aspects of cognitive motor control. Curr Opin Neurobiol 10: 238-241.

Gerstner W, Kreiter AK, Markram H, Herz AV (1997) Neural codes: firing rates and beyond. Proc Natl Acad Sci U S A 94: 12740-12741.

Giachetti A, Cappello M, Torre V (1995) Dynamic segmentation of traffic scenes. Proc IEEE Symp Intell Vehicles, Detroit.

Giachetti A, Torre V (1996) The use of optical flow for the analysis of non-rigid motions. Int J Comput Vision 18: 255-279.

Giachetti A, Campani M, Torre V (1998) The use of optical flow for road navigation. IEEE Trans Robotic Autom 14: 34-48.

Giachetti A (2000) Matching techniques to compute image motion. Image Vision Comput 18: 245-258.

Goldberg JA, Boraud T, Maraton S, Haber SN, Vaadia E, Bergman H (2002) Enhanced synchrony among primary motor cortex neurons in the 1-methyl-4-phenyl-1,2,3,6-tetrahydropyridine primate model of Parkinson's disease. J Neurosci 22: 4639-4653.

Granzow B, Friesen WO, Kristan WB, Jr. (1985) Physiological and morphological analysis of synaptic transmission between leech motor neurons. J Neurosci 5: 2035-2050.

Granzow B, Kristan WB, Jr. (1986) Inhibitory connections between motor neurons modify a centrally generated motor pattern in the leech nervous system. Brain Res 369: 321-325.

Gu XN (1991) Effect of conduction block at axon bifurcations on synaptic transmission to different postsynaptic neurones in the leech. J Physiol 441:755-78.: 755-778.

Gu XN, Muller KJ, Young SR (1991) Synaptic integration at a sensory-motor reflex in the leech. J Physiol 441:733-54.: 733-754.

Gur M, Beylin A, Snodderly DM (1997) Response variability of neurons in primary visual cortex (V1) of alert monkeys. J Neurosci 17: 2914-2920.

Hardingham NR, Larkman AU (1998) Rapid report: the reliability of excitatory synaptic transmission in slices of rat visual cortex in vitro is temperature dependent. J Physiol 507: 249-256.

Heil P (1997) Auditory cortical onset responses revisited. I. First-spike timing. J Neurophysiol 77: 2616-2641.

Heil P, Irvine DR (1997) First-spike timing of auditory-nerve fibers and comparison with auditory cortex. J Neurophysiol 78: 2438-2454.

Hessler NA, Shirke AM, Malinow R (1993) The probability of transmitter release at a mammalian central synapse. Nature 366: 569-572.

Holt GR, Softky WR, Koch C, Douglas RJ (1996) Comparison of discharge variability in vitro and in vivo in cat visual cortex neurons. J Neurophysiol 75: 1806-1814.

Hoover NJ, Weaver AL, Harness PI, Hooper SL (2002) Combinatorial and cross-fiber averaging transform muscle electrical responses with a large stochastic component into deterministic contractions. J Neurosci 22: 1895-1904.

Horn BKP, Schunck BG (2002) Determining optical flow. Artif Intell 17: 185-203.

Jellies J, Johansen KM, Johansen J (1995) Peripheral neurons depend on CNS-derived guidance cues for proper navigation during leech development. Dev Biol 171: 471-482.

Jellies J, Johansen J (1995) Multiple strategies for directed growth cone extension and navigation of peripheral neurons. J Neurobiol 27: 310-325.

Joyce GC, Rack PMH, Westbury DR (1969) The mechanical properties of cat soleus muscle during controlled lengthening and shortening movements. J Physiol 204: 461-474.

Kara P, Reinagel P, Reid RC (2000) Low response variability in simultaneously recorded retinal, thalamic, and cortical neurons. Neuron 27: 635-646.

Kristan WB, Jr., Stent GS (1976) Pepherial feedback in the leech swimming rhythm. Cold Spring Harb Symp Quant Biol 40:663-74.: 663-674.

Kristan WBJr (1982) Sensory and motor neurones responsible for the local bending response in leeches. J Exp Biol 96: 161-180.

Kristan WBJr, Wittenberg G, Nusbaum MP, Stern-Tomlinson W (1988) Multifunctional interneurons in behavioral circuits of the medicinal leech. Experientia 44: 383-389.

Kristan WBJr, Lockery SR, Lewis JE (1995) Using reflexive behaviors of the medicinal leech to study information processing. J Neurobiol 27: 380-389.

Lestienne R (2001) Spike timing, synchronization and information processing on the sensory side of the central nervous system. Prog Neurobiol 65: 545-591.

Levin S, Pearsall G, Ruderman RJ (1978) Von Frey's method of measuring pressure sensibility in the hand: an engineering analysis of the Weinstein-Semmes pressure aesthesiometer. J Hand Surg (Am) 3: 211-216.

Lewis JE, Kristan WBJr (1998) A neuronal network for computing population vectors in the leech. Nature 391: 76-79.

Lewis JE, Kristan WBJr (1998) Representation of touch location by a population of leech sensory neurons. J Neurophysiol 80: 2584-2592.

Lockery SR, Kristan WBJr (1990) Distributed processing of sensory information in the leech. I. Input-output relations of the local bending reflex. J Neurosci 10: 1811-1815.

Lockery SR, Kristan WBJr (1990) Distributed processing of sensory information in the leech. II. Identification of interneurons contributing to the local bending reflex. J Neurosci 10: 1816-1829.

Lockery SR, Sejnowski TJ (1992) Distributed processing of sensory information in the leech. III. A dynamical neural network model of the local bending reflex. J Neurosci 12: 3877-3895.

Lockery SR, Sejnowski TJ (1993) The computational leech. Trends Neurosci 16: 283-290.

Lucas B, Kanade T (1981) An Iterative image registration technique with applications to stereo vision. Proc DARPA Image Und Workshop 21-130.

Mainen ZF, Sejnowski TJ (1995) Reliability of spike timing in neocortical neurons. Science 268: 1503-1506.

Mar A, Drapeau P (1996) Modulation of conduction block in leech mechanosensory neurons. J Neurosci 16: 4335-4343.

Markram H, Tsodyks M (1996) Redistribution of synaptic efficacy between neocortical pyramidal neurons. Nature 382: 807-810.

Mason A, Kristan WBJr (1982) Neuronal excitation, inhibition and modulation of leech longitudinal muscle. J Comp Physiol 146: 527-536.

McAdams CJ, Maunsell JH (1999) Effects of attention on the reliability of individual neurons in monkey visual cortex. Neuron 23: 765-773.

Melinek R, Muller KJ (1996) Action potential initiation site depends on neuronal excitation. J Neurosci 16: 2585-2591.

Middlebrooks JC, Xu L, Eddins AC, Green DM (1998) Codes for sound-source location in nontonotopic auditory cortex. J Neurophysiol 80: 863-881.

Morris LG, Hooper SL (1997) Muscle response to changing neuronal input in the lobster (Panulirus interruptus) stomatogastric system: spike number- versus spike frequency-dependent domains. J Neurosci 17: 5956-5971.

Morris LG, Hooper SL (1998) Muscle response to changing neuronal input in the lobster (Panulirus interruptus) stomatogastric system: slow muscle properties can transform rhythmic input into tonic output. J Neurosci 18: 3433-3442.

Muller KJ, Nicholls JG, Stent GS (1981) Neurobiology of the leech.

Murthy VN, Sejnowski TJ, Stevens CF (1997) Heterogeneous release properties of visualized individual hippocampal synapses. Neuron 18: 599-612.

Mussa-Ivaldi FA, Bizzi E (2000) Motor learning through the combination of primitives. Philos Trans R Soc Lond B Biol Sci 355: 1755-1769.

Nicholls JG, Baylor DA (1968) Specific modalities and receptive fields of sensory neurons in CNS of the leech. J Neurophysiol 31: 740-756.

Nicholls JG, Purves D (1970) Monosynaptic chemical and electrical connexions between sensory and motor cells in the central nervous system of the leech. J Physiol 209: 647-667.

Norris BJ, Calabrese RL (1987) Identification of motor neurons that contain a FMRFamidelike peptide and the effects of FMRFamide on longitudinal muscle in the medicinal leech, Hirudo medicinalis. J Comp Neurol 266: 95-111.

Ort CA, Kristan WBJr, Stent GS (1974) Neuronal Control of Swimming in the Medicinal Leech. II. Identification and Connections of Motor Neurons. J Comp Physiol 94: 121-154.

Pastor J, Soria B, Belmonte C (1996) Properties of the nociceptive neurons of the leech segmental ganglion. J Neurophysiol 75: 2268-2279.

Pearce RA, Friesen WO (1985) Intersegmental coordination of the leech swimming rhythm. II. Comparison of long and short chains of ganglia. J Neurophysiol 54: 1460-1472.

Pearce RA, Friesen WO (1985) Intersegmental coordination of the leech swimming rhythm. I. Roles of cycle period gradient and coupling strength. J Neurophysiol 54: 1444-1459.

Peterson EL (1983) Visual processing in the leech central nervous system. Nature 303: 240-242.

Peterson EL (1984) Photoreceptors and visual interneurons in the medicinal leech. J Neurobiol 15: 413-428.

Pinato G, Torre V (2000) Coding and adaptation during mechanical stimulation in the leech nervous system. J Physiol 529: 747-762.

Pinato G, Battiston S, Torre V (2000) Statistical independence and neural computation in the leech ganglion. Biol Cybern 83: 119-130.

Raz A, Feingold A, Zelanskaya V, Vaadia E, Bergman H (1996) Neuronal synchronization of tonically active neurons in the striatum of normal and parkinsonian primates. J Neurophysiol 76: 2083-2088.

Reich DS, Victor JD, Knight BW, Ozaki T, Kaplan E (1997) Response variability and timing precision of neuronal spike trains in vivo. J Neurophysiol 77: 2836-2841.

Reinagel P, Reid RC (2000) Temporal coding of visual information in the thalamus. J Neurosci 20: 5392-5400.

Reinagel P, Reid RC (2002) Precise firing events are conserved across neurons. J Neurosci 22: 6837-6841.

Rembold CM (1992) Resistance to stretch, [Ca2+]i, and activation of swine arterial smooth muscle. J Muscle Res Cell Motil 13: 27-34.

Sahley CL, Boulis NM, Schurman B (1994) Associative learning modifies the shortening reflex in the semi-intact leech Hirudo medicinalis: effects of pairing, predictability, and CS preexposure. Behav Neurosci 108: 340-346.

Sahley CL, Modney BK, Boulis NM, Muller KJ (1994) The S cell: an interneuron essential for sensitization and full dishabituation of leech shortening. J Neurosci 14: 6715-6721.

Shadlen MN, Newsome WT (1994) Noise, neural codes and cortical organization. Curr Opin Neurobiol 4: 569-579.

Shadlen MN, Newsome WT (1995) Is there a signal in the noise? Curr Opin Neurobiol 5: 248-250.

Shadlen MN, Newsome WT (1998) The variable discharge of cortical neurons: implications for connectivity, computation, and information coding. J Neurosci 18: 3870-3896.

Shaw BK, Kristan WB, Jr. (1995) The whole-body shortening reflex of the medicinal leech: motor pattern, sensory basis, and interneuronal pathways. J Comp Physiol [A] 177: 667-681.

Shaw BK, Kristan WB, Jr. (1997) The neuronal basis of the behavioral choice between swimming and shortening in the leech: control is not selectively exercised at higher circuit levels. J Neurosci 17: 786-795.

Shaw BK, Kristan WB, Jr. (1999) Relative roles of the S cell network and parallel interneuronal pathways in the whole-body shortening reflex of the medicinal leech. J Neurophysiol 82: 1114-1123.

Softky WR, Koch C (1993) The highly irregular firing of cortical cells is inconsistent with temporal integration of random EPSPs. J Neurosci 13: 334-350.

Softky WR (1995) Simple codes versus efficient codes. Curr Opin Neurobiol 5: 239-247.

Sommerfeld A (1974) Mechanics of deformable bodies. New York: Academic Press.

Stent GS, Kristan WBJr, Friesen WO, Ort CA, Poon M, Calabrese RL (1978) Neuronal generation of the leech swimming movement. Science 200: 1348-1357.

Stevens CF, Zador AM (1998) Input synchrony and the irregular firing of cortical neurons. Nat Neurosci 1: 210-217.

Stuart AE (1970) Physiological and morphological properties of motoneurones in the central nervous system of the leech. J Physiol 209: 627-646.

Thorogood MS, Brodfuehrer PD (1995) The role of glutamate in swim initiation in the medicinal leech. Invert Neurosci 1: 223-233.

Tresch MC, Saltiel P, Bizzi E (1999) The construction of movement by the spinal cord. Nat Neurosci 2: 162-167.

Tsau Y, Wu JY, Hopp HP, Cohen LB, Schiminovich D, Falk CX (1994) Distributed aspects of the response to siphon touch in Aplysia: spread of stimulus information and cross-correlation analysis. J Neurosci 14: 4167-4184.

Verri A, Poggio T (1989) Motion field and optical flow: qualitative properties. IEEE Trans Pattern Anal Machine Intell 11: 490-498.

Verri A, Girosi F, Torre V (1989) The mathematical properties of the 2D motion field: from singular points to motion parameters. J Opt Soc Am A 6: 698-712.

Verri A, Aicardi F (1990) Limit cycles of the two-dimensional motion field. Biol Cybern 64: 141-144.

Verri A, Girosi F, Torre V (2002) Differential techniques for optical flow. J Opt Soc Am A 7: 912-922.

Wahl LM, Stratford KJ, Larkman AU, Jack JJ (1995) The variance of successive peaks in synaptic amplitude histograms: effects of inter-site differences in quantal size. Proc R Soc Lond B Biol Sci 262: 77-85.

Wahl LM, Jack JJ, Larkman AU, Stratford KJ (1997) The effects of synaptic noise on measurements of evoked excitatory postsynaptic response amplitudes. Biophys J 73: 205-219.

Warzecha AK, Egelhaaf M (1999) Variability in spike trains during constant and dynamic stimulation. Science 283: 1927-1930.

Warzecha AK, Kretzberg J, Egelhaaf M (2000) Reliability of a fly motion-sensitive neuron depends on stimulus parameters. J Neurosci 20: 8886-8896.

Wilson RJA, Skierczynski BA, Meyer JK, Skalak R, Kristan WBJr (1996) Mapping motor neuron activity to overt behavior in the leech. I. Passive biomechanical properties of the body wall. J Comp Physiol 178: 637-654.

Wilson RJA, Skierczynski BA, Meyer JK, Blackwood S, Skalak R, Kristan WBJr (1996) Predicting overt behavior from the pattern of motor neuron activity: A biomechanical model of a crawling leech. Proc Joint Symp Neural Comput 5: 176-190.

Wittenberg G, Kristan WBJr (1992) Analysis and modeling of the multisegmental coordination of shortening behavior in the medicinal leech. I. Motor output pattern. J Neurophysiol 68: 1683-1692.

Wittenberg G, Kristan WBJr (1992) Analysis and modeling of the multisegmental coordination of shortening behavior in the medicinal leech. II. Role of identified interneurons. J Neurophysiol 68: 1693-1707.

Wu JY, Cohen LB, Falk CX (1994) Neuronal activity during different behaviors in Aplysia: a distributed organization? Science 263: 820-823.

Wu JY, Tsau Y, Hopp HP, Cohen LB, Tang AC, Falk CX (1994) Consistency in nervous systems: trial-to-trial and animal-to-animal variations in the responses to repeated applications of a sensory stimulus in Aplysia. J Neurosci 14: 1366-1384.

Yau KW (1976) Receptive fields, geometry and conduction block of sensory neurones in the central nervous system of the leech. J Physiol 263: 513-538.

Yau KW (1976) Physiological properties and receptive fields of mechanosensory neurones in the head ganglion of the leech: comparison with homologous cells in segmental ganglia. J Physiol 263: 489-512.

Yu X, Nguyen B, Friesen WO (1999) Sensory feedback can coordinate the swimming activity of the leech. J Neurosci 19: 4634-4643.

Zohary E, Shadlen MN, Newsome WT (1994) Correlated neuronal discharge rate and its implications for psychophysical performance. Nature 370: 140-143.